

**A HEURISTIC OPTIMIZATION METHOD FOR THE DESIGN OF
MESO-SCALE TRUSS STRUCTURE FOR COMPLEX-SHAPED
PARTS**

A Thesis
Presented to
The Academic Faculty

By

Jason Nam Nguyen

In Partial Fulfillment
Of the Requirements for the Degree
Master of Science in Mechanical Engineering

Georgia Institute of Technology

August 2012

**A HEURISTIC OPTIMIZATION METHOD FOR THE DESIGN OF
MESO-SCALE TRUSS STRUCTURE FOR COMPLEX-SHAPED
PARTS**

Approved by:

Dr. David W. Rosen, Chair
George W. Woodruff School of Mechanical Engineering
Georgia Institute of Technology

Dr. Seung-Kyum Choi
George W. Woodruff School of Mechanical Engineering
Georgia Institute of Technology

Dr. Chris Paredis
George W. Woodruff School of Mechanical Engineering
Georgia Institute of Technology

Date Approved: June 15, 2012

*I dedicate this thesis to my
family for their unconditional
love and support*

ACKNOWLEDGEMENTS

First of all, I would like to thank my advisor, Dr David W. Rosen, for his guidance and support throughout my graduate school experience. I would also like to thank my committee members, Dr. Chris Paredis and Dr. Seung-Kyum Choi for taking their time to peruse my thesis and provide feedback and suggestions.

In addition, I would like to thank my labmates, Wenchao Zhou, Amit Jariwala, Namin Jeong, Jane Kang, Chad Hume, Sang-in Park, Patrick Chang, Dazhong Wu, and Jiten Patel for their supports and friendships. You guys have helped me so much along the way and made graduate school a much more enjoyable experience. Thank you all and best of luck with your future endeavors.

I also would like to thank my friends for providing friendships and supports when I needed. Thank you for being there for me and not letting time or distance to affect our friendships. I am grateful to have them in my life.

Finally, I would like to thank my mom, dad and sister for their unending love and care. My hard-working parents have made a lot of sacrifices to come to America so that my sister and I can have better education and living condition. I love them so much and I would not have made it this far without them.

TABLE OF CONTENTS

| | |
|---|-------------|
| ACKNOWLEDGEMENTS..... | iv |
| LIST OF TABLES..... | viii |
| LIST OF FIGURES..... | x |
| LIST OF SYMBOLS..... | xiv |
| SUMMARY | xv |
| 1 INTRODUCTION, BACKGROUND AND MOTIVATION..... | 1 |
| 1.1 Introduction | 1 |
| 1.2 Background | 1 |
| 1.2.1 Additive Manufacturing..... | 1 |
| 1.2.2 Design for Additive Manufacturing..... | 5 |
| 1.2.3 Cellular Materials..... | 6 |
| 1.2.4 Meso-scale Lattice Structures | 8 |
| 1.3 Motivation | 8 |
| 1.3.1 Design of Meso-scale Lattice Structure | 8 |
| 1.3.2 The Unit-Cell Approach | 9 |
| 1.4 Goals..... | 10 |
| 1.5 Organization of Thesis | 12 |
| 2 LITERATURE REVIEW..... | 14 |
| 2.1 Lattice Structure Analysis | 14 |
| 2.2 Methods for Designing Lattice Structures | 16 |
| 2.2.1 Size, Shape, and Topology Optimization | 16 |
| 2.2.2 Michell’s Truss Theory..... | 17 |
| 2.2.3 Optimization Approaches | 18 |
| 2.3 Multivariable Optimization Algorithms..... | 21 |
| 2.3.1 Levenberg-Marquardt (LM)..... | 22 |
| 2.3.2 Active Set..... | 23 |
| 2.3.3 Particle Swarm Optimization (PSO)..... | 23 |
| 2.4 Conformal Lattice Structure..... | 24 |
| 2.5 Summary | 25 |

| | | |
|----------|---|-----------|
| 3 | AUGMENTED SMS METHOD | 27 |
| 3.1 | Problem Formulation..... | 27 |
| 3.1.1 | General Problem Formulation..... | 27 |
| 3.1.2 | SMS Problem Formulation | 29 |
| 3.2 | Augmented SMS Method Overview | 32 |
| 3.2.1 | Step 1: Specification of loading, boundary conditions and material properties | 34 |
| 3.2.2 | Step 2a: Generation of ground structure | 34 |
| 3.2.3 | Step 2b: Solid Body Finite Element Analysis..... | 37 |
| 3.2.4 | Step 3: Map FEA nodes to Ground Structure | 40 |
| 3.2.5 | Step 4: Stress Scaling and Normalization..... | 43 |
| 3.2.6 | Step 5: Topology Generation | 56 |
| 3.2.7 | Step 6: Unessential and Duplicated Struts Removal..... | 57 |
| 3.2.8 | Step 7: Diameter Sizing | 58 |
| 3.3 | Comparison Between the Augmented SMS Method and Its Previous Implementations | 61 |
| 3.4 | Unit-Cell Library..... | 62 |
| 3.4.1 | The Optimization Process | 62 |
| 3.4.2 | Unit-Cell Selection..... | 67 |
| 3.4.3 | Mapping | 69 |
| 3.5 | Summary | 70 |
| 4 | DESIGN EXAMPLES..... | 71 |
| 4.1 | 3-D Cantilever Beam..... | 71 |
| 4.1.1 | Problem Description | 71 |
| 4.1.2 | Ground Geometry and Solid Body Analysis | 73 |
| 4.1.3 | Unit-Cell Library | 74 |
| 4.1.4 | Summary..... | 78 |
| 4.2 | 3-D Curved Cantilever Beam..... | 78 |
| 4.2.1 | Problem Description | 78 |
| 4.2.2 | Ground Geometry and Solid-Body Analysis | 80 |
| 4.2.3 | Unit-Cell Library | 81 |
| 4.2.4 | Summary..... | 97 |
| 4.3 | Micro Aerial Vehicle (MAV) Fuselage | 97 |
| 4.3.1 | Problem Description | 97 |

| | | |
|----------|---|------------|
| 4.3.2 | Ground Geometry and Solid Body Analysis | 99 |
| 4.3.3 | Unit-Cell Library | 101 |
| 4.3.4 | Summary | 117 |
| 5 | CONCLUSIONS..... | 119 |
| 5.1 | Summary | 119 |
| 5.2 | Conclusions | 120 |
| 5.3 | Contributions..... | 123 |
| 5.4 | Future Work | 124 |
| 5.4.1 | Unit-Cell Library | 124 |
| 5.4.2 | Systems Integration..... | 125 |
| 5.5 | Closure | 125 |
| | REFERENCES | 126 |

LIST OF TABLES

| | |
|--|----|
| Table 3-1: Qualitative formulation of meso-scale lattice structure design problem [15]. | 28 |
| Table 3-2: Mathematical formulation of meso-scale lattice structure design problem [15] | 28 |
| Table 3-3: Qualitative cDSP formulation for the SMS design problem [15] | 30 |
| Table 3-4: Mathematical cDSP formulation for the SMS design problem[15]..... | 30 |
| Table 3-5: Ground structure definition | 36 |
| Table 3-6: Example of nodal coordinate from solid-body FEA | 39 |
| Table 3-7: Example of stress values from solid-body FEA | 39 |
| Table 3-8: Qualitative cDSP formulation for the optimization of unit cells [15]..... | 62 |
| Table 3-9: Optimization parameter for unit-cell optimization in ANSYS | 65 |
| Table 3-10: Performance table used for selection of unit-cell configuration [15]..... | 69 |
| Table 4-1: Properties for 3-D cantilever beam example..... | 71 |
| Table 4-2: Diameter results for the 3-D cantilever beam | 76 |
| Table 4-3: Diameter result by Chang for 3-D cantilever beam [15]..... | 76 |
| Table 4-4: Actual diameters of the 3-D cantilever beam | 77 |
| Table 4-5: Initial properties of the curve cantilever beam | 79 |
| Table 4-6: Diameter results for the first selection scenario of the curved cantilever beam | 83 |
| Table 4-7: Design space exploration results for the fuselage | 85 |
| Table 4-8: Diameter results for the first selection scenario of the curved cantilever beam using alternative problem formulation..... | 87 |
| Table 4-9: Diameter results for second selection scenario of curved cantilever beam..... | 89 |

| | |
|---|-----|
| Table 4-10: Diameter results for the third selection scenario of the curved cantilever beam | 92 |
| Table 4-11: Diameter results for the final selection scenario of the curved cantilever beam | 94 |
| Table 4-12: Deflection results for curved cantilever beam..... | 95 |
| Table 4-13: Design time results for curved cantilever beam | 96 |
| Table 4-14: Initial properties for the fuselage..... | 99 |
| Table 4-15: Diameter results for the first selection scenario of the fuselage..... | 103 |
| Table 4-16: Diameter results of the second selection scenario for the fuselage | 105 |
| Table 4-17: Diameter results of the third selection scenario of the fuselage | 108 |
| Table 4-18: Design space exploration results for the fuselage | 111 |
| Table 4-19: Diameter results of the final selection scenario for the fuselage..... | 113 |
| Table 4-20: Deflection results for the fuselage..... | 115 |
| Table 4-21: Design time results for the fuselage | 115 |
| Table 4-22: Number of function calls to objective functions for the fuselage | 116 |

LIST OF FIGURES

| | |
|--|----|
| Figure 1-1: Siemens hearing aid manufactured using SLA process (left), customized Invisalign braces from a mold fabricated by SLA (right) [5, 6] | 3 |
| Figure 1-2: Aerospace duct made using SLS [7] | 4 |
| Figure 1-3: Cellular metal lattice structure (left); aluminum foam (right) [10, 11] | 6 |
| Figure 1-4: Octet-truss unit cell and example parts with octet truss meso-structures [14] | 7 |
| Figure 1-5: Thesis organization | 12 |
| Figure 2-1: Unit-cell approach for truss structure analysis | 15 |
| Figure 2-2: (a) Sizing optimization of a truss structure, (b) shape optimization, and (c) topology optimization [24] | 16 |
| Figure 2-3: Truss structure designed using Michell's method | 17 |
| Figure 2-4: Example of the homogenization approach to structural design [38] | 19 |
| Figure 2-5: Truss structure designed using the ground truss approach [24] | 20 |
| Figure 2-6: Uniform and conformal lattice structure | 24 |
| Figure 2-7: CLS construction method [52] | 25 |
| Figure 3-1: Overview of the augmented SMS method | 33 |
| Figure 3-2: Ground structure setting | 35 |
| Figure 3-3: Conformal ground structure | 36 |
| Figure 3-4: Comparison of stress, strain, and strain energy distribution for a 3-D curved cantilever beam | 38 |
| Figure 3-5: Hexahedron with each face dividing into triangles | 41 |
| Figure 3-6: Example of unit cell with outward-pointing normals computed and plotted | 41 |
| Figure 3-7: Unit-cell region | 46 |

| | |
|---|----|
| Figure 3-8: Rotation of coordinate system (x' , y' , z') | 47 |
| Figure 3-9: General state of stress [55]..... | 49 |
| Figure 3-10: Example 1-Parallelogram..... | 50 |
| Figure 3-11: XY-view of the topology for the 3-D parallelogram | 51 |
| Figure 3-12: Isometric view of the topology for the 3-D parallelogram | 51 |
| Figure 3-13: Example 2- rotated parallelogram..... | 52 |
| Figure 3-14: XY-view of the topology for the rotated 3-D parallelogram | 53 |
| Figure 3-15: Isometric view of the topology for the rotated 3-D parallelogram | 53 |
| Figure 3-16: Example 3- deformed and rotated parallelogram..... | 54 |
| Figure 3-17: XY-view of the topology for the rotated and deformed 3-D parallelogram | 55 |
| Figure 3-18: Isometric view of the topology for the rotated and deformed 3-D parallelogram | 55 |
| Figure 3-19: Overview of unit cell optimization process [15]..... | 63 |
| Figure 3-20: Loading conditions for unit-cell optimization [15]..... | 64 |
| Figure 3-21: Combination of optimized unit-cells for shear stress in XY plane for Cantley configuration [15] | 66 |
| Figure 3-22: Unit-cell library [15] | 67 |
| Figure 4-1: 3-D cantilever beam example | 72 |
| Figure 4-2: Cantilever beam divided into multiple unit-cell regions..... | 72 |
| Figure 4-3: von Mises stress (left); X-component of the stress (right)..... | 73 |
| Figure 4-4: Cantilever beam truss structure before topology alteration | 75 |
| Figure 4-5: Topology of the cantilever beam after D_{cutoff} is utilized | 75 |
| Figure 4-6: Final topology of the 3-D cantilever beam using active-set method | 77 |
| Figure 4-7: Least-square minimization result for 3-D cantilever beam using ground truss approach..... | 78 |

| | |
|--|----|
| Figure 4-8: 3-D curved cantilever beam | 79 |
| Figure 4-9: Base-lattice structure of the curve cantilever beam | 80 |
| Figure 4-10 : Von Mises stress (left); y-component of stress distribution (right) | 81 |
| Figure 4-11: Topology for the first selection scenario of the curved cantilever..... | 82 |
| Figure 4-12: Side view of the topology for the first selection scenario of the curved cantilever beam | 82 |
| Figure 4-13: Final topology for the first selection scenario of the curved cantilever beam using active-set method..... | 84 |
| Figure 4-14: Design space exploration for the first scenario of the curved cantilever beam | 85 |
| Figure 4-15: Design space exploration with finer resolution around the solution for the first selection scenario of the curved cantilever beam | 86 |
| Figure 4-16: Levenberg-Marquardt result for first selection scenario the curved cantilever beam using ground truss approach..... | 87 |
| Figure 4-17: Topology for second selection scenario of curved cantilever beam | 88 |
| Figure 4-18: Side view of the topology for the second selection scenario of the curved cantilever bream..... | 89 |
| Figure 4-19: Final topology for the second selection scenario of the curved cantilever beam using active-set method..... | 90 |
| Figure 4-20: Topology of the third selection scenario for the curved cantilever beam | 91 |
| Figure 4-21: Side view of the third selection scenario for the curved cantilever beam.... | 91 |
| Figure 4-22: Final topology for the third selection scenario of the curved cantilever beam using active-set method..... | 92 |
| Figure 4-23: Topology for the final selection scenario of the curved cantilever beam | 93 |
| Figure 4-24: Side view of the final selection scenario of the curved cantilever beam | 94 |
| Figure 4-25: Final topology for the final selection scenario of the curved cantilever beam using active-set method..... | 95 |

| | |
|---|-----|
| Figure 4-26: Loading and boundary condition on the fuselage | 98 |
| Figure 4-27: Multiple views of the fuselage | 99 |
| Figure 4-28: Multiple views of the ground structure for the fuselage | 99 |
| Figure 4-29: Solid-body analysis result for the fuselage | 100 |
| Figure 4-30: Topology for the first selection scenario of the fuselage | 102 |
| Figure 4-31: Side view of the first selection scenario of the fuselage | 102 |
| Figure 4-32: Final topology for the first selection scenario of the fuselage using least-square minimization..... | 103 |
| Figure 4-33: Topology for the second selection scenario of the fuselage | 104 |
| Figure 4-34: Side view of the second selection scenario of the fuselage | 105 |
| Figure 4-35: Final topology for the second selection scenario of the fuselage using active-set method | 106 |
| Figure 4-36: Topology for the second selection scenario of the fuselage | 107 |
| Figure 4-37: Side view of the third selection scenario for the fuselage..... | 107 |
| Figure 4-38: Final topology for the third selection scenario of the fuselage using least-square minimization..... | 109 |
| Figure 4-39: Design space for the third selection scenario of the fuselage | 110 |
| Figure 4-40: Zoomed-in design space of exploration for the third selection scenario of the fuselage | 111 |
| Figure 4-41: Topology for the final selection scenario of the fuselage | 112 |
| Figure 4-42: Side view of the final selection scenario for the fuselage..... | 113 |
| Figure 4-43: Final topology for the final selection scenario of the fuselage using least-square minimization..... | 114 |
| Figure 4-44: Convergence plot for active set method..... | 117 |

LIST OF SYMBOLS AND ABBREVIATIONS

| | |
|-----------|----------------------------------|
| CAD..... | Computer-Aided Design |
| FEA..... | Finite Element Analysis |
| MSLS..... | Meso-Scale Lattice Structures |
| SLA..... | Stereolithography |
| SMS..... | Size Matching and Scaling Method |
| STL..... | Standard Tessellation Language |

SUMMARY

Advances in additive manufacturing technologies have brought a new paradigm shift to both design and manufacturing. There is a much bigger design space in which designers can achieve a level of complexity and customizability, which are infeasible using traditional manufacturing processes. One application of this technology is for fabrication of meso-scale lattice structures (MSLS). These types of structures are designed to have material where it is needed for specific applications. They are suitable for any weight-critical applications, particularly in industries where both low weight and high strength are desired. MSLS can easily have hundreds to thousands of individual struts, where the diameter of each strut can be treated as a design variable. As a result, the design process poses a computational challenge. Since the computational complexity of the design problem often scales exponentially with the number of design variables, topological optimization that requires multi-variable optimization algorithm is infeasible for large-scale problems.

In previous research, a new method was presented for efficiently optimizing MSLS by utilizing a heuristic that reduces the multivariable optimization problem to a problem of only two variables. The method is called the Size Matching and Scaling (SMS) method, which combines solid-body analysis and predefined unit-cell library to generate the topology of the structure. However, the method lacks a systematic methodology to generate the initial ground geometry for the design process, which limits the previous implementations of the SMS method to only simple, axis-aligned structures.

In this research, an augmented SMS method is presented. The augmented method includes the integration of free-mesh approach in generating the initial ground geometry. The software that embodies that ground geometry generation process is integrated to commercial CAD system that allows designer to set lattice size parameters through graphical user interface. In this thesis, the augmented method and the unit-cell library are applied to various design examples.

The augmented SMS method can be applied effectively in the design of conformal lattice structure with highly optimized stiffness and volume for complex surface. Conformal lattice structures are those conformed to the shape of a part's surface and that can used to stiffen or strengthen a complex and curved surface. This design approach removes the need for a rigorous topology optimization, which is a main bottleneck in designing MSLS.

CHAPTER 1

INTRODUCTION, BACKGROUND AND MOTIVATION

1.1 Introduction

Additive manufacturing can be used to produce a vast array of structures, some of which would be impossible to manufacture using traditional manufacturing processes. This technology has been used for many years to do rapid prototyping, and is now being utilized more widely for manufacturing parts that are used in the final products. Designers are now able to achieve a level of complexity and customizability that is infeasible using standard machining processes. One application of this technology is for fabrication of customized, lightweight meso-scale lattice structures. Meso-scale lattice structures are a type of cellular material with strut diameters in the range of 0.1 to several millimeters and strut lengths of millimeters to centimeters. They have several advantages such as high strength-to-weight ratio and strong thermal and acoustic insulation properties. These types of structures are suitable for any weight-critical applications, particularly in the aerospace and automotive industries. This research will present a method for the design of meso-scale lattice structures that conform to a pre-existing geometry.

1.2 Background

1.2.1 Additive Manufacturing

Additive manufacturing refers to the use of additive fabrication technology to manufacture finished parts for assembly into final products. Additive fabrication technology is a process that fabricates 3-D objects by stacking layers of thin 2-D cross-

sectional slices of materials. The process begins with a solid model CAD drawing of the object. The CAD model is then converted to STL files and sent to an additive manufacturing machine [1]. STL files describe a collection of triangles that cover the boundary of the CAD model. They describe the surface geometry of a 3-D object without any representation of color, texture or other common CAD model attributes.

Additive manufacturing technologies can be grouped into different categories based on the machine architecture and materials transformation physics. These categories include: photopolymerization, powder bed fusion, extrusion-based systems, printing, sheet lamination, beam deposition, and direct write technologies [2]. Today five technologies are commonly in use in additive manufacturing, including stereolithography, fused deposition modeling, laser sintering, digital light processing, and 3-D printing [1]. Each technology has its own set of characteristics, such as manufacturing speed, resolution, accuracy, and surface finish that are suitable for specific applications. The two most widely used technologies are stereolithography and selective laser sintering. They are discussed in the next two sections.

1.2.1.1 Stereolithography

Stereolithography (SLA) is the first fully commercialized rapid prototyping technology and it is still the most widely used [1]. It is a process in which a 3-D solid part is created by selectively curing a liquid photopolymer resin using a UV laser. In SLA, there is a platform in a vat of liquid, photocurable polymer, i.e. epoxy or acrylate resin. During the SLA process, the platform is lowered incrementally into the vat of resin with a depth equal to the slice thickness, then a UV laser scans and cures the slice of the exposed resin. After that layer is solidified, the platform moves down incrementally and

the liquid resin spreads on top of the previously solidified layer. The laser then traces out that layer on top of the previous one. The process is repeated until the part is complete.

For many years, SLA was mainly used as a prototyping tool; however, several companies are now using SLA for production manufacturing. Additive manufacturing enables one-off, custom manufacturing of ten to hundreds of thousands of parts. For example, Siemens, Phonak, Widex and other hearing aid manufacturers use SLA machines to produce hearing aid shell [3]. Align Technology uses SLA to fabricate molds for producing customized clear braces (Invisalign®) [4]. Figure 1-1 shows examples of products manufactured using SLA machines.



Figure 1-1: Siemens hearing aid manufactured using SLA process (left), customized Invisalign braces from a mold fabricated by SLA (right) [5, 6]

1.2.1.2 *Selective Laser Sintering*

Selective laser sintering (SLS) uses a high-powered laser to selectively heat the grains of a powder to their melting temperature and then fuse them to form the cross-section of a part. During the SLS process, a roller spreads a thin layer of powder across the build

platform. The SLS machine preheats the powder in the build platform to a temperature just below its melting point in order to minimize the laser power requirement. A CO₂ laser scans the cross-section area generated from the 3D CAD model of the part and selectively fuses the powder. After each cross-section is scanned, the build platform is lowered by one layer, a new layer of powder is applied on top of the previous layer, and the fusion process is repeated. These steps are repeated until the part is complete.

SLS can fabricate parts from a variety of powdered materials including polymers i.e. nylons and polystyrene and metals i.e. steel and titanium. Boeing and its suppliers use SLS to manufacture various parts for F-18 fighter jets. In this case, additive manufacturing technology enables low volume production. In addition, additive manufacturing can greatly simplify product assembly by allowing parts that are typically manufactured as multiple components to be fabricated as one piece. An example of aerospace ducts built using the SLS process is shown in Figure 1-2.



Figure 1-2: Aerospace duct made using SLS [7]

1.2.1.3 Advantages of Additive Manufacturing

Additive manufacturing has revolutionized product development and manufacturing. It has several key advantages over traditional manufacturing methods such as computer numerical control (CNC) machining. They include: [2]

- **Speed:** For a geometrically complex part, CNC machines require considerable set up and process planning. In contrast, an additive manufacturing machine can make the same part in one step. Because of the reduction in process steps, many components can be built in a shorter time frame using additive manufacturing technology.
- **Complexity:** Additive manufacturing has a distinct advantage over CNC machining because it allows the fabrication of parts whose geometric complexity makes them unfeasible to fabricate with subtractive methods.
- **Customizability:** Additive manufacturing process allows customization of parts without modification of the manufacturing process and toolings. Only the CAD model of a part needs to be altered for the customization.

1.2.2 Design for Additive Manufacturing

The unique capabilities of additive technology have created new opportunities for product customization, improvements in product performance, and lower overall manufacturing cost. These unique capabilities include shape complexity, material complexity and hierarchical complexity. Shape complexity refers the ability of additive manufacturing to produce very complex shapes with different sizes. Material complexity refers to its ability to manufacture parts with complex material compositions since different materials can be processed on different layers of a structure. Hierarchical

complexity encompasses the capacity of additive manufacturing system to fabricate multi-scale structures from the microstructure through geometric macrostructures to the part-scale macrostructure [8]. This research presents a design method that enables designers to take advantage of the shape complexity capability of additive manufacturing processes. Specifically, we focus on the design of cellular structures.

1.2.3 Cellular Materials

Cellular material have a biologically inspired origin, as many naturally occurring materials have porous constructions e.g. woods, bone, coral. Cellular materials are designed to have material only where it is needed for specific applications. They have several key advantages, such as strong thermal and acoustical insulation properties and high strength to weight ratio [9]. Some examples of cellular materials are foam, honeycomb, and lattice, etc. They are shown in Figure 1-3. These materials are suitable for any weight-critical application, particularly in the aerospace and automotive industries.

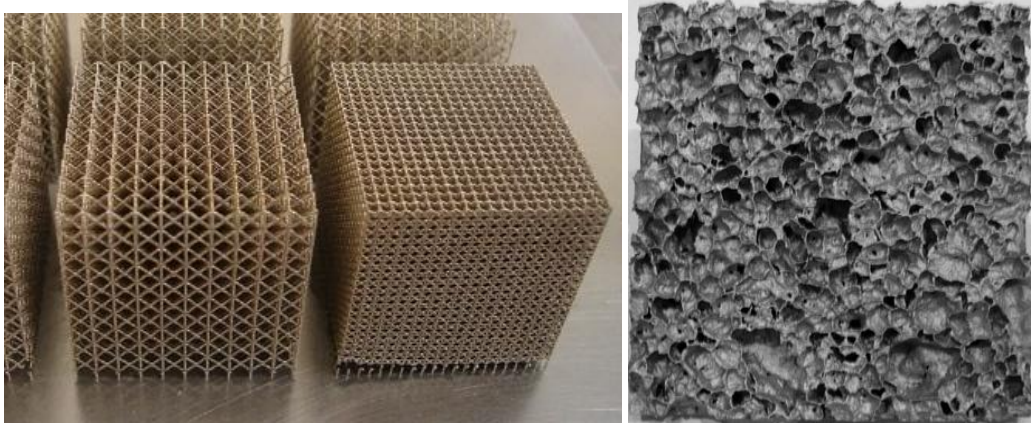
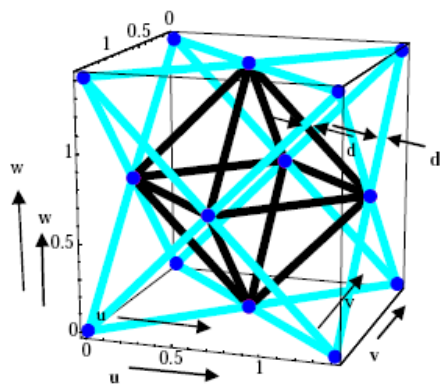


Figure 1-3: Cellular metal lattice structure (left); aluminum foam (right) [10, 11]

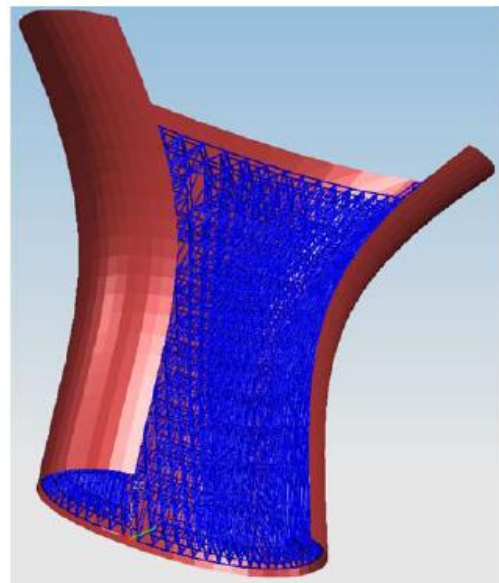
There are two categories of cellular materials: those produced using stochastic processes (e.g. foaming) and those designed using deterministic processes (e.g. designed lattice materials). Lattice materials have an inherent advantage over foams in providing stiff and strong material [12]. Deshpande et al. point out that foam's strength scales roughly to $\rho^{1.5}$, while the strength of lattice material scales to ρ , where ρ is the volumetric density of the material [13]. Therefore, a lattice material with a $\rho = 0.1$ is about three times stronger than a foam with the same volumetric density. The strength difference is attributed to the way that foam deforms by cell wall bending while lattice elements stretch and compress. Figure 1-4 shows the octet truss that has been studied extensively and examples of parts that utilize the octet truss.



(a) Octet Truss



(b) Skin with 2 layers of lattice structure made using SL



(c) Skin with single layer of lattice structure

Figure 1-4: Octet-truss unit cell and example parts with octet truss meso-structures [14]

1.2.4 Meso-scale Lattice Structures

This research will focus on the design of meso-scale lattice structures (MSLS), a type of cellular material with strut diameters in the range of 0.1 to several millimeters and strut lengths of millimeters to centimeters. Examples of MSLS are shown in Figure 1-4.

1.3 Motivation

1.3.1 Design of Meso-scale Lattice Structures

One application of additive technology is for the fabrication of customized, lightweight material called MSLS. This material is highly suitable for any weight-critical applications, particularly in the automobile and aerospace industries, which desire components with high strength and low weight. However, conventional CAD and CAE systems are computationally insufficient to handle MSLS-based designs because these structures can contain hundreds of thousands of individual struts. Furthermore, existing design methods for such structures are very limited due to the large number of design variables and options [14]. Following are the three main drawback of existing methods [15]:

- **Incorrect/Non-optimal Solutions:** Because of the sheer quantity of design variables, the design space often contains many local minima. Therefore, the solution often fails to converge on the global solution because the optimization problem is highly dependent on the initial starting value.
- **Repeatability:** Most multivariable optimization algorithms, such as genetic algorithm and particle swam optimization, are highly stochastic in nature, which

can introduce a certain amount of randomness into a solution. Therefore, repeatability of design results will be an issue in the design of MSLS.

- **Computational complexity/Long Design Time:** Since the computational complexity of the design problem often scales exponentially with the number of design variables, topological optimization that requires multi-variable optimization algorithm is infeasible for large design problems. For a structure that has more than one thousand struts, these methods will either not converge or they will converge in an unreasonable time frame.

1.3.2 The Unit-Cell Approach

In order to mitigate the computational complexity created by the need for multivariable optimization, there has been much research devoted to improving or developing more efficient optimization methods. However, previous research has only reduced the computational burdens to a certain extent. There is still a need for a new method to streamline the design process of MSLS.

In their research, Graf and Chang presented an alternative approach to the design of MSLS, called the “Size Matching and Scaling,” or SMS method. The key feature of this method is utilization of a heuristic that reduces the multivariable optimization problem to a problem of only two variables [15, 16].

1.3.2.1 Approach

The heuristic used by Graf and Chang is based on the observation that the stress distribution in a MSLS will be similar to the stress distribution in a solid body of the same overall shape. Hence, stress analysis of the target lattice structure as a solid body is performed using finite-element analysis. In addition, the target truss structure is divided

into smaller regions, called unit cells. Based on the computed local stress state, unit cells from a predefined “unit-cell library” are selected, assigned to each region in the target truss structure, and sized to support those stress states. The diameters of these struts are normalized and valued from zero to one. The optimal diameters of these struts are then computed by performing a two-variable minimization to determine the smallest diameter in the structure, D_{\min} and the largest diameter in the structure, D_{\max} . A more detailed description of this method is presented in Chapter 3.

1.3.2.2 Drawbacks/Limitations

Although very effective in the design of MSLS, there are significant limitations with the existing SMS method. These issues must be addressed in order for the method to be more effective and versatile. The limitations are as follows:

- The first key limitation is with the segmentation of the target structure into smaller regions, called unit cells. The unit cells are currently generated manually by the designer using a 3-D mapped mesh approach. This manual approach limits the MSLS design to simple geometry and shape.
- The second key limitation is that the SMS method cannot be used in structures that have curved or non-rectangular surfaces. The current method can only be applied to simple and axis-aligned structures. It requires the local coordinate system of the unit cells to be the same as the global coordinate system.

1.4 Goals

The goal of this thesis is to develop a method to design and efficiently optimize MSLS for complex-shaped parts. It should be easy to use, time-efficient, and provide a less manual construction of the model.

In previous research conducted by this laboratory, computer-aided design technologies were developed for efficiently generating and representing MSLS [17]. Given selected part model surfaces, MSLS can be generated to conform to the shapes of the surfaces. This free-mesh approach will be integrated into the SMS method to design MSLS for complex-shaped parts including structures that have curved or non-rectangular surfaces. There are several subtasks to be completed in order to achieve this goal. They are as follows:

- The stress results from the solid-body finite element analysis must be correlated to the appropriate unit cells. Since the geometry of the part model will no longer be simple and axis-aligned, the current SMS method would fail to determine which unit cell the solid-body nodes belong to. A new algorithm must be developed for this mapping process.
- Based on the computed local stress state, the unit cells from a defined unit-cell library are selected and sized. Since the local coordinate systems of the unit cells will not necessarily be the same as the global coordinate systems, a transformation of stress from the global coordinate to the local coordinate system of each unit cell is required.

1.5 Organization of Thesis

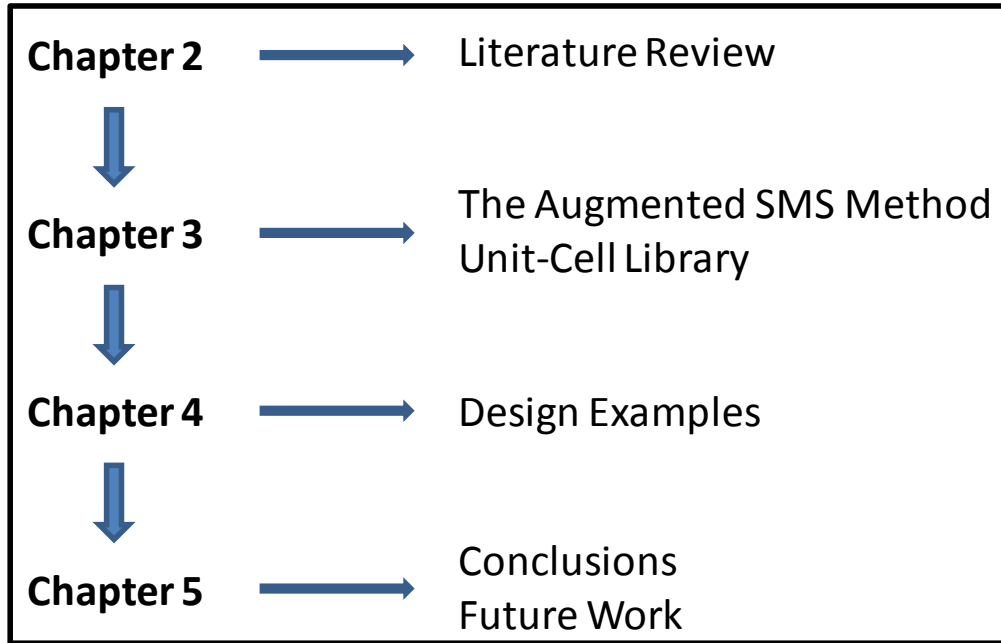


Figure 1-5: Thesis organization

The remaining chapters of this thesis are organized as presented in Figure 1-5.

Details are summarized below:

- In chapter two, a literature survey is conducted to cover the research relevant to the SMS method. This includes an overview of previous research in the design and analysis of cellular structures, and the approaches for optimization of these structures. In addition, gap analysis is conducted on existing research.
- In chapter three, the augmented SMS method is presented. This includes the integration of the free-mesh approach in the SMS method and modifications of existing methods to be used for complex-shaped parts with curved and non-rectangular surfaces. The unit-cell library is also outlined in this chapter. This includes the optimization process for the unit-cell entry and the selection process.

- In chapter four, several example problems are presented. The first example serves to validate and compare the augmented method with the existing method. The second example illustrates that the capability of the new method extends beyond the existing method. The third example applies the augmented SMS method to design and optimize MSLS for a micro air vehicle (MAV) fuselage. This is truly a complex-shaped part that could not be designed using the existing SMS method.
- In chapter five, the conclusion is drawn based on the analysis of the results. The limitations and potential future work are also outlined.

CHAPTER 2

LITERATURE REVIEW

In this chapter, a literature survey of relevant research is conducted. Several aspects of cellular structure design including analysis methods and optimization methods are discussed. This chapter also provides an overview of the method for generating and representing meso-scale lattice structures, which will be integrated into the augmented SMS method.

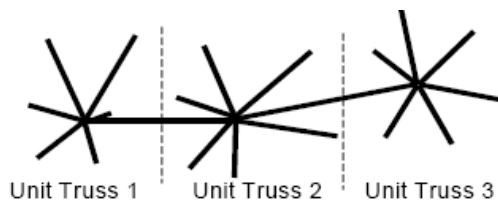
2.1 Lattice Structure Analysis

In order to effectively design cellular structures, we must be able to accurately model, determine the mechanical properties, and quantify the performance of these structures. One main task is to determine the assumptions and limitations involved in developing these models. Many methods have been developed to analyze various cellular structures. For instance, Ashby et al. has conducted extensive research in the area of metal foams [12]. Wang and McDowell have performed a comprehensive review of analytical modeling, mechanics, and characteristics of various metal honeycombs [18, 19]. However, the focus of this section is on the analysis of truss structures, a type of cellular structure.

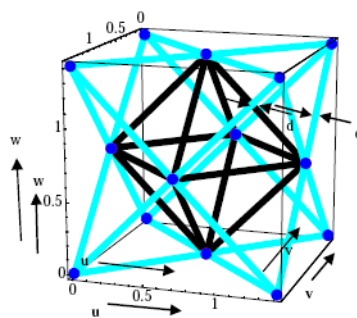
Since truss structures comprise a series of struts and nodes, their properties are different from solid components. Truss structures were initially analyzed under the assumptions that struts have pin-pin joints and only undergo axial loading. Wallach and Gibson use this assumption to analyze lattice sheets undergoing axial loads in the x, y and z directions [20]. This work returned results with percent errors ranging from 3% to 27%

in comparison with experimental results. Chiras et al. extended this assumption to analyze similar structures undergoing bending and shear loading.

A truss structure, however, can be decomposed into mesostructure unit cells for design and analysis purposes. Each mesostructure unit cell can be further broken down into smaller truss structures. Deshpande et al. has investigated extensively the properties of these smaller building blocks, particularly the octet-truss structure. However, the analysis also assumed that the struts only experience axial forces [13]. Johnson et al. provided a more comprehensive analytical model of the truss structure by considering each strut as a beam experiencing axial, bending, shearing, and torsion effects. The octet-truss structure was analyzed using a unit-truss model that consists of a node and set of half-struts connecting to the node [21]. The analysis is done using the finite-element approach. Wang et al. have applied this unit-truss method to design and represent lattice structure [22, 23]. Examples of the unit trusses and the octet truss are shown in Figure 2-1.



(a) Series of 3 unit truss structures



(b) Octet truss

Figure 2-1: Unit-cell approach for truss structure analysis

2.2 Methods for Designing Lattice Structures

2.2.1 Size, Shape, and Topology Optimization

Cellular materials are designed to have material only where it is needed for a specific application. The optimization of the geometry and topology of the structural lay-out has great impact on the performance of the structures [24]. The design synthesis method for cellular materials consists of size, shape, and topology optimization to address different aspect of the structural design problem.

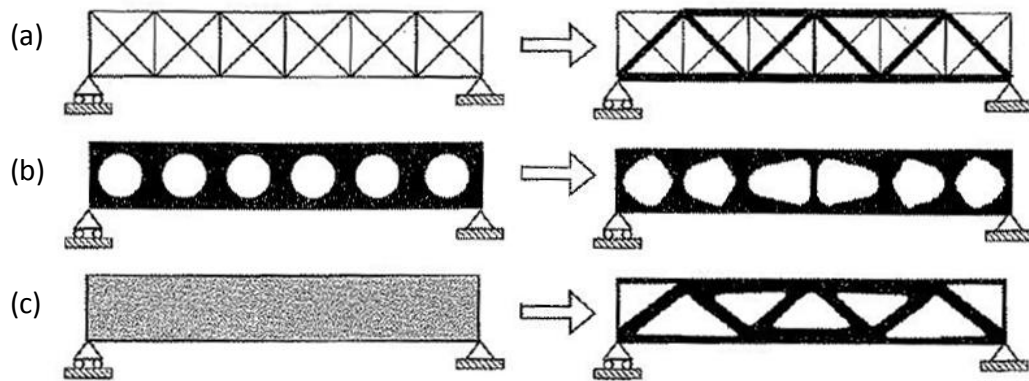


Figure 2-2: (a) Sizing optimization of a truss structure, (b) shape optimization, and (c) topology optimization [24]

In order to understand optimization of structures, the definitions of three categories of structural optimization must be stated. These definitions follow those from Bendsøe and Sigmund [24]. A typical size optimization involves finding the optimal cross-sectional area of each strut in a truss structure [25]. Shape optimization computes the optimal form that defined by the boundary curves or boundary surfaces of the body [26, 27]. The process may involve moving nodes to change the shape of the structure; however, the element-node connectivity remains intact. Topology optimization, according to Rozvany, finds optimal connective or spatial sequences of members or elements in a structure [28]. In topological optimization, the physical size, shape, and connectivity of the structure are

not known. The only known properties are the volume of the structure, the loads, and the boundary conditions [24]. It can be seen that topology optimization involves both size and shape optimization. Three categories of structural optimization are illustrated in Figure 2-2. It can be seen that size and shape optimizations consider the material distribution in the structure to satisfy certain loading conditions while maintaining the same topology. On the other hand, the initial and optimal structures are completely different in the case of topology optimization. In this research, optimization variables of the truss structures are strut diameters. However, each unit cell of the MSLS can have a different configuration depending on the selection criteria. Therefore, ‘‘topology optimization’’ will be the term used in this research for designing and optimizing MSLS.

2.2.2 Michell’s Truss Theory

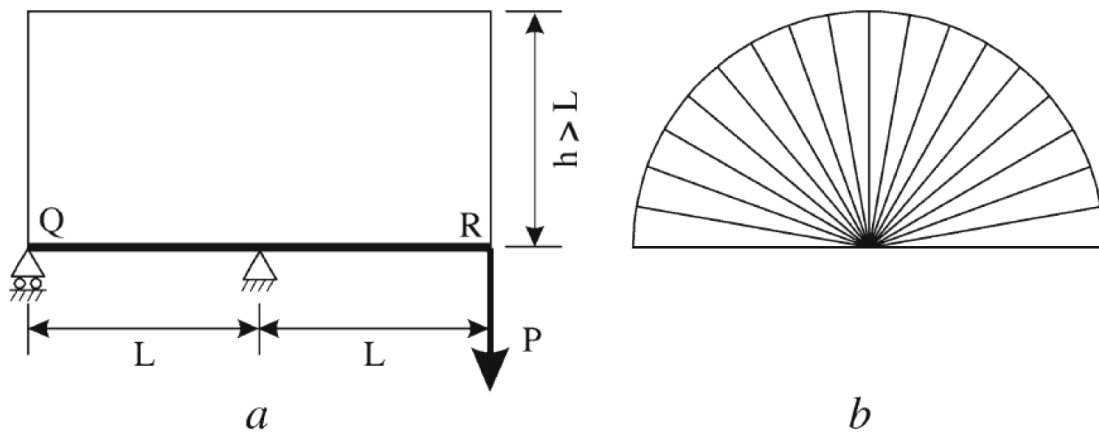


Figure 2-3: Truss structure designed using Michell’s method

Structural optimization for cellular structures dates as far back as a century ago. In 1904, George Michell, an Australian engineer, published a theory that defines the existence of an analytically optimal truss structure under certain loading conditions [29]. He described a simple 2D truss structure consisting of two mutually orthogonal fields of

tension/compression, with only members that are directed along the principal strain [24]. An example of Michell trusses is shown Figure 2-3.

Michell trusses have become the foundation for analytical theory of topology optimization for nearly a century. Several extensions of Michell trusses have been investigated, such as multi-material structures, geometrically non-linear trusses, or structure containing pre-existing struts [30-32]. However, Michell trusses are limited to two dimensions and are not conducive to practical manufacturing due to varying lengths and curved beams needed for optimal solution. Hence, it is very limited in application.

2.2.3 Optimization Approaches

The topology optimization techniques used to design truss structures are based on one of two approaches: the homogenization (continuum) approach and the ground (discrete) truss approach. Topology optimization is intrinsically a discrete optimization problem [33]. By using continuous variables such as cross-sectional area, void sizes and material density, these two approaches transform the discrete problem into a continuous one [34]. The details of these two approaches and the advantages/disadvantage of each approach are discussed in the next couple of sections.

2.2.3.1 Homogenization Approach - Continuum Structural Optimization

The homogenization approach in topology optimization is a material distribution method that considers the design space as an artificial composite material with an infinite number of periodically distributed small holes. The problem is transformed from a topology optimization problem to a sizing optimization problem by considering the sizes of these small holes as design variables. The main task is to create a microstructure model using a material density function. In the final optimal structure, regions with

density at or near one are filled while regions with density at or near zero are empty. The method was pioneered by Bendsøe and Kikuchi in 1988 [35]. More microstructures have been developed to improve the homogenization method, including ranked layered microstructures, micro-microstructure, and free mixture representation [24]. The method is advantageous in that it allows true optimization without the need to remesh the finite-element model [24]. However, there can be ambiguity in material allocation for areas that do not have a clear definition of high or low density. Various methods have been developed to alleviate the problem with varying degree of success [36, 37]. An example of the homogenization approach in structural design is shown Figure 2-4.

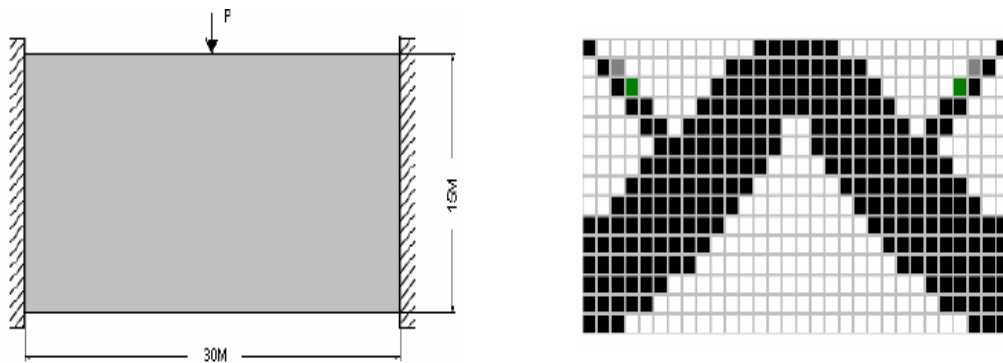


Figure 2-4: Example of the homogenization approach to structural design [38]

2.2.3.2 Ground Truss Approach-Discrete Structural Optimization

The ground truss approach starts with a ground structure, which is a grid of all elements connecting the nodes in the design space. The optimal truss structure is realized by selecting an optimal substructure from this pre-defined ground structure. Ultimately, the ground-truss approach is a sizing optimization problem, where the cross-sections of ground truss members are the continuous design variables for the optimization. The

cross-sections of the struts are sized to support the applied loads on the structure. Struts with cross-sections near zero are then removed to obtain the optimal structure [39]. Since the ground truss approach is highly dependent on the initial ground structure, much research has been conducted to include geometry optimization in the approach by considering the locations of the nodes as second design variables [40]. In general, the ground truss approach is much faster than the homogenization approach. An example of a truss structure designed using the ground truss approach is shown in Figure 2-5.

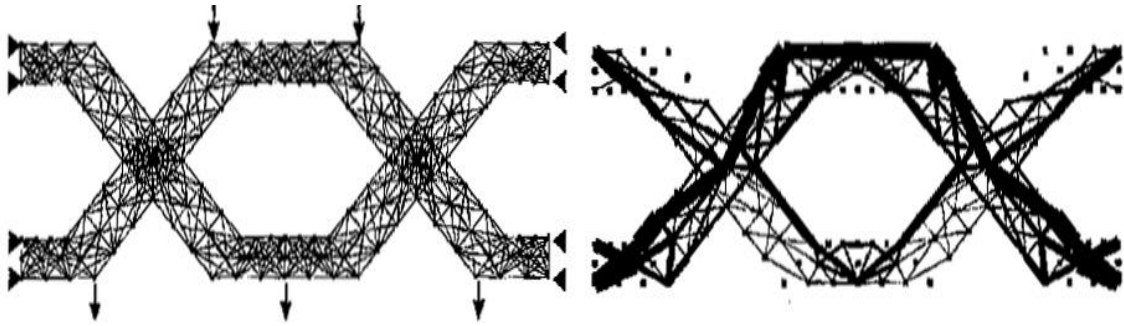


Figure 2-5: Truss structure designed using the ground truss approach [24]

For a typical single load situation, the design problem for the ground truss approach is formulated as minimizing deflection and volume subject to static equilibrium and stress constraints [25, 41]. Recently, a new framework has been developed to design meso-scale structures by combining deterministic topology optimization and reliability constraints. This topology optimization under uncertainty is referred to as reliability-based topology optimization, in which probabilistic constraints specify the required reliability level of the system [42].

2.3 Multivariable Optimization Algorithms

Regardless of what structural optimization approach is used for the design, an actual optimization routine must still be performed. There are many different optimization algorithms depending on the specific applications. However, the optimization algorithms used mainly in topology optimization of truss structures are those for solving nonlinear constrained optimization problems. Rozvany and Zhou categorized these optimization algorithms into direct methods and indirect method [43, 44]. Direct methods, such as mathematical programming, consist of iteratively calculating the value of the objective function, its gradient with respect to all the design variables, and a change of design variables resulting in cost reduction until the local minimum of the objective function is found [44]. According to Rozvany et al., these methods are very robust. However, the calculation of gradients can be time-consuming, and these methods can only optimize a limited number of design variables. On the other hand, indirect methods, such as optimality criterion, attempt to satisfy some characteristics of the structure instead of directly optimizing the objective function [45]. For instance, in a full stress topological design approach, the trusses are designed based on the assumption that each strut in an optimal structure is subjected to its limiting stress under at least one loading condition. The fundamental idea behind this approach was introduced by George Michell, whose trusses require that all struts in compression and tension to have identical stress [29, 46]. In many cases, optimality criteria, such as uniform stresses, are equivalent to direct criteria, such as minimum compliance, and therefore provide the same solutions [27].

In this research, three particular optimization algorithms are used or discussed: Particle Swam Optimization (PSO), Levenberg-Marquardt (LM) and Active-set Programming. They are discussed in detail in the next three sections.

2.3.1 Levenberg-Marquardt (LM)

The Levenberg-Marquardt algorithm is a gradient-based optimization algorithm that performs well for least-square minimization problems. Least square minimization is a problem formulation that seeks to minimize the sum of the square of the error between the target value of the goal and the actual value of the goal. The formulation is represented mathematically as [14]:

$$S(X) = \sum_i (P_{i,target} - P_{i,actual}(X))^2 \quad (2-1)$$

where P_i can be the volume of the structure, or its compliance, etc... In order to minimize the objective function, its derivative is set to zero.

$$\nabla S(X) = 2 \sum_{i=1}^n \left[\frac{\delta P_{i,actual}(X)}{\delta X} \right] [P_{i,target} - P_{i,actual}(X)] = 0 \quad (2-2)$$

In cellular structure design, the number of design variables greatly exceeds the number of objectives, which is similar to fitting a lower order model to a large data set. Several methods have been developed to solve these problems, such as the Gauss-Newton and Levenberg-Marquardt methods [47]. In this research, the Levenberg-Marquardt method is selected because of its robustness when the variation in the partial derivative term, also known as Jacobian, $J(X)$, is small. In this research, a MATLAB nonlinear least-square solver from the optimization toolbox, *lsqnonlin*, is used.

2.3.2 Active Set

The active set algorithm is a mathematical programming algorithm (direct method) that uses a gradient to optimize a large-scale optimization problem [48]. The problem is formulated using an objective function and a set of constraints that define the set of all values to search for the optimal solution. It aims to predict which inequality constraints are active in a given minimization function, which reduces the complexity of the search. In this research, the MATLAB function, *fmincon*, will be used to implement the active set algorithm to find the minimum of constrained nonlinear multivariable functions. This implementation uses a sequential quadratic programming (SQP) method in which the function solves a quadratic programming problem at each iteration [49]. Since *fmincon* is a gradient-based method, the algorithm is limited to problems where the objective and constraint functions and their first derivative are continuous.

2.3.3 Particle Swarm Optimization (PSO)

Particle swarm optimization (PSO) is a stochastic optimization method that can be used for direct or indirect methods, depending on the problem formulation. PSO was originally introduced by Kennedy and Eberhart as an extension of the genetic algorithm (GA) to simulate social behavior by emulating the movement of birds in a flock during the search for food [50]. The process updates the current position of each particle swarm using a velocity vector. The velocity vector is updated based on the history of each particle, as well as the experience by the swarm as a whole. The process is implemented numerically as shown below [51]:

$$x_{k+1}^i = x_k^i + v_{k+1}^i \Delta t \quad (2-3)$$

$$v_{k+1}^i = \underbrace{w_k \times v_k^i}_{\text{velocity inertia}} + \underbrace{c_1 r_1 \times \left(\frac{p_k^i - x_k^i}{\Delta t} \right)}_{\text{cognitive behavior}} + \underbrace{c_2 r_2 \times \left(\frac{p_k^g - x_k^i}{\Delta t} \right)}_{\text{social behavior}} \quad (2-4)$$

p_k^i & p_k^g respectively represent the best position of particle i and the global best position of the entire swarm; and r represents a random number. Hence, PSO is stochastic in nature because the particle swarm process is governed by a pseudo-random number used to calculate the velocity vector of the swarm. PSO often converges faster than GA and is robust and well-suited to handle non-linear and non-convex design spaces with discontinuities even though it does not guarantee to find a solution. PSO is not implemented in the augment SMS method, but it was used in previous research as a validation tool [16].

2.4 Conformal Lattice Structure

Conformal lattice structures are MSLS that conformed to the shape of a part's surface and that can be used to stiffen or strengthen a complex and curve surface. These structures will be the primary focus of this research. Figure 2-6 shows the difference between a uniform lattice and a conformal lattice.

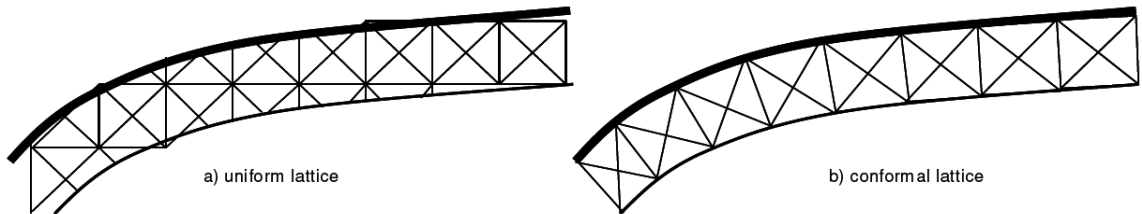


Figure 2-6: Uniform and conformal lattice structure

Previous research conducted in this laboratory resulted in method to create conformal lattice structures. The method consists of two main steps: generate a conformal

hexahedral mesh and populate the volume between the mesh on the original surface and the offset surface with unit cells of cellular materials [17]. This method automates the design process for a MSLS for an input surface. It efficiently generates and represents a MSLS. The overall method for generating a conformal lattice structure is shown Figure 2-7. This new method will be integrated with the augmented SMS method to automatically generate the ground / base- lattice structure.

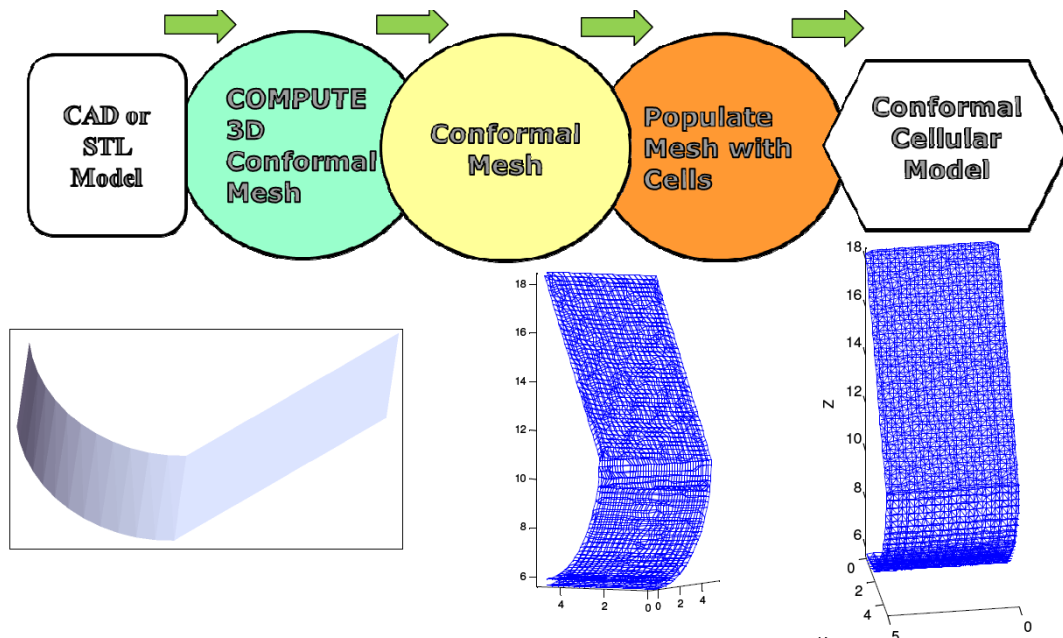


Figure 2-7: CLS construction method [52]

2.5 Summary

Chapter 2 provided a literature review of previous works related to designing and optimizing meso-scale lattice structures. Several methods of trusses analysis were presented as means to quantify the performance of truss structures. The unit-truss method was selected for this research because of the previous documented success in modeling the structure. Michell's truss, an analytical optimal truss structure, is presented, but the solution is not very practical. Hence, there is a need for structural optimization.

Much research has been conducted on the problem of design and optimizing cellular structures. It can be seen that optimization is by far the most time-consuming step of the process. Two main optimization approaches were outlined including: homogenization approach and ground truss. There are certain advantages and disadvantages to each approach. Regardless of what approach is used, a multivariable optimization is required. There are many different optimizations methods, depending on the applications. Several optimization techniques were presented including: active set, least square minimization and particle swarm optimization. Finally, a new method for generating conformal lattice structure was briefly outlined. It provides a new way to generate the ground structure for the augmented SMS method.

CHAPTER 3

AUGMENTED SMS METHOD

In this section, the augmented Size Matching and Scaling (SMS) Method will be presented. The augmented method will resolve the technical limitations from the previous implementations of the method by integrating a free mesh approach to the existing method. This design method will be able to efficiently design and optimize meso-scale lattice structure on complex shaped parts by utilizing a heuristic that reduces multivariable optimization problem to a problem of only two variables.

3.1 Problem Formulation

A general design problem formulation for meso-scale lattice structure is formulated and can then be adapted for the specific characteristics of SMS method.

3.1.1 General Problem Formulation

Each meso-scale lattice structure design problem has its own loading condition, geometric properties and desired performance specification. However, they can all be characterized as multi-objective design problems using the Compromise Decision Support Problem (cDSP) method [53]. The general qualitative problem formulation for design optimization of meso-scale lattice structure is provided in Table 3-1. The equivalent mathematical formulation is provided in Table 3-2.

Table 3-1: Qualitative formulation of meso-scale lattice structure design problem [15]

| | |
|------------------|--|
| Given: | Starting ground structure, loading and boundary condition |
| Find: | Strut diameter sizes |
| Satisfy: | Upper and lower diameter bounds, maximum volume constrains and maximum stress constrains |
| Minimize: | Compliance, deviation from target volume |

Table 3-2: Mathematical formulation of meso-scale lattice structure design problem [15]

| | |
|------------------|---|
| Given: | p^{BG}, p^F, p^M, i |
| Find: | Strut diameter, $D_i \in \{0, [D_{LB}, D_{UB}]\}$ (a) |
| Satisfy: | $\sigma_i \leq \sigma_{max}$ (b) |
| | $V \leq V_{max}$ (c) |
| Minimize: | $Z = (W_d \times d)^2 + (W_V \times V)^2$ (d) |

In Table 3-2, the symbols p^{BG} , p^F , p^M represent the boundary, loading and material properties respectively. The strut diameter, D_i , can either range from the lower diameter bound, D_{LB} , to the upper diameter bound, D_{UB} , or zero. The symbol σ_i represents the axial stress value in each i strut. The symbols V and d represent the volume and the deformation of the structure. W_d and W_V represent weighting variables for d and V in the minimization function, Z . The volume of the structure is calculated by summing the volume of all the struts in the structure, which are assumed to be cylinders:

$$V = \sum \pi \times \frac{D_i^2}{4} \times l_i \quad (3-1)$$

where D_i and l_i represent the diameter and length of each of the i strut in the structure. In this calculation, the overlapping volumes where the struts meet are not subtracted from

the overall volume of the structure because they are assumed to have negligible contributions in order to simplify the calculation.

This problem is traditionally solved using rigorous global optimization, which considers the diameter of each strut as a design variable. It typically starts with a ground structure and is inherently a size optimization problem. However, when the diameter of a strut is below the lower bound, it will be removed from the structure. The problem then becomes a topological optimization because the topology of the structure has changed. Depending on the size and complexity of the structure, this design method is often computationally impractical because the number to design variable can be prohibitively large.

3.1.2 SMS Problem Formulation

Size Matching and Scaling (SMS) method uses a heuristic to reduce the multivariable optimization problem to a problem of only two variables. The heuristic is based on the observation that the stress distribution in a MSLS will be similar to the stress distribution in a solid body of the same overall shape. Hence, a solid body is generated that envelopes the part model surfaces and the MSLS and a stress analysis is performed using finite-element analysis. Based on the computed local stress states, unit cells from a predefined unit-cell library are selected and sized to support those stress states. The optimal diameters of these struts are then computed by performing a two-variable minimization. The general problem formulations presented in Table 3-1 and Table 3-2 can be modified to use for SMS method. The modified qualitative problem formulation is presented in Table 3-3. The equivalent mathematical formulation is provided in Table 3-4.

Table 3-3: Qualitative cDSP formulation for the SMS design problem [15]

| | |
|------------------|---|
| Given: | Bounding dimensions and unit-cell distribution within the bounding dimensions, loading and boundary conditions, material properties, unit-cell library configurations |
| Find: | Lattice topology in each unit-cell region, strut diameter values |
| Satisfy: | Upper and lower diameter bounds, target volume and maximum stress constrains |
| Minimize: | Compliance, deviation from target volume |

Table 3-4: Mathematical cDSP formulation for the SMS design problem[15]

| | |
|------------------|---|
| Given: | $p^{BG}, p^F, p^M, p^{UC}, S_{j,k}^L, i, k$ |
| Find: | $D_{i,k} = [S_{i,j}^u \times S_{i,j}^L \times (D_{MAX} - D_{MIN})] + D_{MIN} \quad (a)$ $D_{MIN}, D_{MAX} \quad (b)$ $S_{i,j}^u = \frac{\sum \sigma_n - \sigma_{i,j}^{min}}{\sigma_{i,j}^{max} - \sigma_{i,j}^{min}} \quad (c)$ |
| Satisfy: | $D_{LB} \leq D_{MIN} \leq D_{MAX} \leq D_{UB} \quad (d)$ $\sigma_i \leq \sigma_{max} \quad (e)$ $V \leq V_{max} \quad (f)$ |
| Minimize: | $Z = (W_d \times d)^2 + (W_V \times \frac{V-V_t}{V_t})^2 \quad (g)$ |

In Table 3-4, the symbols $i, j,$ and k represent each unit-cell region in the structure, each unit-cell configuration in the unit-cell library, and the strut number in each of the j configuration in the library respectively; n represents the nodes from the solid-body finite element analysis.

In contrast to the general formulation, SMS method requires additional information besides the starting topology, and the boundary condition. External sources of information include the unit-cell library and the solid-body finite element analysis. Using those information, the determination of the struts diameter, shown in (a) of Table 3-4, is

no longer a multivariable optimization problem. It can be seen that $D_{i,k}$ can be determined using the pre-scaled maximum and minimum diameter value, D_{MAX} and D_{MIN} , a stress scaling factor, $S_{i,j}^u$ and a unit-cell scaling factor, $S_{i,j}^l$. The two scaling factors, $S_{i,j}^u$ and $S_{i,j}^l$, are provided by the unit-cell library and the solid-body stress analysis respectively. Hence, only D_{MAX} and D_{MIN} need to be determined through optimization. The optimization of D_{MAX} and D_{MIN} is done using the minimization function Z , shown in (g) of Table 3-4. The minimization function is formulated in the least-square format to minimize the deflection of the structure, d , and deviation of the structural volume from a target volume, V_t . W_d and W_V represent the weighting variables for d and V .

The optimization process of D_{MAX} and D_{MIN} requires calculation of deflection, volume, and associate stresses using finite element analysis of the truss structure. The finite-element package, which assumes each truss member as a beam element, was developed in MATLAB by Hongqing Vincent Wang in satisfaction of his doctoral dissertation [22]. Once the optimization is done, the diameter of each strut is obtained using equation shown in (a) of Table 3-4. The optimized maximum and minimum diameter of the structure are denoted as D_{max} and D_{min} to differentiate from the pre-scaled maximum and minimum diameter value, D_{MAX} and D_{MIN} . It is important to note that the finite element analysis of the truss structure is conducted using the scaled/true diameters of the structure.

In order to show the flexibility of the SMS method, an alternative problem formulation with a different objective function is also presented. This problem formulation will be applied to design example 2, curved cantilever beam problem. The

diameters will be determined by constrained minimization approach using active-set algorithm. The topology optimization problem for minimizing structural volume can be represented as

Minimize: Volume of the Structure, $V(D_{MIN}, D_{MAX})$

Subject to: $d_{actual} - d_{target} \leq 0$

$$D_{LB} \leq D_{MIN} \leq D_{MAX} \leq D_{UB}$$

where d is the deflection of the structure, and D_{LB} and D_{UB} represent the lower and upper bounds for D_{MIN} and D_{MAX} .

3.2 Augmented SMS Method Overview

The SMS method can be divided into eight discrete tasks that are completed in seven steps. These steps are summarized in Figure 3-1. There is an output, shown, in the shaded box under each step, which is also the input used in the subsequent step. Each step of the SMS method will be outlined in the following format:

- **Detail description of each step:** The process of each step will be discussed in detail.
- **Primary deliverable of the step:** The result of the step will be discussed.
- **Additional information:** This section can include information such as assumption, data storage format, limitation of the step and the key difference versus the previous implementations.

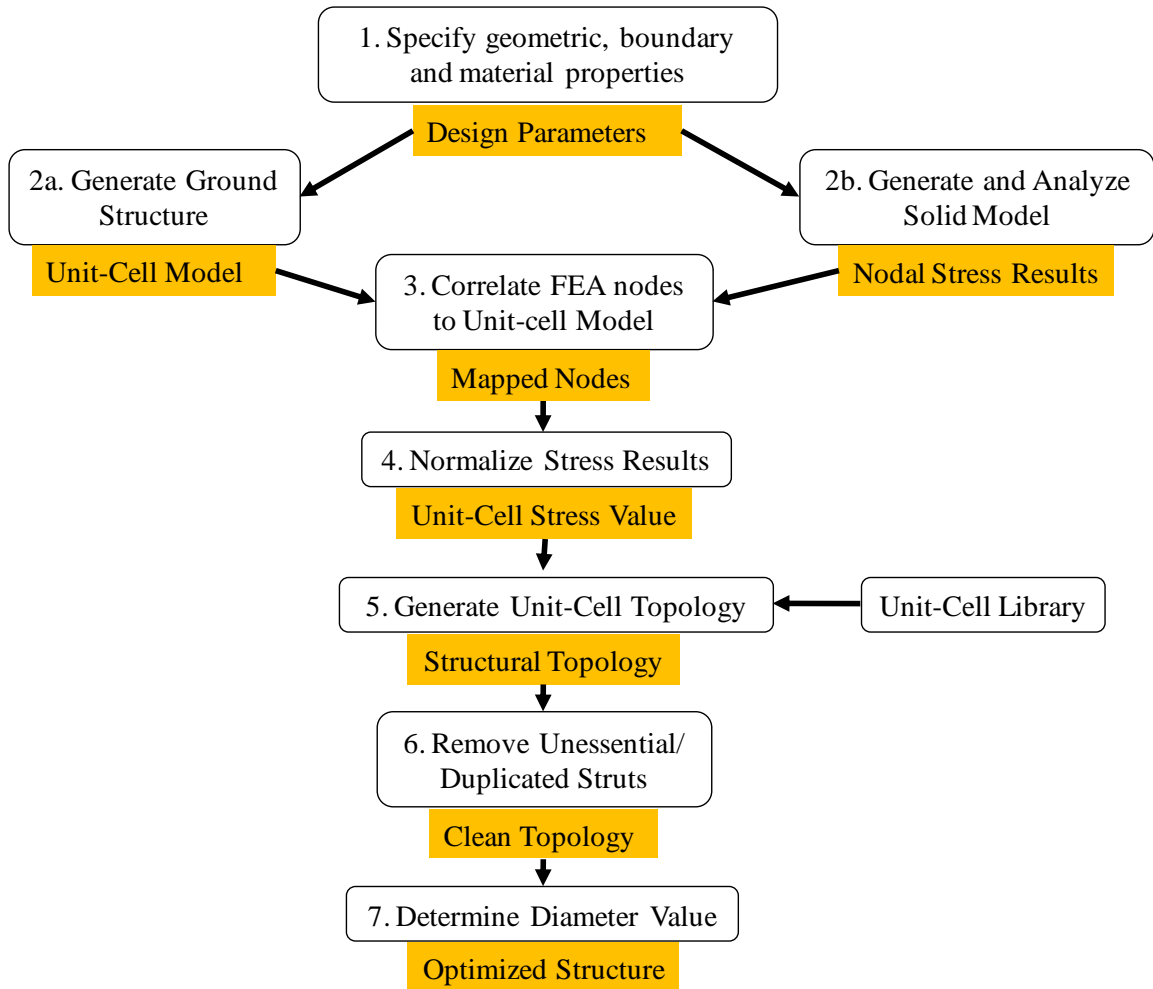


Figure 3-1: Overview of the augmented SMS method

3.2.1 Step 1: Specification of loading, boundary conditions and material properties

3.2.1.1 Method

In this first step of the method, the boundary conditions, material properties, and loading conditions are specified for the target meso-scale lattice structure. These properties will be utilized to perform the stress analysis of both the solid-body representation in step 2b and the truss structure during the optimization process of step 7. These values include the material properties such as Poisson's ratio, Young's modulus of elasticity, and the desired loading and boundary conditions.

3.2.1.2 Primary deliverable

The primary deliverable of this step is a collection of all the loading, boundary conditions, and material properties of the structure. These values will be used in the remaining steps of the design process. That data storage format for the deliverable is a set of constants that can be accessed by any steps of the SMS method.

3.2.1.3 Additional Information

This step of the SMS method aims to characterize the design problem by specifying the analytic properties of the structure. This step can be considered as the "problem definition" task of the method.

3.2.2 Step 2a: Generation of ground structure

In this step of the method, the ground structure of the meso-scale lattice structure is created. The ground structure only specifies the bounding geometry of the truss structure and contains no actual struts or materials. In this implementation of the SMS method, a

free mesh approach is utilized to generate the ground structure that conforms to an arbitrary complex surface. Computer-aided technologies were developed for efficiently generating and representing the lattice structure [54] . The software that embodies this process is integrated into Unigraphics NX. The add-on is called TrussCreator. Given selected part model surfaces, a ground structure can be generated to conform to the shapes of the surfaces. Designers have the ability to set tolerances, lattice structure size parameters, and the number of layers. The dialog boxes for inputting the settings are shown in Figure 3-2. An example of a conformal ground structure is shown in Figure 3-3.

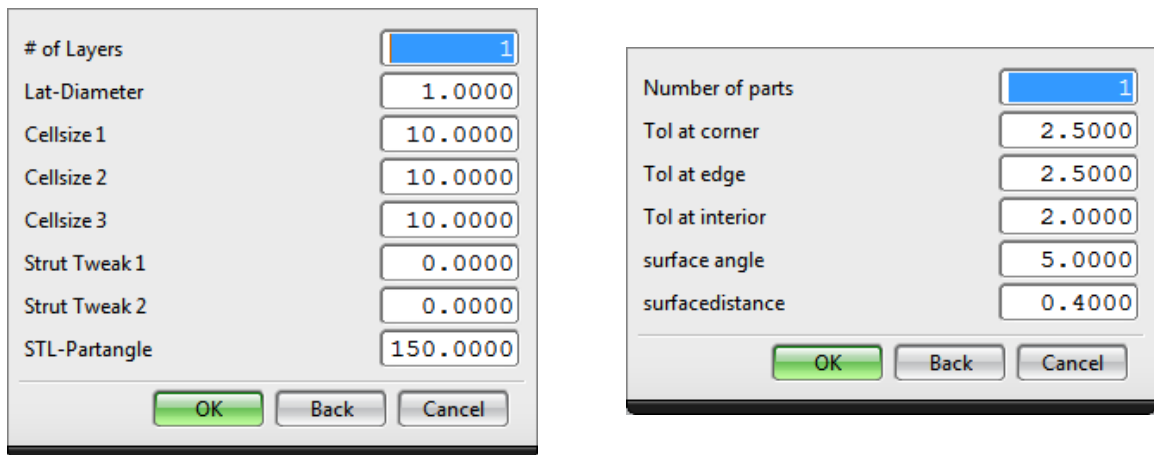


Figure 3-2: Ground structure setting

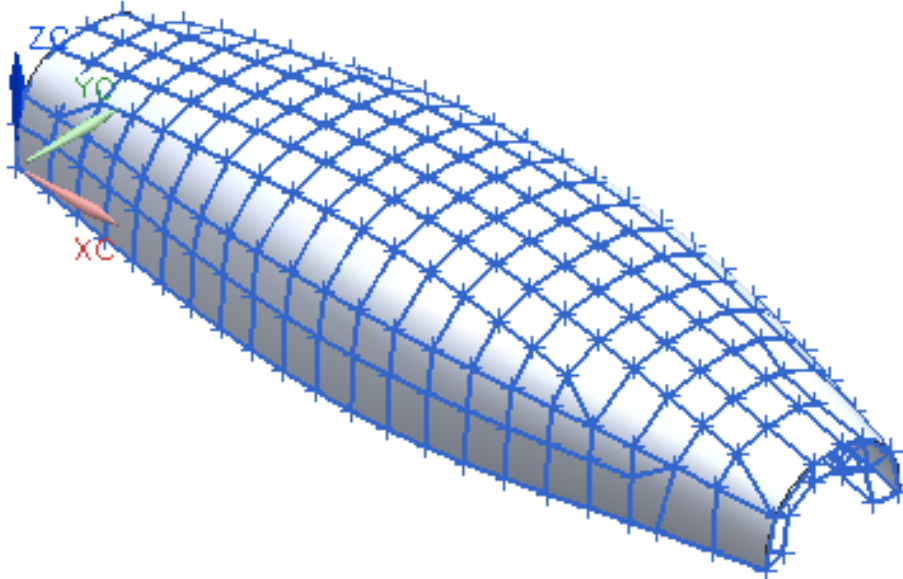


Figure 3-3: Conformal ground structure

3.2.2.1 Primary Deliverable

At the end of this step, a ground structure should be successfully generated to conform to the shape of a given selected part model surface. This includes the set of nodes that make up each unit-cell region in the structure, in particular the nodes number and their Cartesian coordinates. Table 3-5 shows an abbreviated ground structure definition for Figure 3-3.

Table 3-5: Ground structure definition

| Unit cell | Nodes | | | | | | | |
|-----------|-------|-----|-----|-----|-----|-----|-----|-----|
| 1 | 1 | 4 | 3 | 2 | 5 | 8 | 7 | 6 |
| 2 | 17 | 11 | 12 | 18 | 19 | 14 | 15 | 20 |
| 3 | 23 | 21 | 1 | 9 | 24 | 22 | 5 | 10 |
| ... | ... | ... | ... | ... | ... | ... | ... | ... |

| Node | X | Y | Z |
|------|-------|-------|-------|
| 1 | 253.9 | 52.60 | 14.11 |
| 2 | 253.9 | 52.56 | 14.21 |
| 3 | 0 | 52.53 | 14.28 |
| ... | ... | ... | ... |

3.2.2.2 Additional Information

In previous implementations, the SMS method was unable to generate the ground geometry without manual guidance. In addition, the ground structure is required to be divided into uniformly-sized hexahedral regions. Therefore, the previous implementations of the SMS method cannot be used in complex-shaped parts with highly curved or non-rectangular surfaces. By integrating the free mesh approach into the augmented SMS method, the designer will have the ability to design conformal meso-scale lattice structure on any arbitrary complex surfaces. Since the software that embodies that process is integrated into Unigraphics NX 6.5, the generation of ground geometry becomes an autonomous step where the designers have the ability define the size of the unit cell.

3.2.3 Step 2b: Solid Body Finite Element Analysis

3.2.3.1 Method

In this step of the method, a solid body is generated that envelopes the part model surfaces and the meso-scale lattice structure and a stress analysis is performed using finite-element analysis. The loading and boundary condition, and material properties for the structural analysis are specified in step 1 of the method. The purpose of this step is to obtain the stress distribution of the solid-body structure and extrapolate this information to determine the stress distribution and the local stress states in the truss structures. This is based on the observation that the stress distribution in a meso-scale lattice structure will be similar to the stress distribution in a solid body of the same overall shape. Once the analysis is complete, the von Mises stress distribution of the structure is obtained.

The primary deliverable of this step is the general state of stress at each node, which is characterized by six independent normal and shear stress components.

Different metrics can be used to determine the material distribution besides stress distribution such as strain energy and strain distribution. All these metrics have very similar distribution, shown in Figure 3-4.

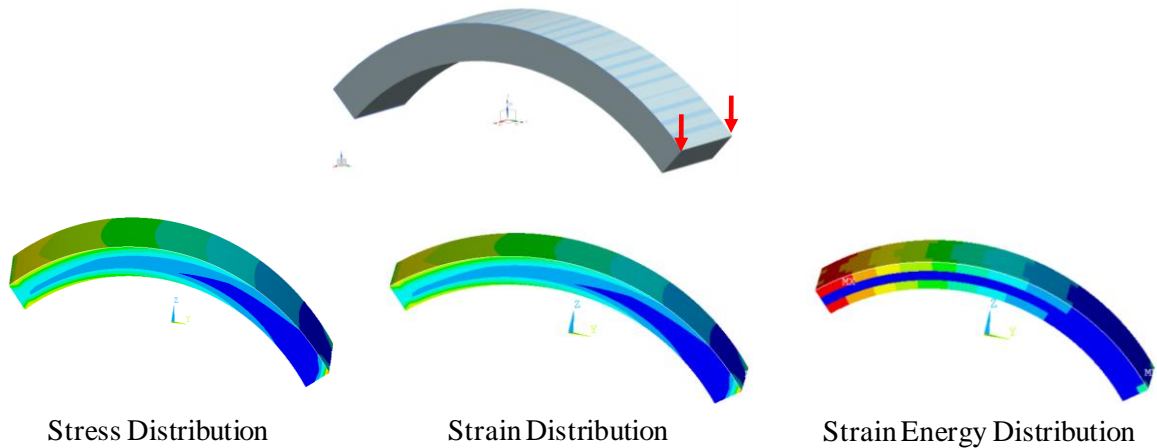


Figure 3-4: Comparison of stress, strain, and strain energy distribution for a 3-D curved cantilever beam

In this method, the stress distribution with six independent normal, shear stress components, σ_{xx} , σ_{yy} , σ_{zz} , τ_{xy} , τ_{xz} , and τ_{yz} , is used to determine the topology of the structure because each configuration in the unit-cell library is optimized for the certain stress direction. Strain energy distribution only has one value per element with no direction; therefore, it cannot be used for this method. On the other hand, strain distribution is node-specific and can be broken into six-directional component; thus it can be used as an alternative for stress distribution.

3.2.3.2 Primary Deliverable

The primary delivery for this step is a list of nodal locations and six independent normal and shear stress components of each node. An example of abbreviated data returned from ANSYS 14 analysis for structure in Figure 3-4 is shown in Table 3-6 and Table 3-7.

Table 3-6: Example of nodal coordinate from solid-body FEA

| NODE | X | Y | Z |
|------|--------------|----------------|----------------|
| 1 | 0.0000000000 | -53.3939955017 | -2.86865689265 |
| 2 | 0.0000000000 | -51.4614475110 | -1.10695933720 |
| 3 | 0.0000000000 | -49.4708096835 | 0.588823977812 |
| 4 | 0.0000000000 | -47.4243290572 | 2.21677884698 |
| 5 | 0.0000000000 | -45.3243157058 | 3.77506762996 |
| 6 | 0.0000000000 | -43.1731401306 | 5.26193132578 |
| 7 | 0.0000000000 | -40.9732305847 | 6.67569155839 |
| 8 | 0.0000000000 | -38.7270703325 | 8.01475247113 |
| 9 | 0.0000000000 | -36.4371948462 | 9.27760252812 |
| 10 | 0.0000000000 | -34.1061889472 | 10.4628162189 |

Table 3-7: Example of stress values from solid-body FEA

| NODE | SX | SY | SZ | SXY | SYZ | SXZ |
|------|--------------|----------|--------------|--------------|--------------|--------------|
| 1 | -0.13150E-02 | -0.17936 | -0.43053E-01 | 0.24556E-01 | -0.11017 | -0.26649E-03 |
| 2 | -0.82954E-02 | -0.14999 | -0.61421E-01 | 0.88933E-02 | -0.82986E-01 | -0.53503E-02 |
| 3 | -0.16578E-03 | -0.13247 | -0.67364E-01 | 0.57652E-02 | -0.80078E-01 | -0.47344E-02 |
| 4 | -0.18313E-03 | -0.12735 | -0.75548E-01 | 0.33320E-02 | -0.81390E-01 | -0.30514E-02 |
| 5 | 0.51678E-03 | -0.12483 | -0.76880E-01 | 0.20072E-02 | -0.81151E-01 | -0.22032E-02 |
| 6 | 0.79946E-03 | -0.12420 | -0.74869E-01 | 0.11452E-02 | -0.79845E-01 | -0.16552E-02 |
| 7 | 0.10089E-02 | -0.12446 | -0.70988E-01 | 0.61122E-03 | -0.77764E-01 | -0.13426E-02 |
| 8 | 0.11223E-02 | -0.12511 | -0.66208E-01 | 0.26413E-03 | -0.75119E-01 | -0.11530E-02 |
| 9 | 0.11829E-02 | -0.12584 | -0.61049E-01 | 0.35437E-04 | -0.72048E-01 | -0.10329E-02 |
| 10 | 0.12074E-02 | -0.12646 | -0.55810E-01 | -0.12058E-03 | -0.68650E-01 | -0.95042E-03 |

3.2.3.3 Additional Information

The analysis of the solid body must meet several criteria.

- The dimension and shape of the solid body must be identical to the ground structure
- The loading, boundary condition and material properties must be identical to those specified in step 1 for the ground structure.
- The number of finite-element nodes must be equal to or greater than the number of unit cells in the ground structure. However, the mesh of the solid model should be such that there are at least several finite-element nodes in each unit cell to better approximate the average stress.

3.2.4 Step 3: Map FEA nodes to Ground Structure

3.2.4.1 Method

In order to use the finite-element analysis result obtained from step 2b, the stress results must be appropriately mapped to the ground structure. The goal of this step is to determine which finite-element nodes correlate to which unit-cell region in the ground structure. Since the free mesh approach is utilized to generate the ground structure, the augmented SMS method is no longer limited to simple and axis-aligned geometry. As the result, the unit cells do not have to be uniformly-sized hexahedra oriented along the global coordinate system. Therefore, a new algorithm must be developed to identify which unit-cell region the finite-element nodes fall into.

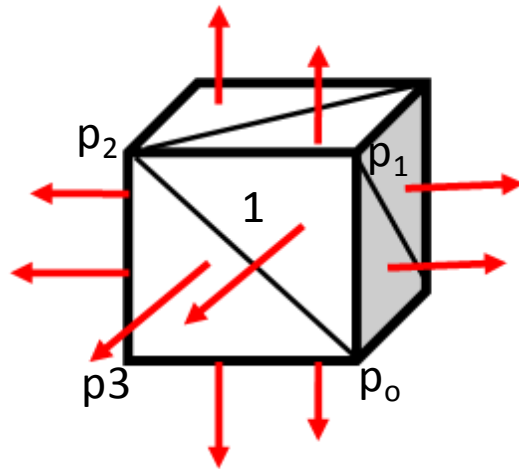


Figure 3-5: Hexahedron with each face dividing into triangles

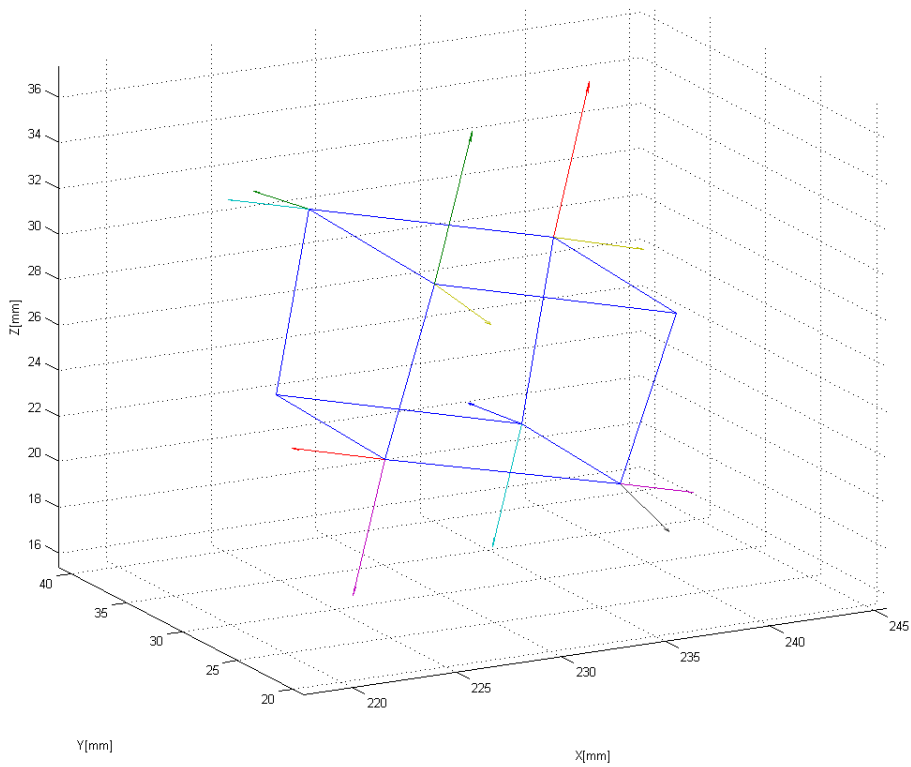


Figure 3-6: Example of unit cell with outward-pointing normals computed and plotted

The process starts by dividing each face of the unit cell into triangles as shown in Figure 3-5 . This step is conducted because triangles are convex and planar. In addition, every polygon can be broken up into a set of triangles. After this step is complete, we need to arrange the vertices of each triangle in a counter-clockwise order. An outward-pointing normal for each triangle can then be obtained by computing the cross-product of two of the edges. For example, the outward-pointing normal for triangle 1 is given by $(p_1 - p_0) \times (p_2 - p_1)$. The right-hand rule for cross-product ensures that this is the outward-pointing normal and not the in-ward pointing normal for triangle 1. An example of a unit cell with outward-pointing normals computed and plotted in MATLAB is shown in Figure 3-6. Once all the outward-pointing normals are obtained for the unit cells, we can determine whether or not a finite-element node falls into the unit cell by computing the dot-products between the outward-pointing normal of each triangles and the vector from a vertex of each triangle to the node. In the case of the hexahedron shown in Figure 3-6, there will be a total of twelve triangles with twelve outward-pointing normals and twelve dot product operations. If and only if all the dot product results are either 0 or less than 0, then the finite-element node belongs to that unit cell. In the case that one of the dot products is equal to 0, then the finite-element node is on the border between multiple unit cells and will be included in each of these respective unit cells.

3.2.4.2 Primary Deliverable

Once the node mapping process is done, each unit cell will contain a list of finite element nodes that will be included in the calculation of the stress distribution in that unit cell.

3.2.4.3 Additional Information

This step is one of the major key differences between the augmented SMS method and its previous implementations. In the previous implementation of the methods, it was fairly simple to determine which unit cell the solid-body nodes fall into because of the simple shape of the part. In the current implementation, a new algorithm is developed to handle the added geometric complexity of the part, which arises from the integration of the free mesh approach into the method.

In the case where a unit cell have non-planar faces, each face of the unit cell can be divided into two triangles in two different ways using two different diagonals. Depending on which diagonal is selected, there is a potential miscorrelation between the finite-element nodes and the unit cell in the ground structure. However, through the investigation of the meshes generated by Truss Creator, it is rare for a mesh element to have non-planar faces. Therefore, the impact of using different diagonals is insignificant.

In this step, it is crucial to have the finite element model to be finely meshed in order to have sufficient number of nodes in each unit cell to better approximate the average stress for each unit cells.

3.2.5 Step 4: Stress Scaling and Normalization

3.2.5.1 Method

This step of the method has 2 sequential operations: averaging and normalization.

The details of each operation are described below.

3.2.5.1.1 *Averaging*

After step 3 is complete, the stress values from the finite-element nodes in each unit cell are then averaged to determine average stress values of six independent normal and shear stress components for each unit cell. The results are six average stress values: σ_{xx} , σ_{yy} , σ_{zz} , τ_{xy} , τ_{xz} , and τ_{yz} . Only the absolute values of the stresses are averaged because only the magnitude and not the direction is important for calculating the stresses in the unit cell.

3.2.5.1.2 *Normalization*

The stress results from finite-element analysis are only relevant for the solid-body structure. The actual numerical values cannot be used for the SMS method because they are not equivalent to those in the truss structure. Instead, the stress distribution throughout the model is more useful than the actual values of the stresses. Therefore, the stresses are normalized from zero to one such that the largest value of stress is equal to one and smallest stress is near zero. These six scaling values correlate to six entries of each configuration in the unit cell and will be utilized to size the struts during the topology generation process in step 5.

In the topology generation, the diameter values of the selected unit-cell configuration from the preconfigured unit-cell library are scaled against the associated stress values (σ_{xx} , σ_{yy} , σ_{zz} , τ_{xy} , τ_{xz} , and τ_{yz}) and then mapped to the unit cells in ground structure. However, since the solid-body results are all provided relative to the global coordinate system and the local coordinate systems of the unit cells in the ground structure can be different from the global coordinate system, stress transformations are needed to ensure correct topology generation. The stress transformation from the global coordinate system

to local coordinate system of a unit cell consists of a change of rectangular coordinate systems made by rigid-body rotation of the axes while keeping the origin fixed. However, since the unit cell is not necessarily a cuboid hexahedron, its orthonormal local coordinate system can be determined using the following approach. As can be seen in Figure 3-7, each unit cell from the ground structure is characterized by 8 nodes in each of the corners, the edges of the unit cell can be used to determine its local coordinate system. Three edges of the unit cell, edge 1-2, edge 1-4, and edge 1-5, which correspond to the x, y, and z axes respectively, are selected as reference edges. For each edge that corresponds to the direction of a certain axis, the angle between that edge and the corresponding reference edge is calculated, e.g. in the x-axis direction, the angle between edge 1-2 and edge 5-6, edge 1-2 and edge 8-7, and edge 1-2 and edge 4-3 is calculated by performing a dot product operation. The resultant angles that correspond to a certain direction e.g. x-axis direction, are then averaged. This step is repeated for the other two directions. The reference edge with the lowest averaged angle is selected as the starting axis for that particular direction. The reference edge with the second lowest averaged angle is selected as a second axis. However, these two axes are not necessarily orthogonal. Therefore, a cross product is performed between the first and second axes to find the third orthonormal axis. Then another cross product operation between the third and first axes gives the second orthonormal axis. This approach allows us to determine the local orthonormal coordinate system of a unit cell from the ground structure.

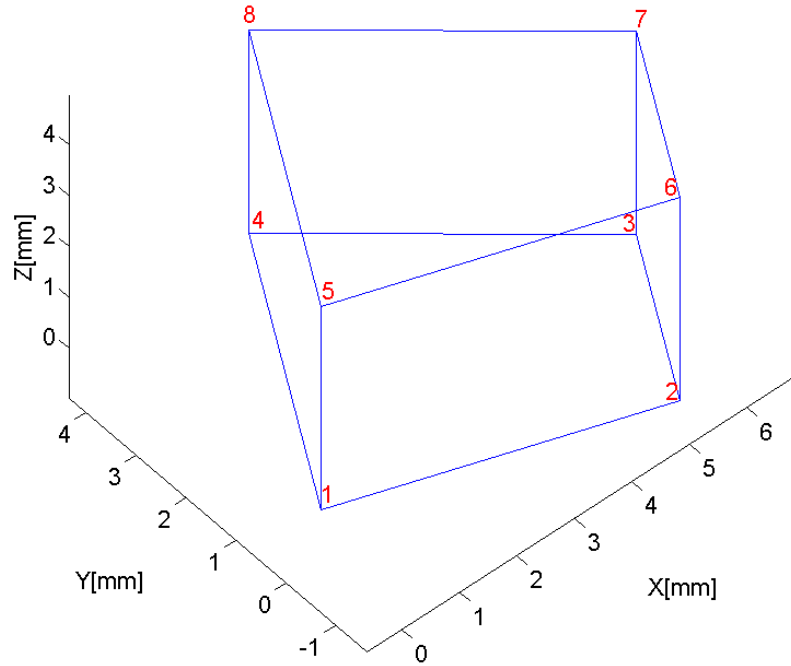


Figure 3-7: Unit-cell region

After obtaining the local orthonormal coordinate system for the unit cell, the relative orientation between the local and global coordinate system can be determined. The global coordinate system, xyz , and local coordinate system, $x'y'z'$, are shown in Figure 3-8, where α_1 is the angle between the x' and x axes, β_1 is the angle between x' and y axes, θ_1 is the angle between x' and z axes, α_2 (not shown) is the angle between the y' and x axes, and so forth.

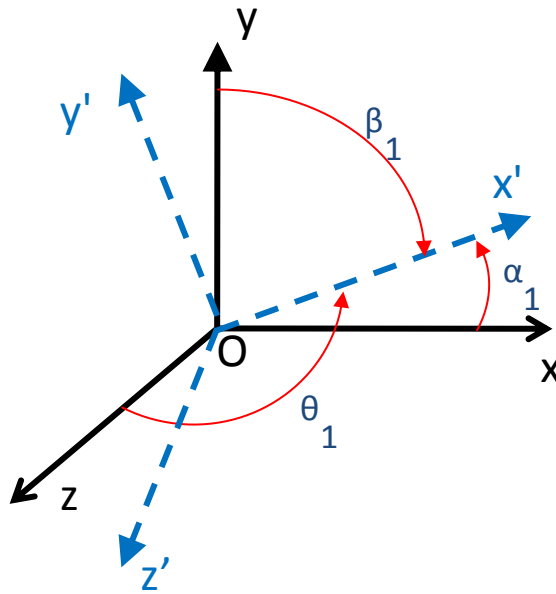


Figure 3-8: Rotation of coordinate system (x', y', z')

Let R be the rotation matrix that transforms the vector components in the original coordinate system to those in the primed system, then

$$\begin{Bmatrix} x' \\ y' \\ z' \end{Bmatrix} = \begin{bmatrix} R_{11} & R_{12} & R_{13} \\ R_{21} & R_{22} & R_{23} \\ R_{31} & R_{32} & R_{33} \end{bmatrix} \begin{Bmatrix} x \\ y \\ z \end{Bmatrix} \quad (3-2)$$

From Equation 3-2, it can be seen that the unit vector x' can be expressed in the original coordinate system as

$$x' = R_{11}x + R_{12}y + R_{13}z \quad (3-3)$$

When $x, y, z, x', y',$ and z' are unit vectors, R_{11} can be expressed by Equation 3-4 using the definition of the dot product.

$$R_{11} = |x'|/|x| \cos(\alpha_1) = (1)(1) \cos(\alpha_1) = \cos(\alpha_1) \quad (3-4)$$

Therefore, x' can be expressed in term of x , y and z using Equation 3-5.

$$x' = \cos(\alpha_1) x + \cos(\beta_1) y + \cos(\theta_1) z \quad (3-5)$$

Similarly, axes y' and z' can be expressed in term of x , y , and z using Equation 3-6 and Equation 3-7.

$$y' = \cos(\alpha_2) x + \cos(\beta_2) y + \cos(\theta_2) z \quad (3-6)$$

$$z' = \cos(\alpha_3) x + \cos(\beta_3) y + \cos(\theta_3) z \quad (3-7)$$

In matrix form, the coordinate transformation is shown in Equation 3-8.

$$\begin{Bmatrix} x' \\ y' \\ z' \end{Bmatrix} = \begin{bmatrix} \cos(\alpha_1) & \cos(\beta_1) & \cos(\theta_1) \\ \cos(\alpha_2) & \cos(\beta_2) & \cos(\theta_2) \\ \cos(\alpha_3) & \cos(\beta_3) & \cos(\theta_3) \end{bmatrix} \begin{Bmatrix} x \\ y \\ z \end{Bmatrix} \quad (3-8)$$

The stress state at a point P is characterized by six independent normal and shear stress components, as shown in Figure 3-9. These components can be organized into a matrix:

$$\begin{bmatrix} \sigma_{xx} & \tau_{xy} & \tau_{xz} \\ \tau_{yx} & \sigma_{yy} & \tau_{yz} \\ \tau_{zx} & \tau_{zy} & \sigma_{zz} \end{bmatrix} \quad (3-9)$$

The grouping of these stress components becomes the components of a second-order stress tensor. This stress tensor is defined in the deformed state of the material and is known as the Cauchy stress tensor [55].

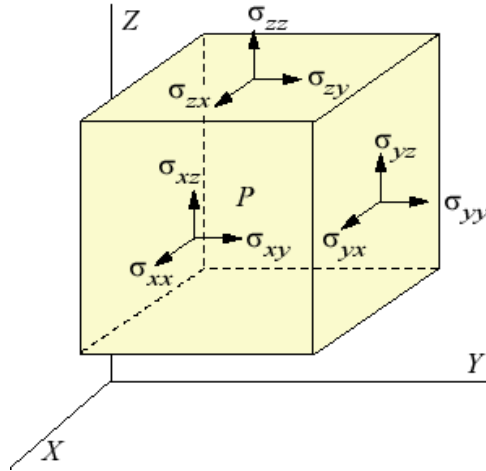


Figure 3-9: General state of stress [55]

With the rotation matrix given in Equation 3-8, the Cauchy stress tensor in the local coordinate system (x', y', z') can be obtained using Equation 3-10.

$$[\sigma'] = R[\sigma]R^T \quad (3-10)$$

where R is the rotation matrix calculated in Equation 3-8, R^T is its transpose, σ is the Cauchy stress tensor in global coordinate system (x, y, z) , and σ' is the Cauchy stress tensor in the local coordinate system (x', y', z') . This follows the rule of changing second-order tensor components under rotation of axes [55].

A few design examples are tested to validate that the stress transformation works properly to generate the correct topology.

3.2.5.1.2.1 Example 1

Example 1 is a 3-D parallelogram with the loading conditions as shown in Figure 3-10. The average stresses in the global coordinate system are $\sigma_{xx} = 0.1245$ MPa, $\sigma_{yy} = -0.3283$ MPa, $\sigma_{zz} = 0.0593$ MPa, $\tau_{xy} = 0.0494$ MPa, $\tau_{xz} = 0.0207$ MPa, and $\tau_{yz} = 0.0231$ MPa. The local coordinate system of the unit cell is the same as the global coordinate

system; therefore, the average stress in the local coordinate system is the same as in the global coordinate system. The resultant topology, which the thickest struts are in the Y-direction, matches the intuitive expectation as shown in Figure 3-11 and Figure 3-12.

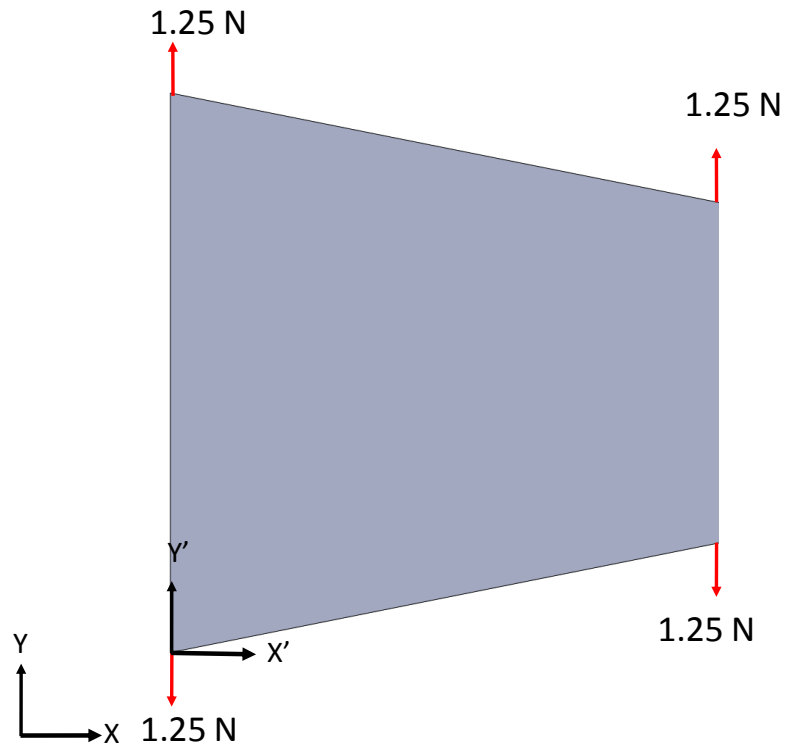


Figure 3-10: Example 1-Parallelogram

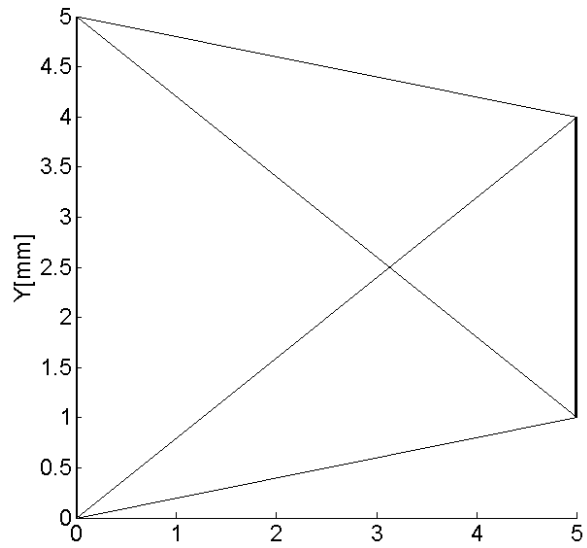


Figure 3-11: XY-view of the topology for the 3-D parallelogram

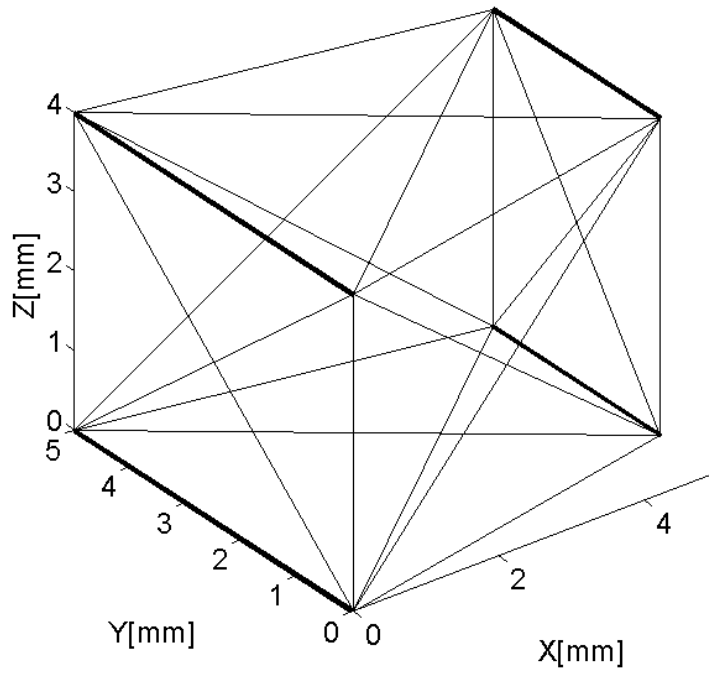


Figure 3-12: Isometric view of the topology for the 3-D parallelogram

3.2.5.1.2.2 Example 2

Example 2 is the same 3-D parallelogram but rotated by -30° around the Z-axis. The physical representation of the problem is shown in Figure 3-13.

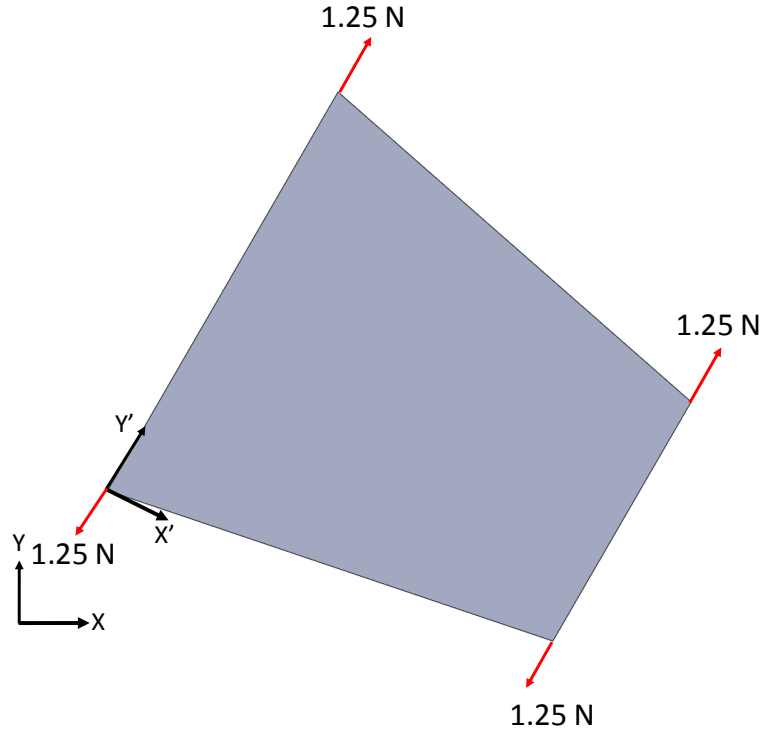


Figure 3-13: Example 2- rotated parallelogram

The average stresses in the global coordinate system are $\sigma_{xx} = 0.1439$ MPa, $\sigma_{yy} = -0.2547$ MPa, $\sigma_{zz} = 0.0593$ MPa, $\tau_{xy} = 0.1562$ MPa, $\tau_{xz} = 0.0198$ MPa, and $\tau_{yz} = 0.0214$ MPa. The average stresses in the local coordinate system are $\sigma_{x'x'} = 0.1245$ MPa, $\sigma_{y'y'} = -0.3283$ MPa, $\sigma_{z'z'} = 0.0593$ MPa, $\tau_{x'y'} = 0.0494$ MPa, $\tau_{x'z'} = 0.0214$ MPa, and $\tau_{y'z'} = 0.0198$ MPa. The resultant topology, which has the thickest struts Y'-direction of the unit-cell local coordinate system, matches the intuitive expectation as shown in Figure 3-14 and Figure 3-15. The average local stress in example 2 matches closely with the average local stress from example 1.

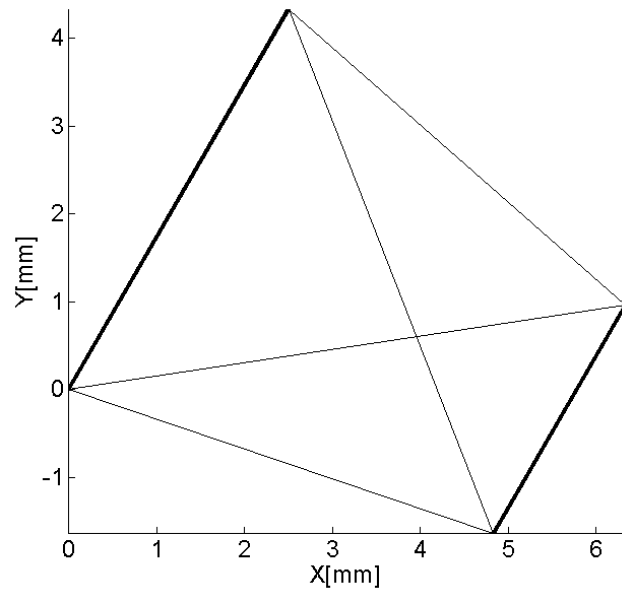


Figure 3-14: XY-view of the topology for the rotated 3-D parallelogram

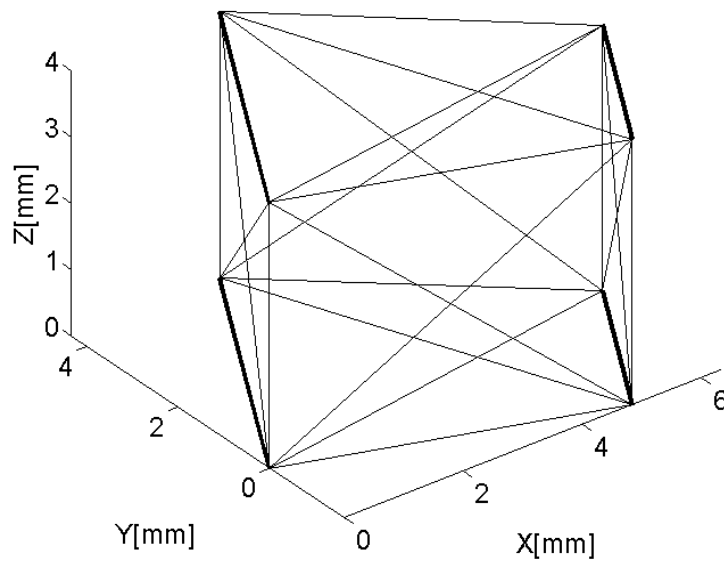


Figure 3-15: Isometric view of the topology for the rotated 3-D parallelogram

3.2.5.1.2.3 Example 3

Example 3 is a deformed 3-D parallelogram but rotated by -30° around the Z-axis.

The physical representation of the problem is shown in Figure 3-16.

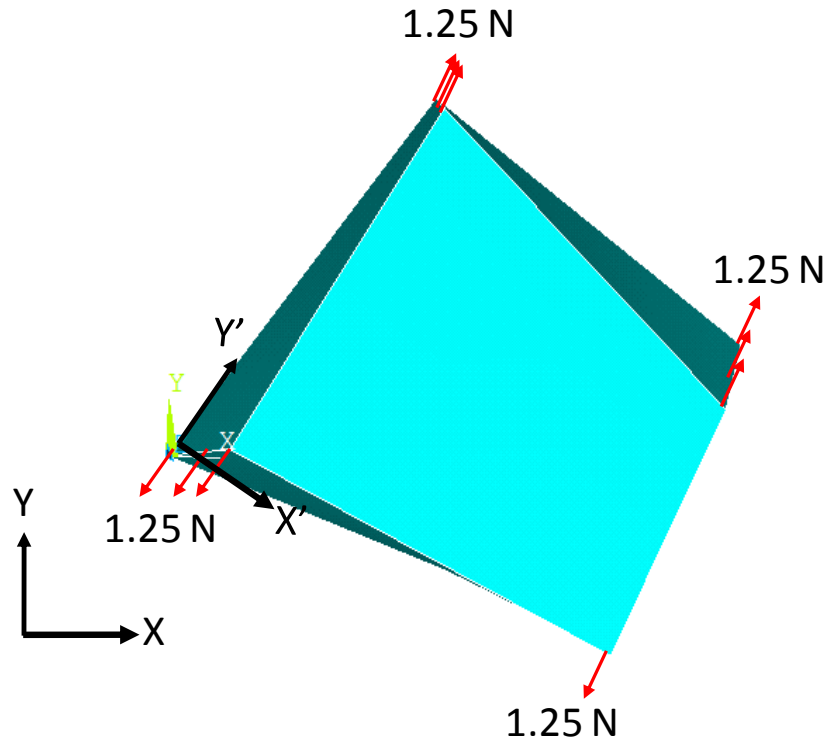


Figure 3-16: Example 3- deformed and rotated parallelogram

The average stresses in the global coordinate system are $\sigma_{xx} = 0.1194$ MPa, $\sigma_{yy} = 0.1699$ MPa, $\sigma_{zz} = 0.0428$ MPa, $\tau_{xy} = 0.1074$ MPa, $\tau_{xz} = 0.0176$ MPa, and $\tau_{yz} = 0.0158$ MPa. The average stresses in the local coordinate system are $\sigma_{x'x'} = 0.1020$ MPa, $\sigma_{y'y'} = 0.2185$ MPa, $\sigma_{z'z'} = 0.0422$ MPa, $\tau_{x'y'} = 0.0457$ MPa, $\tau_{x'z'} = 0.0158$ MPa, and $\tau_{y'z'} = 0.0176$ MPa. The resultant topology, where the thickest struts are in the Y' -direction, matches the intuitive expectation as shown in Figure 3-17 and Figure 3-18.

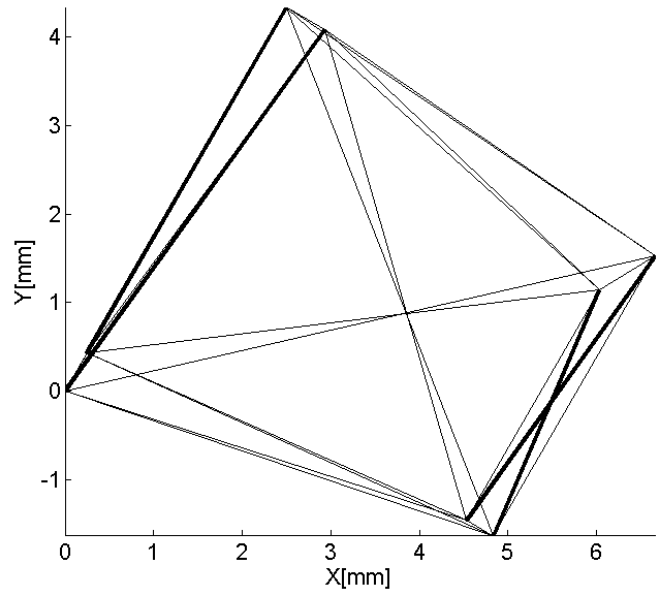


Figure 3-17: XY-view of the topology for the rotated and deformed 3-D parallelogram

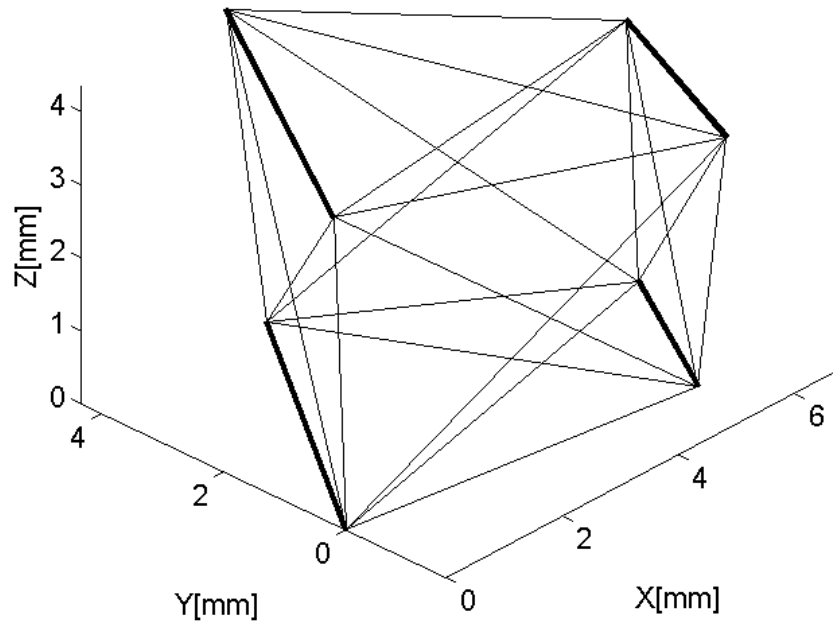


Figure 3-18: Isometric view of the topology for the rotated and deformed 3-D parallelogram

3.2.5.2 Additional Information

Since the previous implementations of the SMS method did not have the capability to generate the ground structure for the complex-shaped parts, the method was limited to simple and axis-aligned geometry. There was no need to consider stress transformation. It could not be applied for structures that require the unit cells to have local coordinate systems that are not the same as the global coordinate system. The augmented SMS method integrates the free mesh approach to generate the ground geometry. As a result, the method can be applied to complex-shaped part and requires stress transformation from the global coordinate system to the local coordinate system of the unit cell to ensure correct topology generation using the predefined unit-cell library.

One key assumption in this step is that the average stress is a good approximation for the stress distribution in the structure. It is important to ensure that there is small stress variation within a unit cell for the assumption to be valid. This assumption allows us to ignore the geometric skewness of the unit cell in the ground structure during the stress transformation and only consider the rigid-body rotation. The assumption is also used to formulate the unit-cell library.

3.2.6 Step 5: Topology Generation

3.2.6.1 Method

Once the six normalized stresses are determined for each unit cell, the unit-cell library is used to map different configurations to each unit cell in the ground structure. Each unit cell in the ground structure will be mapped with one of the seven configurations from the unit-cell library. The mapping and selection process will be described in details in Section 3.3.

3.2.6.2 Primary Deliverable

After this step is complete, the structure will have a topology designed for the anticipated stress distribution in the truss structure. The struts diameters are valued between zero and one with one being the thickest and zero being the thinnest; thus, the relative thickness of one strut to another is known. However, these normalized diameters must be correlated with actual strut diameter values in step 7 of the method.

3.2.6.3 Additional Information

In order to generate correct topology for the ground structure, the stresses must be correctly transformed from the global to local coordinate system in step 4. This ensures that the optimized unit-cell configurations from the unit-cell library are correctly oriented under the expected loading condition.

3.2.7 Step 6: Unessential and Duplicated Struts Removal

3.2.7.1 Method

Since the unit cells are populated individually, there will be instances of overlapping struts between adjacent unit cells. These struts will have identical start and end nodes. To resolve this ambiguity, the largest diameter strut is kept and all other smaller struts are removed. Duplicated nodes are also removed.

For simple design problems, struts that have little contribution to the structural performance are also removed. A parameter, called cutoff diameter, is utilized in this process, where D_{cutoff} is a value between D_{min} and D_{max} . All the struts that are smaller than D_{cutoff} are removed from the structure to reduce the overall volume of the structure.

$$D_{cutoff} = c \times (D_{max} - D_{min}) + D_{min} \quad (3-11)$$

where c is the cutoff percentage, which was set at 2.5% , or 0.025 in previous implementation. This method of removing essential struts works well for simple design such as cantilever beam, but is not effective for complex structure. Therefore, it will only be used for the first design example of a 3-D cantilever beam.

3.2.7.2 Primary deliverable

After this step, a clean topology is generated with all the duplicated struts removed. This ensures accurate calculation of volume and deflection of strut structure in the next step of the method.

3.2.8 Step 7: Diameter Sizing

3.2.8.1 Method

The strut diameters are normalized from zero to one in step 5 of the method. This provides the diameter values relative to each other in the structure. However, these normalized diameter values must be replaced with the actual diameter values to satisfy the loading and volume condition. It can be seen from the problem formulation for the SMS method shown in Table 3-4, the only parameters missing to determine the diameter of each strut are the D_{MIN} and D_{MAX} , where D_{MAX} and D_{MIN} correspond to pres-scaled thickest and thinnest diameters, respectively. After D_{MIN} and D_{MAX} are calculated, the diameters of each strut can be determined using Equation 3-12 below:

$$D_{i,k} = [S_{i,j}^u \times S_{i,j}^L \times (D_{MAX} - D_{MIN})] + D_{MIN} \quad (3-12)$$

where $D_{i,k}$ is the diameter value of the k^{th} strut in the i^{th} unit cell, $S_{i,j}^u$ is the scaling factor associated with the unit-cell library, $S_{i,j}^L$ is the scaling factor found in step 4 of the method. The thickest and thinnest diameters of the structure are denoted as D_{max} and D_{min} .

3.2.8.1.1 Two-variable Approach to Determine D_{MIN} and D_{MAX}

In two-variable approach, values D_{MIN} and D_{MAX} are determined by performing two-variable minimization of the objective function (g) from the problem formulation in Table 3-4. It is rewritten below as a function of both D_{MIN} and D_{MAX} .

$$Z(D_{MIN}, D_{MAX}) = (W_d \times d(D_{MIN}, D_{MAX}))^2 + \left(W_V \times \frac{V(D_{MIN}, D_{MAX}) - V_t}{V_t} \right)^2 \quad (3-13)$$

where $V(D_{MIN}, D_{MAX})$, volume and $d(D_{MIN}, D_{MAX})$, deformation are functions of only D_{MIN} and D_{MAX} . Deformation, d , does not correlate to any metric, but instead represents any unit of measure that is directly proportional to structural stiffness, such as tip deflection or strain energy.

The target structure must attempt to minimize both volume and deflection. However, these two goals have competing effects. The volume constraint will drive the strut diameter down while compliance constraint will drive them up. The target deflection is always set to zero. Two algorithms used to perform this two-variable minimization are Levenberg-Marquardt algorithm and active-set algorithm. Levenberg-Marquardt algorithm has documented success in design and optimization of meso-scale lattice structure [14]; while active-set algorithm is documented to have success in optimization of multivariable, nonlinear and constrained optimization problem. These algorithms were discussed in details in chapter 2.

3.2.8.1.2 One-variable Approach to Determine D_{MIN} and D_{MAX}

Graf noted in his research that for a particular truss structure there is an ideal relationship between D_{MIN} and D_{MAX} such that when the ratio is approximately equal to 28% for a specific target volume, the structure would have the least deflection [16]. This finding has significant effect because it would reduce the two-variable equation involving D_{MIN} and D_{MAX} to a one-variable equation. D_{MIN} can be expressed as a function of D_{MAX} :

$$D_{MIN} = 0.28 \times D_{MAX} \quad (3-14)$$

Combining Equation 3-6 and Equation 3-7, the equation to determine the diameter of each strut becomes:

$$D_{i,k} = [0.72(S_{i,j}^u \times S_{i,j}^L) + 0.28] \times D_{MAX} \quad (3-15)$$

Similar to the two-variable approach, the truss structure attempts to minimize the objective function (g) from the problem formulation in Table 3-4. However, the objective function in this case is only a function of one variable. Thus it would reduce the complexity of the optimization problem and potentially design time. The MATLAB function, *fminbnd*, will be used to find the minimum of single-variable function on fixed interval. Its algorithm is based on golden search and parabolic interpolation [56]. In this research, both one-variable and two-variable approaches will be used. The results will be compared in terms of the deformation and design time.

3.2.8.2 Primary Deliverable

This is the final step of the SMS method. After this step is complete, the final meso-scale lattice structure with optimized diameters is generated.

3.2.8.3 Additional Information

The key assumption in this step is that the struts are cylinders; therefore, the only optimization parameter is diameter value. In addition, the finite-element analysis assumes each strut as a beam element experiencing axial and bending effects.

3.3 Comparison Between the Augmented SMS Method and Its Previous Implementations

Major changes between the augmented SMS method and its previous implementations are summarized below:

- The integration of free mesh approach in generating ground structure is a major addition to the SMS method. This allows the method to design and optimize meso-scale truss structure conforming to any arbitrary complex surfaces. The software that embodies this ground structure generation process was also integrated into a commercial CAD system to give designers the ability to easily set lattices structure size parameters through graphical user interface.
- Several steps of method required modifications in order to utilize this new capability. A new algorithm was developed for the third step of the method, which correlates the finite-element nodes to the unit cells in the ground structure. This step is very crucial to the overall success of the method because it allows the method to correctly calculate the stress distribution within the truss structure. Another key modification is the addition of stress transformation from the global coordinate system to the local coordinate systems of the unit cells in the ground structure. This allows the method to correctly generate the topology for the truss structure.

3.4 Unit-Cell Library

In the previous implementation of the SMS method, Chang developed a unit-cell library to generate the topology for the truss structure [15]. There are seven different unit-cell configurations in the library. Each configuration has six entries with each specialized for six independent normal, shear stress components. This library will be used in this augmented method for generation of lattice topology. The following sections outline the library, the optimization, mapping, and selection process for the entries in the library.

3.4.1 The Optimization Process

3.4.1.1 Problem Formulation

The problem formulation utilized for the optimization of unit cells is shown in Table 3-8.

Table 3-8: Qualitative cDSP formulation for the optimization of unit cells [15]

| | |
|------------------|--|
| Given: | Loading and Fixity Conditions, Starting Lattice Topology |
| Find: | Truss Diameters/Lattice Topology |
| Satisfy: | Target Strain Energy Maximum Stress Value |
| Minimize: | Volume |

For unit-cell optimization, the objective is to minimize the volume of the unit cell. The stiffness is set as a constraint to force the performance of all the optimized unit-cells to be equal. Strain energy ΔU , is the metric to measure stiffness, which is calculated as:

$$\Delta U = \frac{\Delta F}{2} d \quad (3-16)$$

where $\frac{\Delta F}{2}$ is the average magnitude of the load and d is the total displacement of the structure. Strain energy is widely used in topological optimization problem.

3.4.1.2 Process Overview

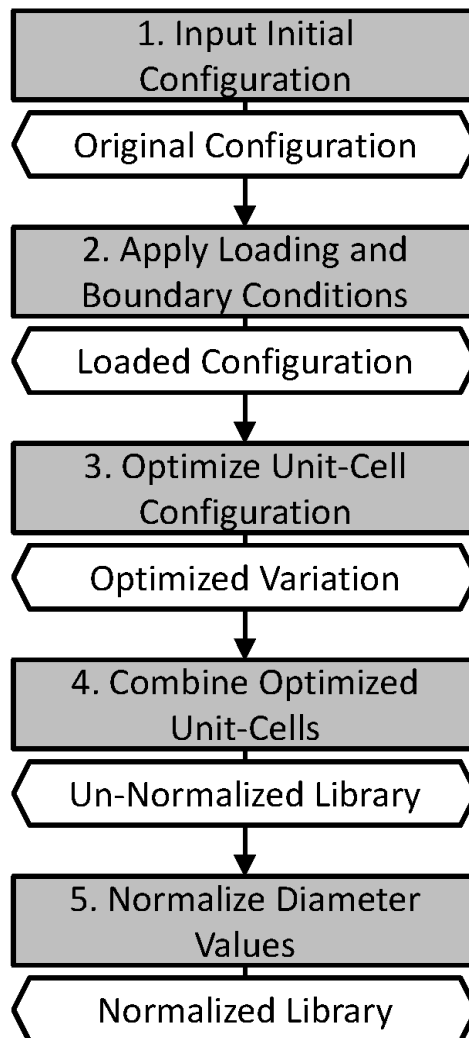


Figure 3-19: Overview of unit cell optimization process [15]

The optimization process for the unit cell is divided into five separate steps. The overview of the process is shown in Figure 3-19.

3.4.1.2.1 Step 1: Insert Initial Unit-Cell Configuration

Each unit cell is defined in a cuboid region by 8 nodes in each of the corner. A diameter value of “1” is assigned to all the struts in the unit cell.

3.4.1.2.2 Step 2: Apply Loading Conditions

In this step, the unit cell is loaded with six loading conditions, each for a component of the stress state. The loading conditions are shown in Figure 3-19.

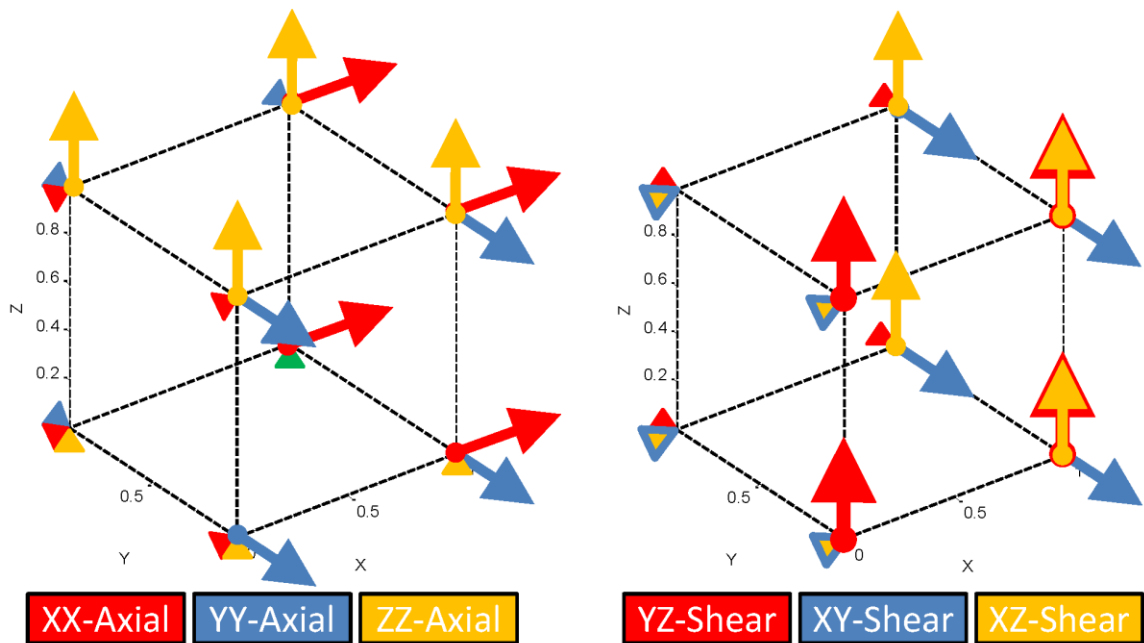


Figure 3-20: Loading conditions for unit-cell optimization [15]

These loading conditions must be applied in multiple directions. For instance, there are 4 shear directions in the XY plane including τ_{xy} , $-\tau_{xy}$, τ_{yx} , $-\tau_{yx}$. The unit-cell must be optimized individually for each direction and then combined to form the final optimized unit-cell.

3.4.1.2.3 *Step 3: Optimize Unit Cell*

After defining the base-lattice structure and the loading condition, the unit-cell was optimized using the parameters in Table 3-9. The analysis and optimization was done in ANSYS 13.0

Table 3-9: Optimization parameter for unit-cell optimization in ANSYS

| | |
|--------------------------------------|--------|
| Strain Energy Constraints (mJ) | 50 |
| Poisson Ratio | 0.3 |
| Elastic Modulus (N/cm ²) | 1960 |
| Loading Magnitude (N) | 10 |
| Element Type | BEAM 4 |

3.4.1.2.4 *Step 4: Combine Optimized Unit-Cells*

Since the loading conditions are applied in multiple directions, the results from each direction must be combined to form an optimized unit cell. The process is illustrated in Figure 3-21 for shear stress in the XY plane. When combining the results, the largest diameter for each strut is kept and all other instances are deleted.

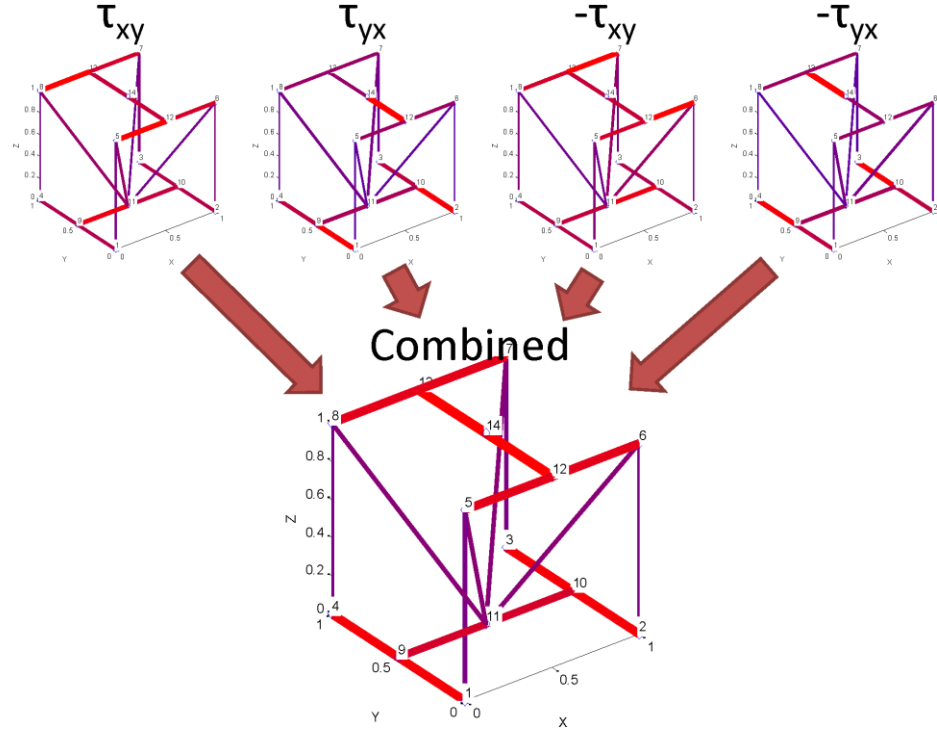


Figure 3-21: Combination of optimized unit-cells for shear stress in XY plane for Cantley configuration [15]

3.4.1.2.5 Step 5: Normalize Unit-Cells

After all the configurations are optimized, the diameters of the unit cell are normalized from 0 to 1:

$$D_{j,k,l}^{norm} = D_{j,k,l} / D_l^{max} \quad (3-17)$$

where j represents each strut for each k^{th} configurations for each of l stress directions. k goes from one to seven because there are seven configuration. l goes from one to six because there are six stress directions, σ_{xx} , σ_{yy} , σ_{zz} , τ_{xy} , τ_{xz} , and τ_{yz} . Hence, D_l^{max} represents the largest diameter value among the six stress directions. $D_{j,k,l}^{norm}$ becomes the unit-cell library scaling factor that is used in the diameter determination step.

After the normalization process is complete, the unit-cell library is stored in a list with three key parameters: the nodal coordinates, the elements, and the diameters of each element. The complete unit-cell library is shown in Figure 3-22.

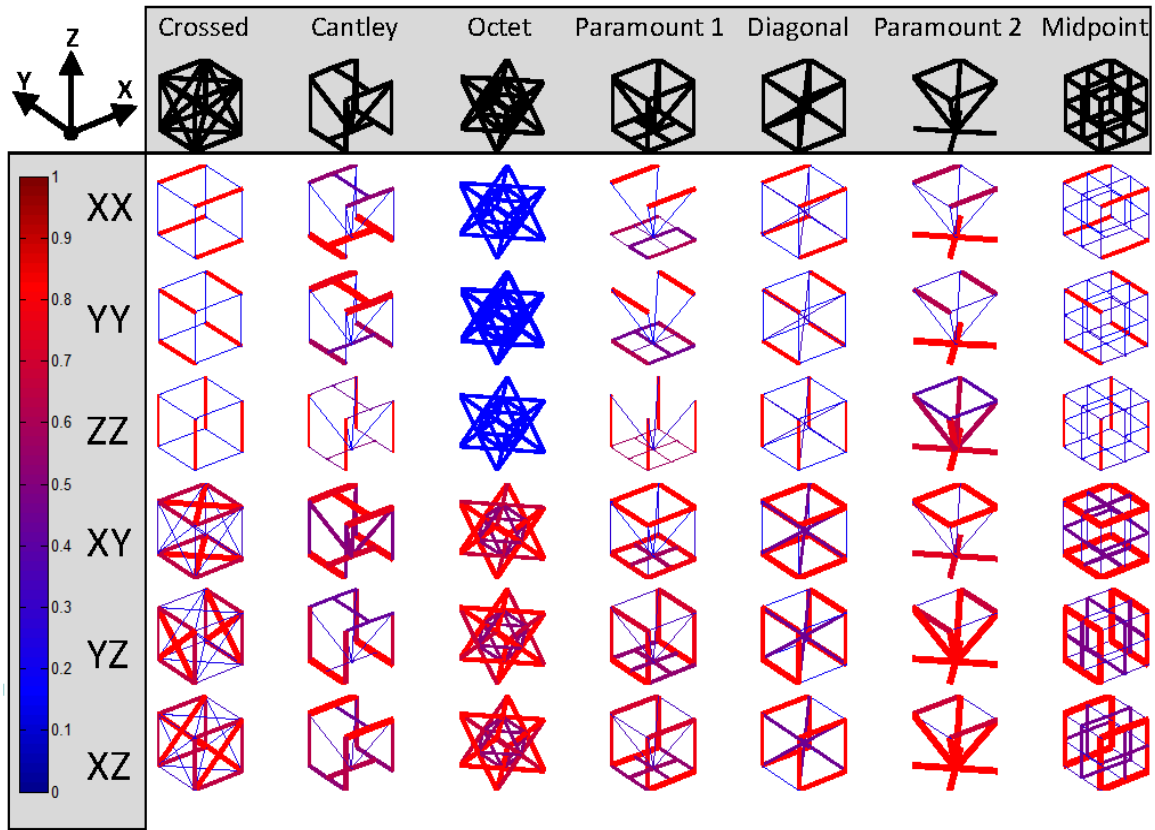


Figure 3-22: Unit-cell library [15]

3.4.2 Unit-Cell Selection

One way to generate the best topology for the structure is to iteratively populate each unit cell in the ground structure with a configuration from the library and analyze the performance of the structure. However, it is computationally infeasible because there are M^N number of possible combinations of topology where M is the number of configurations in the unit-cell library and N is the number of unit cells in the ground structure. For instance, a ground structure with 5 unit cells would already have

$7^5 = 16807$ unique topologies. Therefore, a heuristic was developed for the selection process.

Since all the configurations of the unit-cell library are optimized such that they have identical performance, the structure with the smallest normalized volume is selected. The selection is performed using the Equation 3-18 [15]. This selection process is performed for each unit cell from the ground structure and the configuration with the lowest rating, r , is selected for that unit cell.

$$r = W_v \times \left(\sum V_\sigma \right) + W_{vn} \times (V_{net}) + W_p \times \left(\sum P \right) \quad (3-18)$$

where

$$\sum V_\sigma = V_{xx} + V_{yy} + V_{zz} + V_{xy} + V_{xz} + V_{yz} \quad (3-19)$$

$$\sum P = P_{xx} + P_{yy} + P_{zz} + P_{xy} + P_{xz} + P_{yz} \quad (3-20)$$

For each topology configuration, the volume of each entry in six primary stress directions (σ_{xx} , σ_{yy} , σ_{zz} , τ_{xy} , τ_{xz} , and τ_{yz}) is multiplied by the corresponding normalized stress results from step 4 of the SMS method and then summed to determine $\sum V_\sigma$ as shown in Equation 3-19. For each topology configuration, V_{net} is the net volume of each configuration calculated by combining all six entries in six stress direction and removing the overlapping struts. $\sum P$ for each topology configuration is determined, as shown in Equation 3-20, using a performance table. These values are provided in Table 3-10. They are determined using results from a design example [15]. In this example, a $15 \text{ cm} \times 15 \text{ cm} \times 15 \text{ cm}$ cube is divided into $3 \times 3 \times 3$ of the same unit-cell configuration. The same loading and boundary condition, shown in Figure 3-20, is applied to the cube. There are six loading condition approximating the six axial and shear stresses. Each of these

loading conditions will be applied to all seven configurations in the library; therefore, there will be 42 unique topologies. The strain energy from each topology is calculated. The results are normalized between 0 and 1 and plugged in the performance table to calculate $\sum P$. In addition, there are three weighting values W_v , W_{vn} , and W_p , which can be set manually to vary the importance of each contributing factors to generate different topologies. The configuration with the lowest rating is selected and mapped to that particular unit cell in the ground structure.

Table 3-10: Performance table used for selection of unit-cell configuration [15]

| | XX Axial | YY Axial | ZZ Axial | XY Axial | YZ Axial | XZ Axial |
|------------|----------|----------|----------|----------|----------|----------|
| Crossed | 0.0745 | 0.0693 | 0.0375 | 0.0810 | 0.0747 | 0.0752 |
| Cantley | 0.5399 | 0.4885 | 0.0539 | 0.5418 | 0.5353 | 0.2626 |
| Octet | 0.2281 | 0.2023 | 0.1050 | 0.1004 | 0.0891 | 0.0863 |
| Paramount1 | 0.0197 | 0.0907 | 0.0500 | 0.9865 | 0.3904 | 0.3734 |
| Diagonal | 0.0743 | 0.0704 | 0.0390 | 0.1166 | 0.0881 | 0.0956 |
| Paramount2 | 1.0000 | 1.0000 | 1.0000 | 0.6043 | 0.5569 | 0.5462 |
| Midpoint | 0.1058 | 0.0955 | 0.0507 | 1.0000 | 1.0000 | 1.0000 |

3.4.3 Mapping

Once the best possible configuration is determined for a unit cell in the ground structure, it is mapped to that region. If there is a node from unit-cell configuration that does not exist in the unit cell of the ground structure, it will be added using 3-D linear interpolation. After all the missing nodes are added, the unit-cell configuration can then be populated into the unit cell. The normalized stress values from step 4 of the augmented SMS method are scaled against the normalized diameter values from the unit cell library to determine the relative thickness of one strut to another.

3.5 Summary

In this chapter, the augmented SMS method was presented with each of the steps. The key difference between the augmented SMS method and its previous implementation lies in the generation of the ground structure in step 2 of the method. In this step, an autonomous and free mesh approach is integrated into the augmented SMS method to allow the method to design and optimize conformal lattice structure on complex surface. The process of generating the ground structure for complex-shaped parts was integrated into Unigraphics NX 6.5 to enable the designers to set lattice structure size parameters through graphical user interface. Step 3 and 4 of the method were modified in order to incorporate and take advantage of this new capability in the augmented SMS method.

The augmented method uses the unit-cell library to generate the topology for the target truss structure. The library, including the optimization, selection and mapping process was presented. The augmented SMS method and the unit-cell library will be applied to various designed examples in Chapter 4.

CHAPTER 4

DESIGN EXAMPLES

4.1 3-D Cantilever Beam

4.1.1 Problem Description

For this example, a simple, three-dimensional cantilever is used to demonstrate the augmented SMS method. It is an example problem from Graf's and Chang's work [15, 16]. The initial conditions from their examples are duplicated in order to make a direct comparison. The beam is fixed at one end and loaded with two vertical forces at the free end. Ultimately, the primary goal of this example will be to confirm that the algorithm modifications did not result in any negative changes in the topology and performance of the structure. The physical representation of the design problem is shown in Figure 4-1. The loading condition, material properties and dimensions and unit-cell configurations are provided in Table 4-1.

Table 4-1: Properties for 3-D cantilever beam example

| | |
|--------------------------------------|------|
| Length (mm) | 50 |
| Width (mm) | 10 |
| Height (mm) | 20 |
| Loading Magnitude(N) | 10 |
| Elastic Modulus (N/mm ²) | 1960 |
| Unit-cell size x-direction (mm) | 10 |
| Unit-cell size y-direction (mm) | 10 |
| Unit-cell size z-direction (mm) | 10 |
| Target Volume(mm ³) | 1600 |

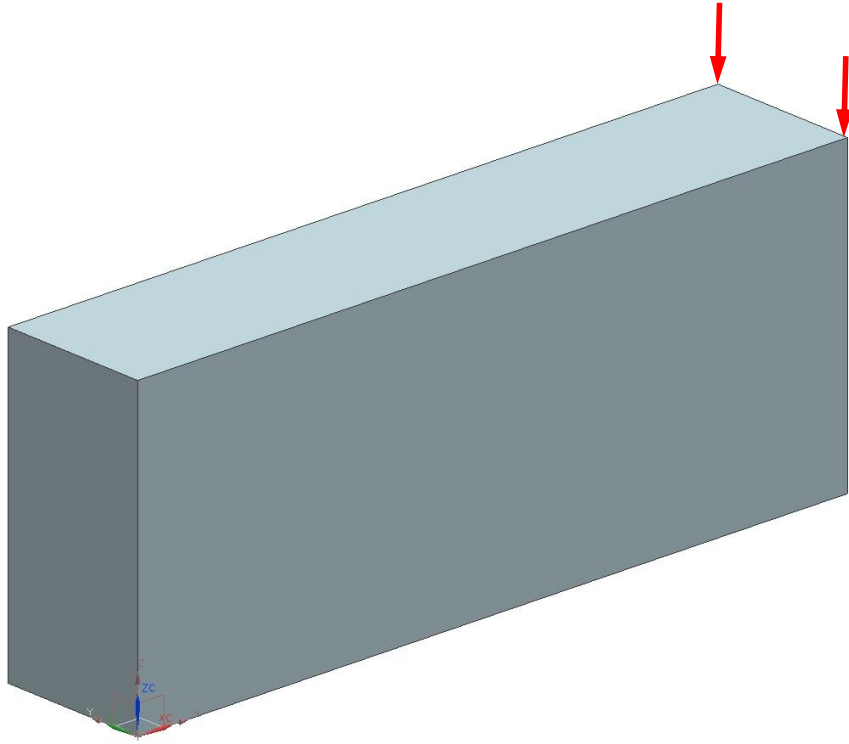


Figure 4-1: 3-D cantilever beam example

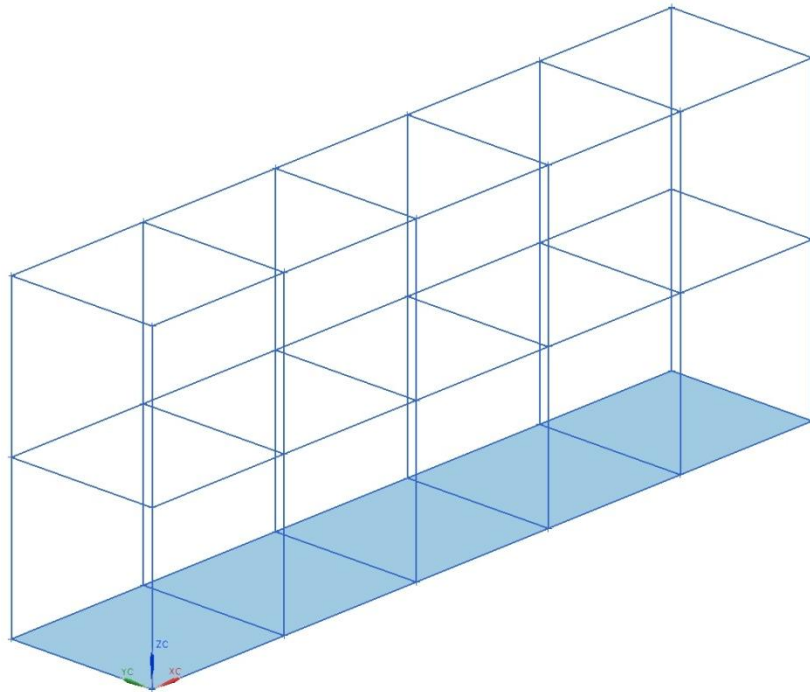


Figure 4-2: Cantilever beam divided into multiple unit-cell regions

4.1.2 Ground Geometry and Solid Body Analysis

A base lattice structure is generated for the cantilever beam using TrussCreator in Unigraphics NX with the desired unit-cell sizes provided in Table 4-1. An image of the base lattice structure of the cantilever beam is shown in Figure 4-2. The next step in the process is to perform solid-body finite element analysis. This step is done using ANSYS with the appropriate bounding, loading condition and material property provided in Table 4-1. It is important to note that the finite element model is constructed with a higher mesh density than the base lattice structure to allow multiple finite element nodes in each unit cell. Figure 4-3 shows the von Mises stress for the cantilever beam as well as the X-component (along the length of the beam) of the stress distribution.

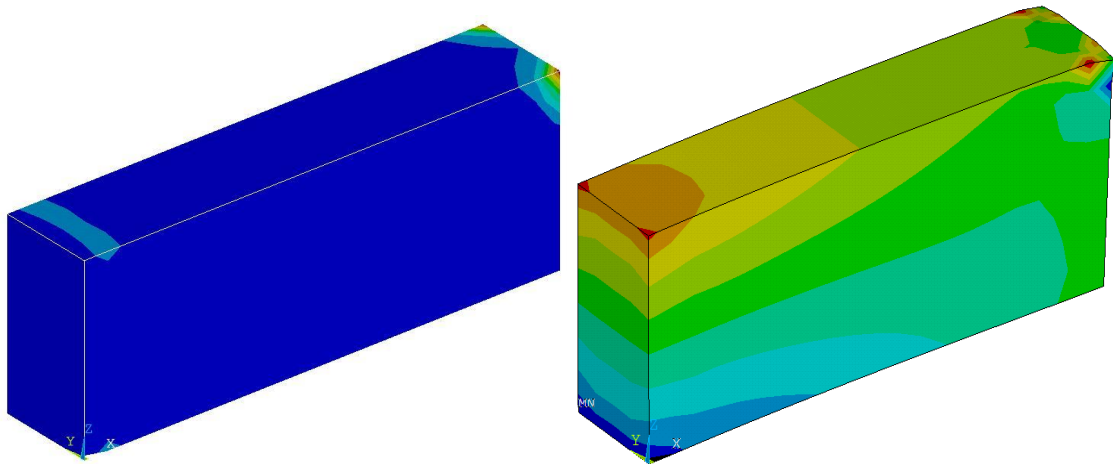


Figure 4-3: von Mises stress (left); X-component of the stress (right)

From the solid-body finite element analysis of the structure, it can be seen that the stress is highest at the tip of the beam where the forces are applied and at the upper region of the fixed end. Therefore, it can be expected that the largest struts are along the length down the center of the beam and at the point where the load is applied. After the solid

body analysis is complete, the results can be mapped to the structure. There are six different stresses in each of the unit cells, three normal stresses and three shear stresses. Since the structure is aligned with the global coordinate system, the stress transformation from the global coordinate system to local coordinate system of each unit cell is not necessary. The nodal stresses in each of the unit cells are averaged and then normalized based on the largest stress present in the structure to determine the scaling factors for the diameter of each strut.

4.1.3 Unit-Cell Library

Once the scaling factors for the diameter of each strut is known, the unit-cell library and selection method are used to generate the topology for the SMS method. The weighting values W_v , W_{v_n} and W_p in Equation 3-18 are set to 2, 0 and 1 respectively. W_v , W_{v_n} , and W_p represent the weighting variables for $\sum V_\sigma$, V_{net} , and $\sum P$ in the rating equation. These numbers were determined heuristically to produce the best performing topology for the given structure [15]. With the given weighting values, the augmented SMS method selects cross configuration for the topology. Figure 4-4 shows the topology matches the expectation. It shows intuitive strut placement with thickest struts along the length of the beam near the fixed end and at the tip where the force is applied.

The topology from Figure 4-4 undergoes topology alteration to remove duplicated and unnecessary struts. Figure 4-5 shows the topology of the cantilever beam after D_{cutoff} is utilized. The cutoff diameter is valid for this example because no critical struts that affect the beam structural integrity are removed.

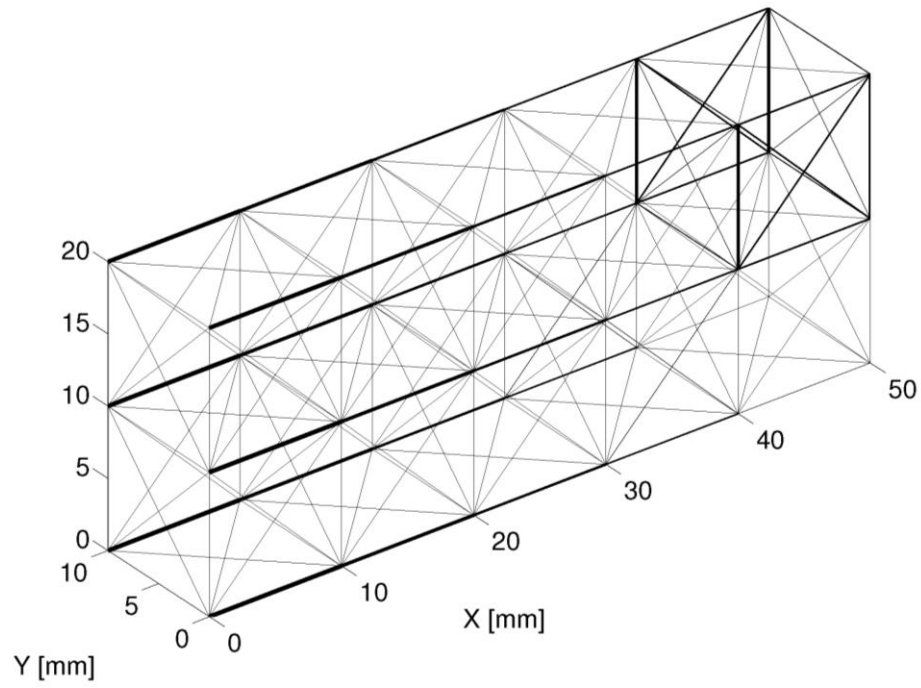


Figure 4-4: Cantilever beam truss structure before topology alteration

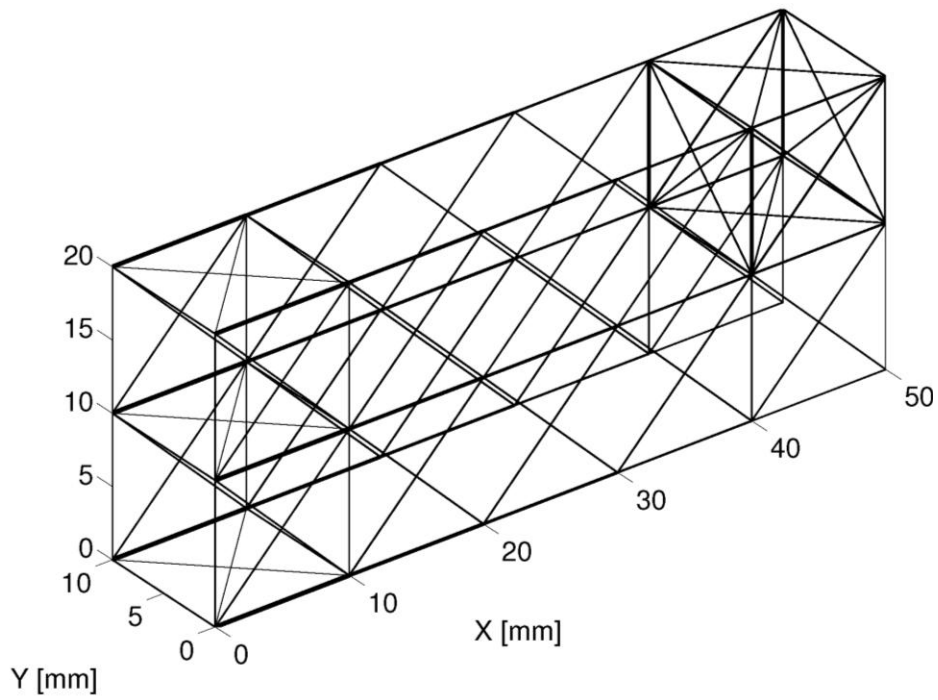


Figure 4-5: Topology of the cantilever beam after D_{cutoff} is utilized

Table 4-2: Diameter results for the 3-D cantilever beam

| <u>Optimization Approach</u> | 28% Assumption | Active-Set | Least-square Minimization | Ground Truss LM |
|--|-----------------------|-------------------|----------------------------------|------------------------|
| Deflection(mm) | 0.636 | 0.569 | 0.569 | 0.3488 |
| Volume (mm³) | 1600 | 1600 | 1600 | 1600 |
| D_{MIN} (mm) | 0.85 | 0.51 | 0.51 | -- |
| D_{MAX} (mm) | 3.05 | 4.55 | 4.55 | -- |
| D_{cutoff} (mm) | 0.91 | 0.61 | 0.61 | -- |
| D_{MIN}/D_{MAX} (%) | 28.00 | 11.2 | 11.2 | -- |
| Design Time (s) | 3.2 | 18.0 | 20.9 | 1195.3 |

Table 4-3: Diameter result by Chang for 3-D cantilever beam [15]

| <u>Optimization Approach</u> | 28% Assumption | Active-Set | Least-square Minimization |
|--|-----------------------|-------------------|----------------------------------|
| Deflection(mm) | 0.636 | 0.569 | 0.569 |
| Volume (mm³) | 1600 | 1600 | 1600 |
| D_{MIN} (mm) | 0.85 | 0.51 | 0.51 |
| D_{MAX} (mm) | 3.05 | 4.55 | 4.55 |
| D_{cutoff} (mm) | 0.91 | 0.61 | 0.61 |
| D_{MIN}/D_{MAX} (%) | 28 | 11.2 | 11.2 |
| Design Time (s) | 3.0 | 18.8 | 20.1 |

The diameter results for the topology optimization are provided in Table 4-2. For the optimization result, the deflection of the tip of the beam i.e. the displacement of the loaded nodes is used to measure stiffness. Active-set and least-square minimization are able to return better stiffness performance than the 28% assumption solution even though they take longer to converge. These results agree well with the design example done by Chang, shown in Table 4-3. Since the strut diameters of the structure are calculated based scaling factors taken from the unit-cell library and the solid-body analysis, D_{min} and D_{max} of the structure after scaling against those factors are shown in Table 4-4 . The diameter

results of next two design examples are also tabulated after they are scaled against the scaling factors.

Table 4-4: Actual diameters of the 3-D cantilever beam

| <u>Optimization Approach</u> | 28% Assumption | Active-Set | Least-square Minimization |
|-------------------------------------|-----------------------|-------------------|----------------------------------|
| Deflection(mm) | 0.636 | 0.569 | 0.569 |
| Volume (mm³) | 1600 | 1600 | 1600 |
| D_{min} (mm) | 0.91 | 0.61 | 0.61 |
| D_{max} (mm) | 1.99 | 2.61 | 2.61 |
| Design Time (s) | 3.2 | 18.0 | 20.9 |

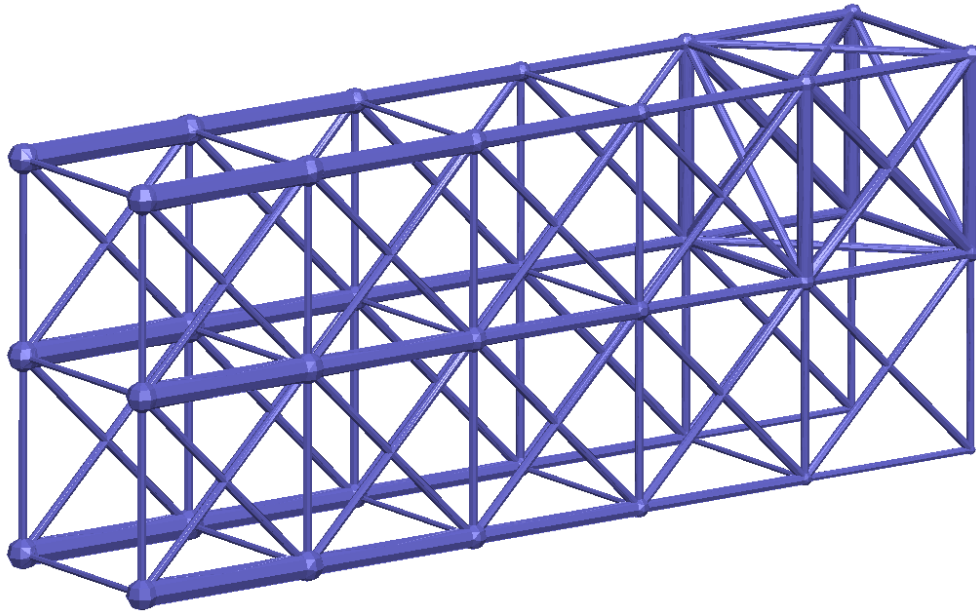


Figure 4-6: Final topology of the 3-D cantilever beam using active-set method

In addition to the augmented SMS method, ground truss approach was utilized to perform the topological optimization. Levenberg-Marquardt algorithm was used to optimize the ground truss. The resultant topology for the Levenberg-Marquardt algorithm is shown in Figure 4-7. When compared with the ground truss approach, the augmented SMS has acceptable performance result, but is able to converge much more

quickly with about 55 times decrease in design time using two-variable approach and about 360 times decrease in design time using one-variable approach.

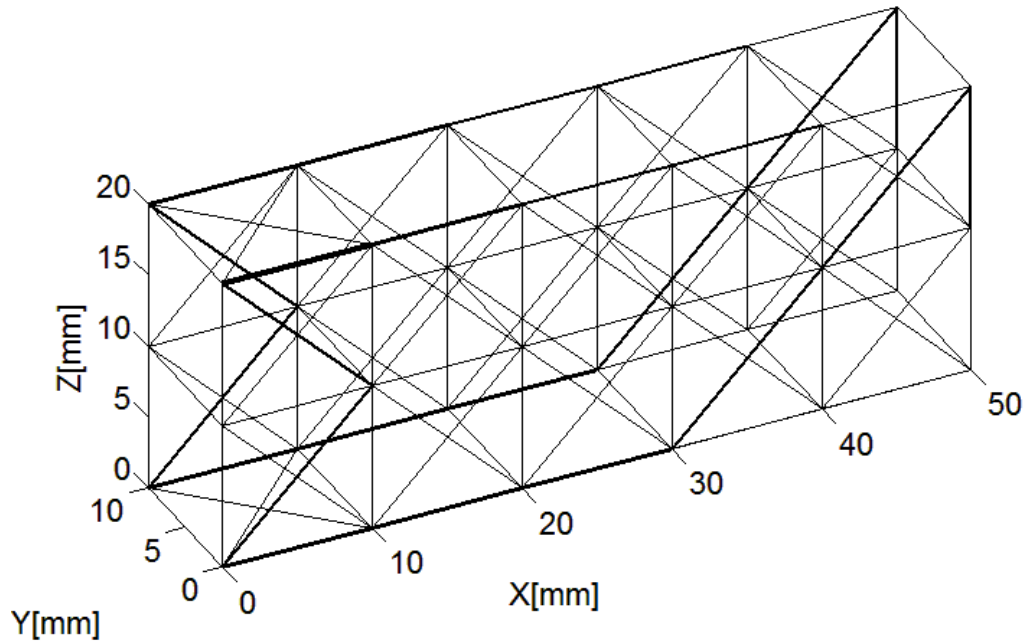


Figure 4-7: Least-square minimization result for 3-D cantilever beam using ground truss approach

4.1.4 Summary

This example serves to validate that the integration of free-mesh approach and the algorithm changes did not have any adverse effects on the topology or structural integrity of the beam.

4.2 3-D Curved Cantilever Beam

4.2.1 Problem Description

The second example is a simple, three-dimensional, curved cantilever beam with rectangular cross section. The beam is fixed at one end and has two point loads applied in the z-direction at the free end. Ultimately, the primary goal of this example is to

illustrate the modified algorithm in steps two, three, and four has allowed the augmented method to overcome the significant limitations with the previous implementations of the SMS method which cannot be utilized in structures with curved surfaces. For this example, the unit-cell regions do not have local coordinate systems that are the same as the global coordinate system. The design problem is shown in Figure 4-8.

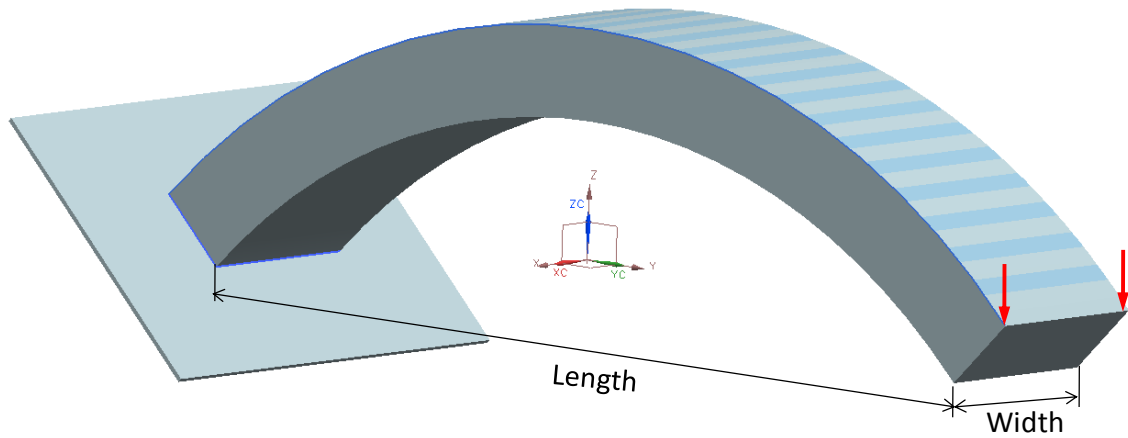


Figure 4-8: 3-D curved cantilever beam

The objective of this problem is to achieve a target volume of 5000 mm^3 while minimizing the tip deflection. The initial properties of this design problem are provided in Figure 4-4.

Table 4-5: Initial properties of the curve cantilever beam

| | |
|-------------------------------------|------|
| Outer Radius (mm) | 84.5 |
| Inner Radius (mm) | 74.5 |
| Width (mm) | 20 |
| Length(mm) | 105 |
| Loading Magnitude (N) | 1 |
| Elastic Modulus (N/mm^2) | 1960 |
| Unit-cell size in-plane (mm) | 10 |
| Unit-cell size out-plane (mm) | 10 |
| Target Volume (mm^3) | 5000 |

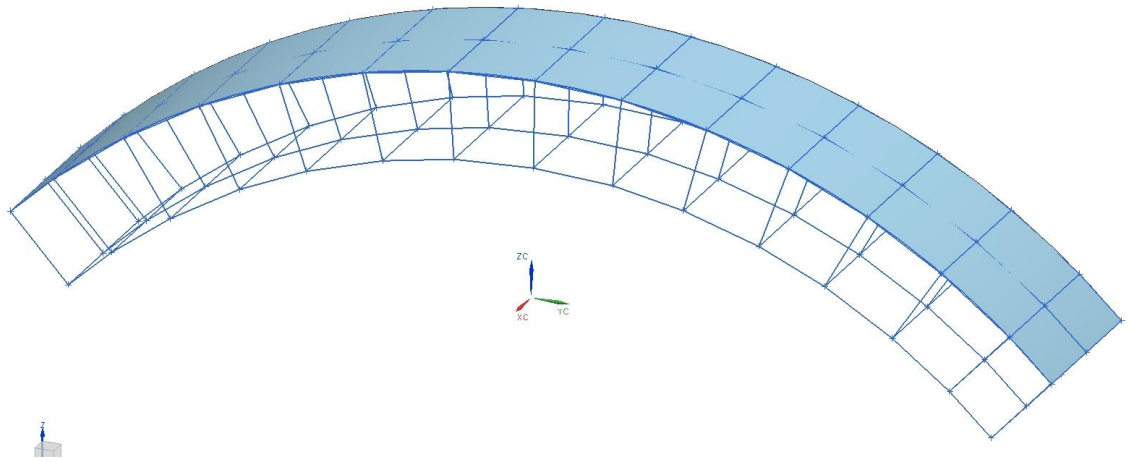


Figure 4-9: Base-lattice structure of the curve cantilever beam

4.2.2 Ground Geometry and Solid-Body Analysis

The curved cantilever beam is divided into multiple unit-cell regions using TrussCreator with the desirable unit-cell sizes as provided in Table 4-5. There are 28 unit cells in the ground structure. Because of the curved surface, the unit-cell regions are no longer perfect cubes. The structure also requires the unit-cell regions to have local coordinate systems different from the global coordinate system. The solid body finite element analysis is shown in Figure 4-10. The Y-component of the stress distribution is also shown in Figure 4-10. From the solid-body finite element results, it can be seen that the highest stress occurs near the fixed end of the beam. Therefore, it can be expected that the thickest struts will be along the length of the beam near the fixed end and thinner struts will be everywhere else.

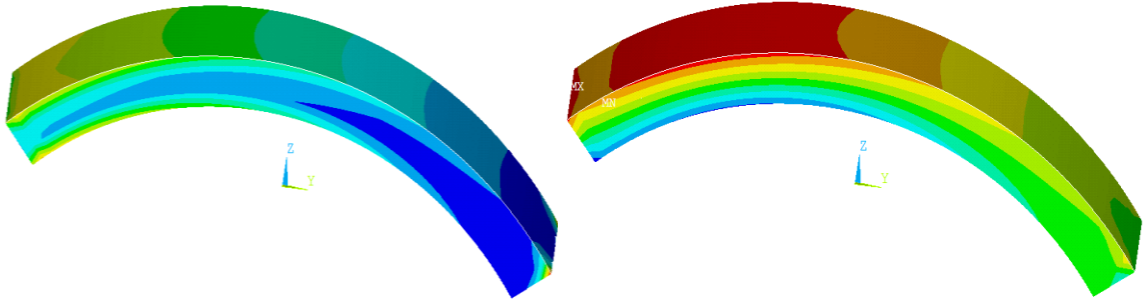


Figure 4-10 : Von Mises stress (left); y-component of stress distribution (right)

The stress results are then mapped to the correct unit-cell regions of the base lattice structure. Essentially, the finite element nodes are checked to find which unit-cell region they belong to. If a node falls into a unit-cell region, then that nodal stress values are included in the calculation of the stresses in that unit-cell region. The general state of stress at each node is characterized by six independent normal and shear stress components. The solid-body finite element analysis results are provided relative to the global coordinate system. Since the local coordinate system of a unit region is different from the global coordinate system, the stress components are transformed from the global to local coordinate system in order to generate correct topology for the structure. The detailed algorithm of this step can be found in chapter three. Once the mapping process is done, the unit-cell library can be used to generate the topology of the structure.

4.2.3 Unit-Cell Library

In this section, four unique topologies of the curved cantilever beam will be created using the unit-cell library and selection scenario with different weighting values. The resultant topology and strut diameter values are provided for each selection. For the selection method, which results in the best structural stiffness, a design space

exploration/grid search and topological optimization using ground truss approach were also conducted.

4.2.3.1 Selection Scenario 1

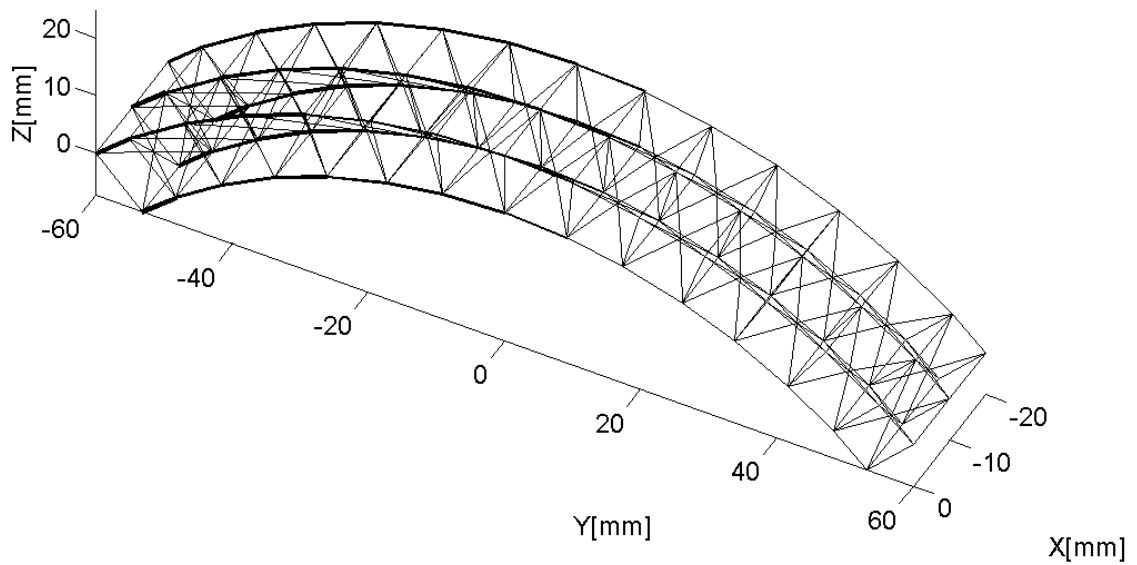


Figure 4-11: Topology for the first selection scenario of the curved cantilever

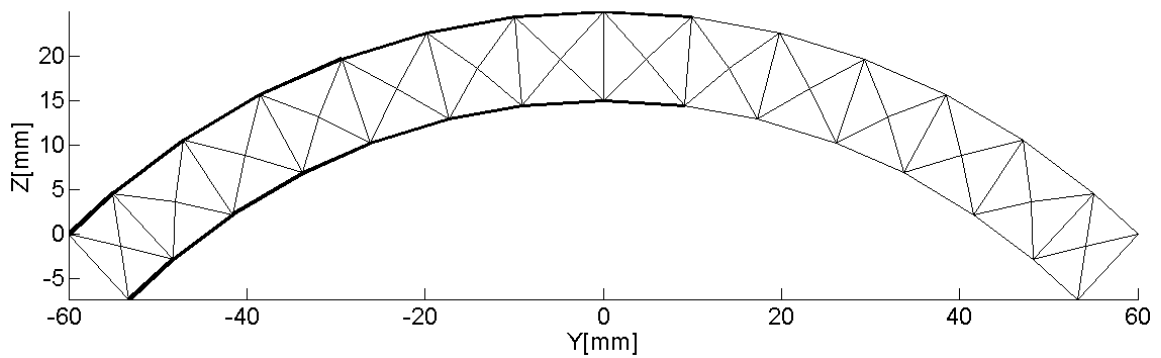


Figure 4-12: Side view of the topology for the first selection scenario of the curved cantilever beam

For the first selection scenario, the weighting values from Equation 3-18 are set at: $W_v = 1$, $W_{vn} = 1$, $W_p = 0$. These values are manually set to vary the importance of each contributing factors in the selection Equation 3-18. The complete topology of the structure is shown in Figure 4-11. A side view is also provided in Figure 4-12. With these values, the topology was generated with 28 diagonal configurations. The strut diameter results are summarized in Table 4-6.

Table 4-6: Diameter results for the first selection scenario of the curved cantilever beam

| <u>Optimization Approach</u> | SMS 28% Assumption | SMS Active-Set | SMS Least-square Minimization | Ground Truss LM |
|-------------------------------------|---------------------------|-----------------------|--------------------------------------|------------------------|
| Deflection(mm) | 1.341 | 0.901 | 0.901 | 0.780 |
| Volume (mm³) | 5501.0 | 5500.5 | 5500.5 | 5501 |
| D_{min} (mm) | 1.13 | 0.65 | 0.65 | -- |
| D_{max} (mm) | 2.43 | 3.88 | 3.88 | -- |
| D_{cutoff} (mm) | N/A | N/A | N/A | -- |
| Design Time (s) | 7.8 | 46.7 | 52.8 | 3260 |

The results show that the 28% method is able to converge about 6 times faster than either two-variable optimizations; however, the deflection result is worse than either two-variable approaches. The two 2-variable optimizations return identical results. However, the active-set method is able to converge faster. The final 3-D topology of the curved cantilever beam using active-set method is shown in Figure 4-13. As mentioned in example 1, it is important to note that the diameter results reported for SMS method are the actual diameters of structure after being scaled against the solid body analysis and unit cell library scaling factors. The pre-scaling D_{MIN} and D_{MAX} for the active set method are 0.4135mm and 7.0704mm respectively.

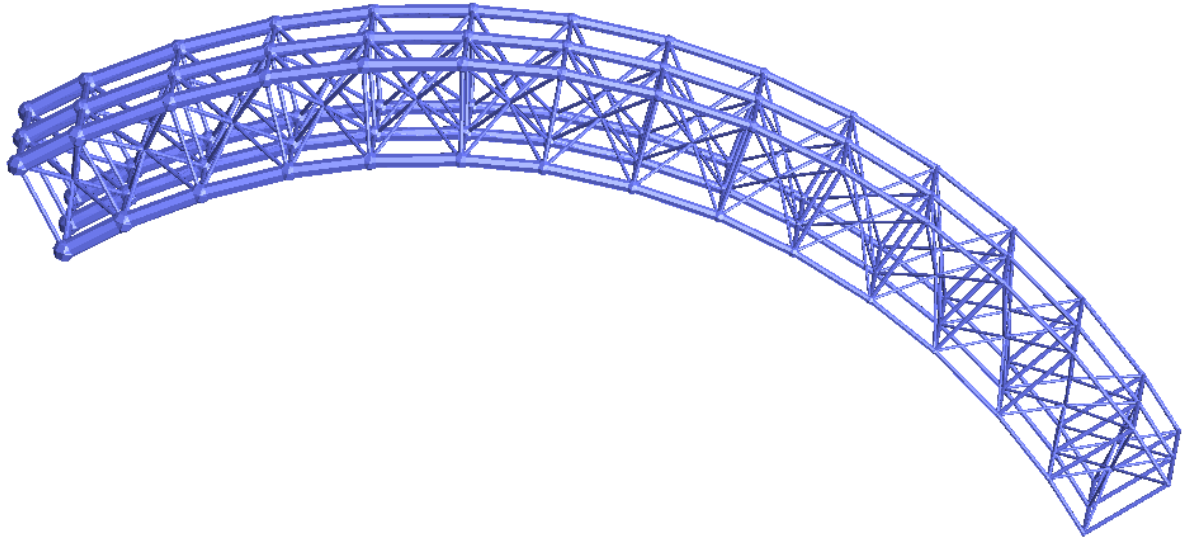


Figure 4-13: Final topology for the first selection scenario of the curved cantilever beam using active-set method

Besides the three optimization approaches, a design space exploration/grid search was conducted. The design space exploration is done using pre-scaling values of diameters. It is important to note that the finite element analysis of the truss structure is conducted using the scaled/true diameters of the structure. This design space exploration was performed by iterating both D_{MIN} and D_{MAX} from 0.1 to 10 mm with an increment of 0.1 mm. The result is plotted in Figure 4-14. Based on the results from the initial exploration, a finer resolution of the design space was conducted around the apparent minimum by searching D_{MIN} from 0.3 to 0.5m and D_{MAX} from 6.9 to 7.3 mm. with an increment of 0.01 mm. The result is plotted in Figure 4-15. The red diamond indicates the minimum found in design exploration. Diameter results that return the lowest objective function value are shown in Table 4-7. The first column is diameter values from the design space exploration before scaling. The second column is true diameters of the structure after they have been scaled using solid-body and unit-cell library scaling factors. These diameter

values are found to be close to the values obtained from the SMS method. Both two-variable optimizations were able to return results with much lesser design time than the design space exploration.

Table 4-7: Design space exploration results for the fuselage

| | Pre-scaled | Scaled |
|--------------------------------|------------|--------|
| Deflection(mm) | 0.900 | 0.900 |
| Volume (mm³) | 5500 | 5500 |
| D_{max} (mm) | 7.09 | 3.87 |
| D_{min} (mm) | 0.41 | 0.64 |
| D_{cutoff} (mm) | N/A | N/A |
| Design Time (s) | 2860 | 2860 |

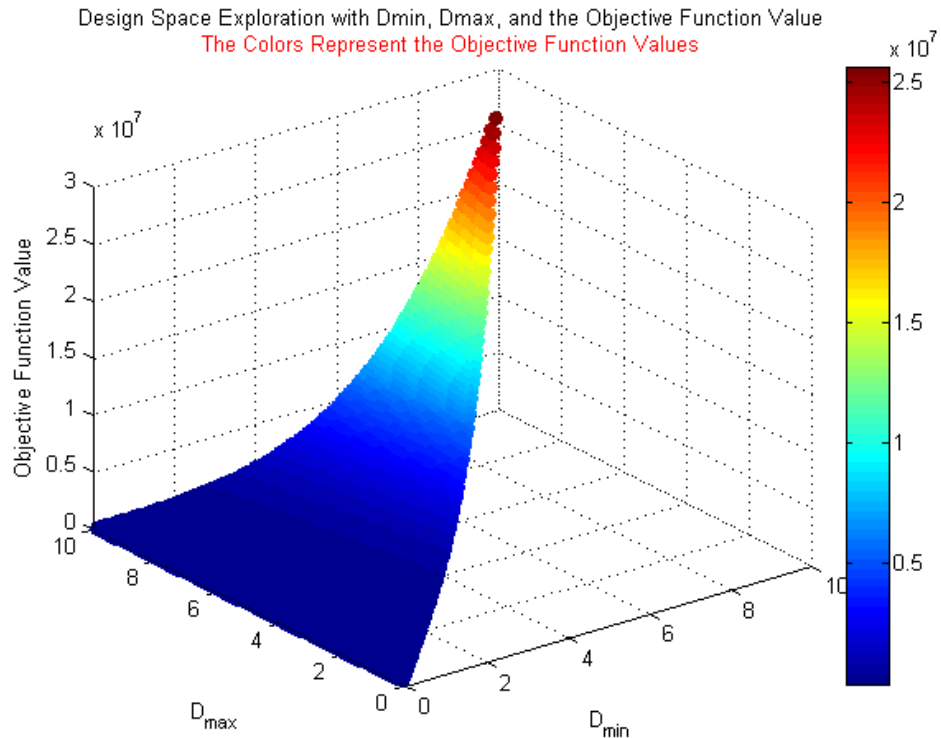


Figure 4-14: Design space exploration for the first scenario of the curved cantilever beam

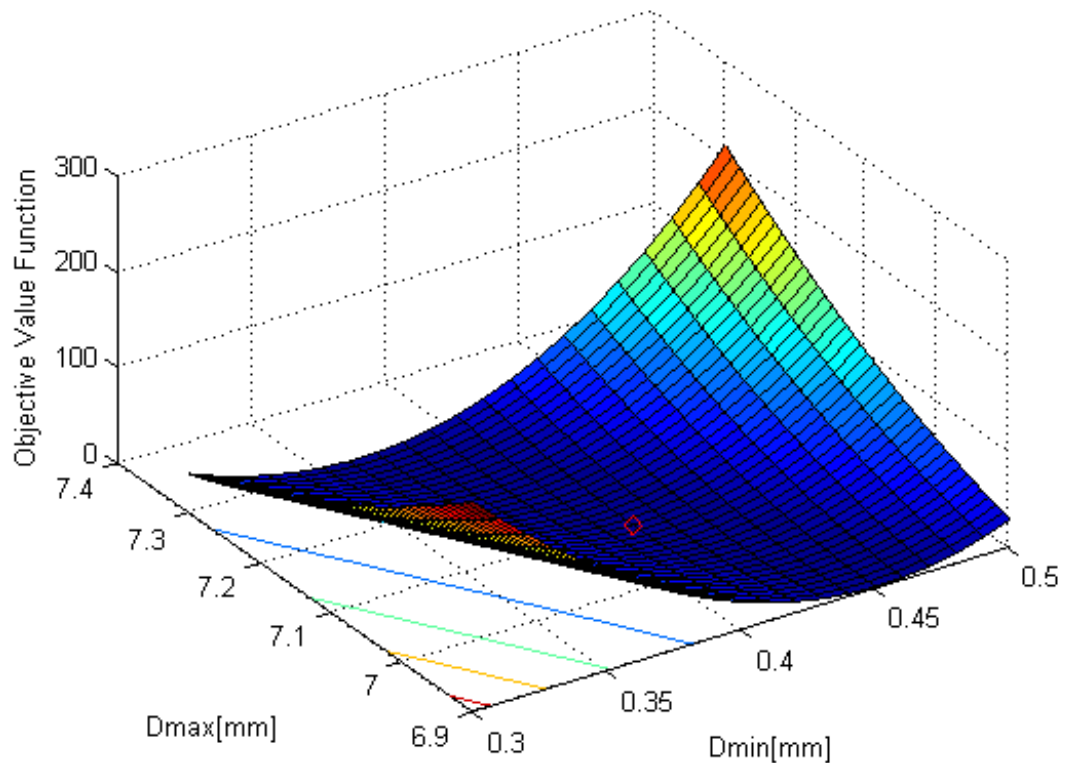


Figure 4-15: Design space exploration with finer resolution around the solution for the first selection scenario of the curved cantilever beam

In addition to the augmented SMS method, ground truss approach was utilized to perform topology optimization for this selection scenario. Levenberg-Marquardt algorithm was used to optimize the ground truss. The resultant topology for the Levenberg-Marquardt algorithm is shown in Figure 4-16. When compared with the ground truss approach, the augmented SMS has comparable performance result, but is able to converge much more quickly with about 70 times decrease in design time using two-variable approach and about 400 times decrease in design time using one-variable approach.

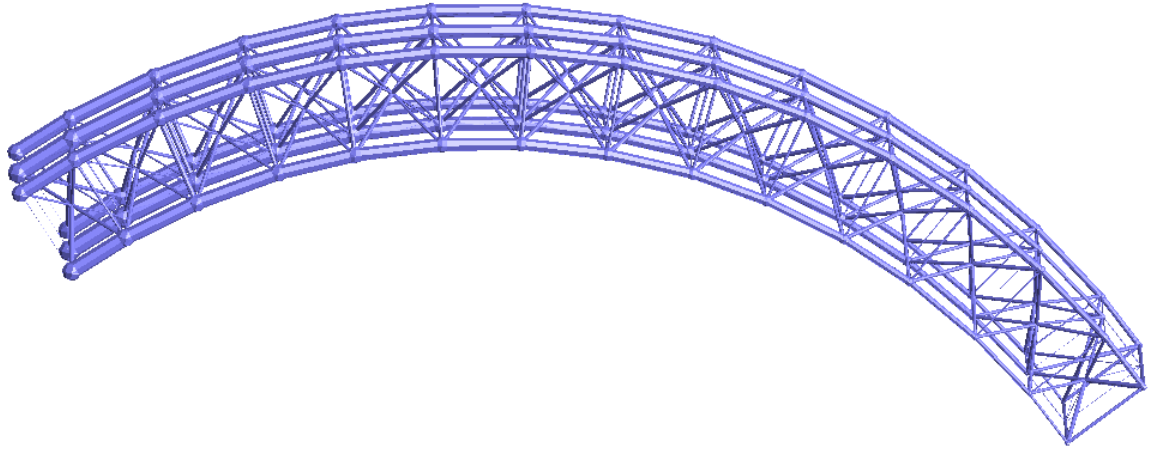


Figure 4-16: Levenberg-Marquardt result for first selection scenario the curved cantilever beam using ground truss approach

4.2.3.1.1 *Alternative Problem Formulation*

An alternative problem formulation, which the volume of the structure is minimized while subjects to a target deflection constraint, is also used for the first selection scenario of the curved cantilever beam. The diameters are determined by constrained optimization approach using active-set method. The deflection target is set to 0.78 mm. The diameter results are shown in Table 4-8.

Table 4-8: Diameter results for the first selection scenario of the curved cantilever beam using alternative problem formulation

| <u>Optimization Approach</u> | SMS 28% Assumption | SMS Active-Set | Ground Truss |
|-------------------------------------|---------------------------|-----------------------|---------------------|
| Deflection(mm) | 0.780 | 0.780 | 0.782 |
| Volume (mm³) | 9359 | 6336 | 4864 |
| D_{min} (mm) | 1.4841 | 0.7040 | -- |
| D_{max} (mm) | 3.1704 | 4.1630 | -- |
| Design Time (s) | 19.7 | 34.1 | 259200 |

Topology optimization using ground truss approach took more than three days to get close to the target deflection. Even though the volume of the structure using ground truss approach is about 20% less than the volume of the structure using the SMS active-set method, the ground truss approach is highly inefficient as it takes 7600 times longer than the SMS method. Topology optimization using ground truss approach is not a feasible solution using this problem formulation.

4.2.3.2 Selection Scenario 2

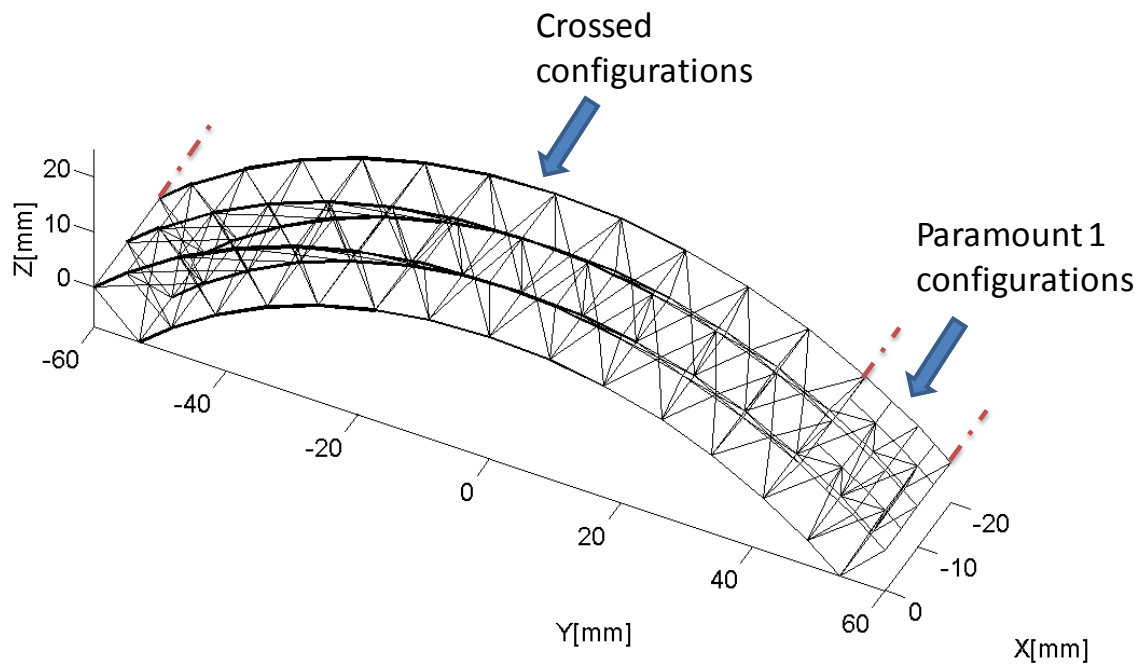


Figure 4-17: Topology for second selection scenario of curved cantilever beam

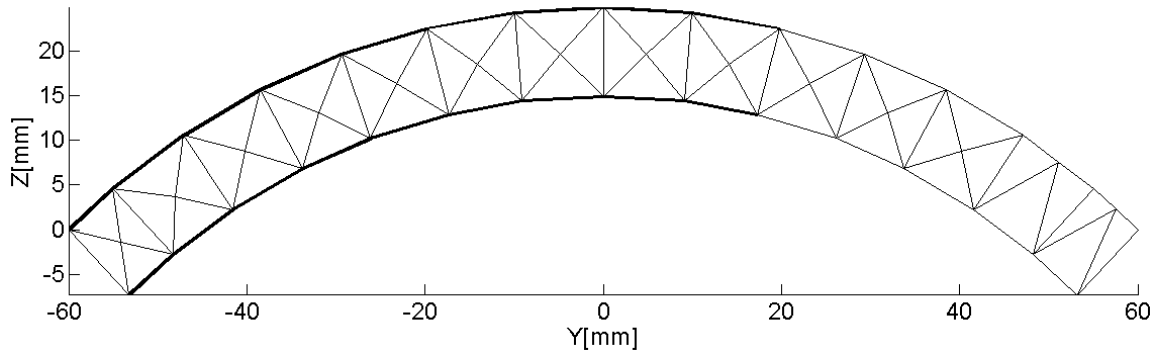


Figure 4-18: Side view of the topology for the second selection scenario of the curved cantilever beam

The weighting values are set at: $W_v = 0$, $W_{vn} = 1$, $W_p = 0$ for this selection scenario. With these values, 4 unit cells were mapped with the paramount 1 configuration and 24 units cells were mapped with diagonal configuration. The complete topology is shown in Figure 4-17. A side view of the topology is also provided in Figure 4-18. The strut diameter results are shown in Table 4-9.

Table 4-9: Diameter results for second selection scenario of curved cantilever beam

| <u>Optimization Approach</u> | 28% Assumption | Active-Set | Least-square Minimization |
|-------------------------------------|-----------------------|-------------------|----------------------------------|
| Deflection(mm) | 1.379 | 1.049 | 1.049 |
| Volume (mm³) | 5501.1 | 5500.7 | 5500.7 |
| D_{min} (mm) | 1.11 | 0.72 | 0.72 |
| D_{max} (mm) | 2.45 | 3.56 | 3.56 |
| D_{cutoff} (mm) | N/A | N/A | N/A |
| Design Time (s) | 8.9 | 49.9 | 55.5 |

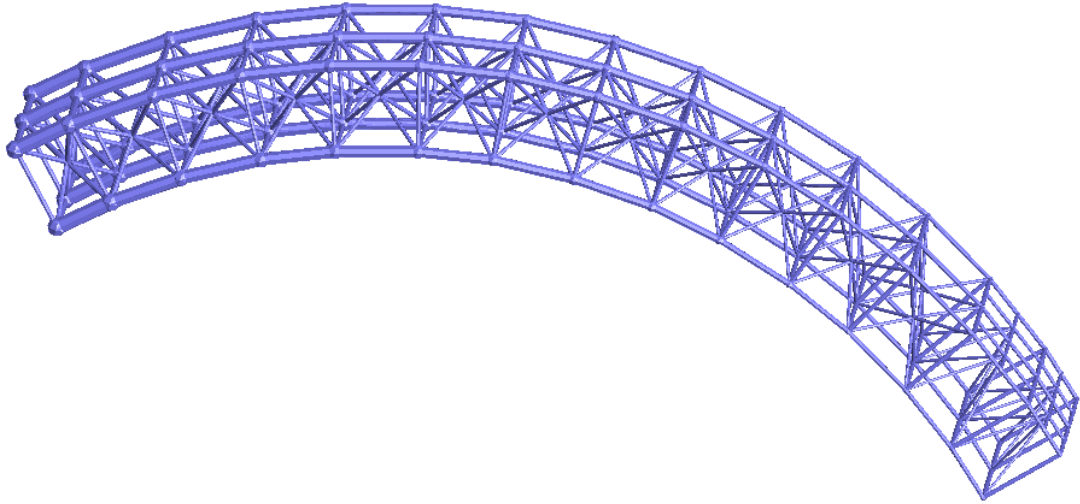


Figure 4-19: Final topology for the second selection scenario of the curved cantilever beam using active-set method

Similar to the first selection scenario, the one-variable assumption took the least amount of time, but returns the worst deflection value. Both two-variable optimizations produce very similar results; however, the active-set method converges faster than the least-square minimization. The final 3-D topology of the curved cantilever beam using active-set method is shown in Figure 4-19.

4.2.3.3 Selection Scenario 3

The third selection scenario has the weighting values set at: $W_v = 0$, $W_{vn} = 0$, $W_p = 1$. With these weighting values, the topology is generated with 28 crossed configurations. The complete topology of the structure is shown in Figure 4-20. The side view of the topology is also provided in Figure 4-21. The topology matches the expectation based on the solid-body analysis.

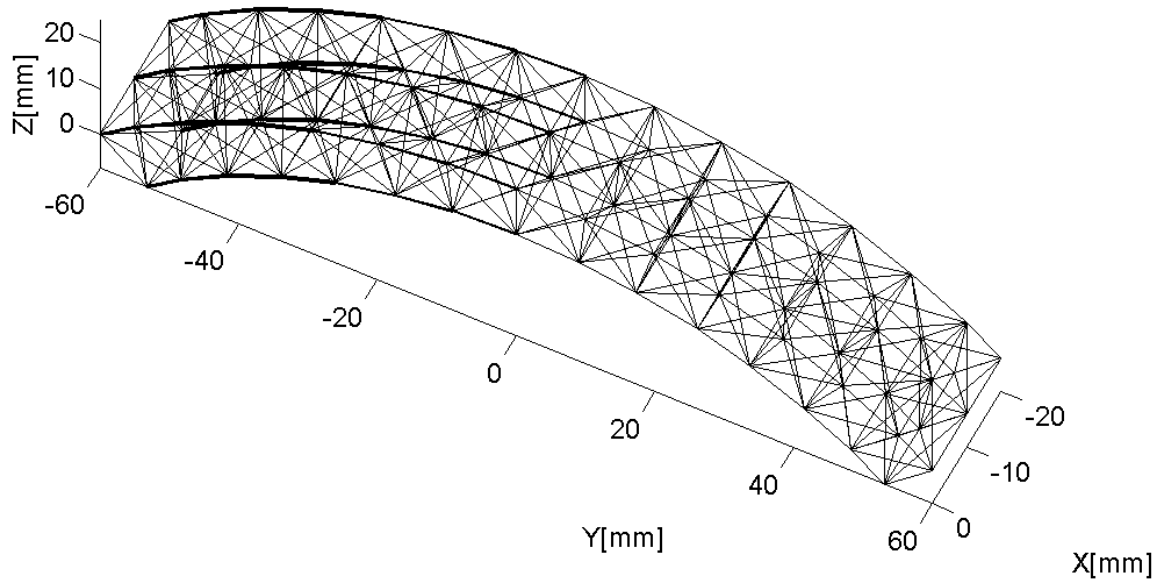


Figure 4-20: Topology of the third selection scenario for the curved cantilever beam

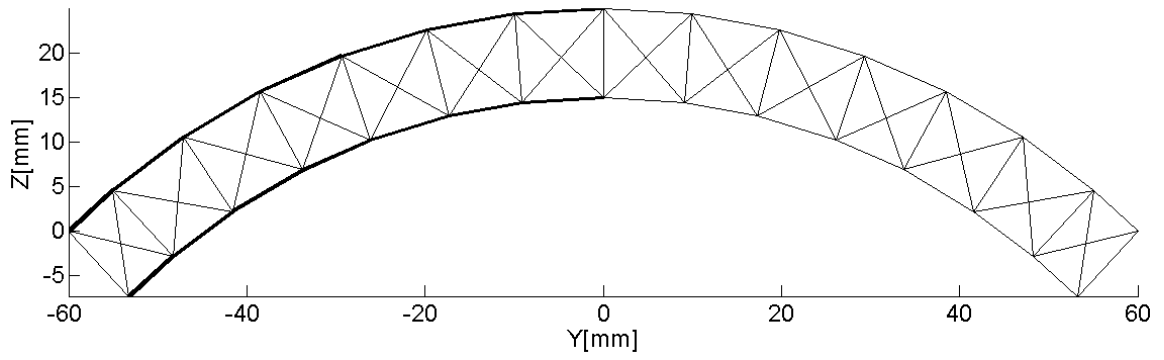


Figure 4-21: Side view of the third selection scenario for the curved cantilever beam

Table 4-10: Diameter results for the third selection scenario of the curved cantilever beam

| <u>Optimization Approach</u> | 28% Assumption | Active-Set | Least-square Minimization |
|-------------------------------------|-----------------------|-------------------|----------------------------------|
| Deflection(mm) | 2.231 | 1.908 | 1.908 |
| Volume (mm³) | 5505.8 | 5502.9 | 5502.9 |
| D_{min} (mm) | 0.92 | 0.59 | 0.59 |
| D_{max} (mm) | 2.09 | 3.01 | 3.01 |
| D_{cutoff} (mm) | N/A | N/A | N/A |
| Design Time (s) | 9.0 | 47.1 | 49.2 |

The strut diameter results are shown in Table 4-10. Once again, the 28% assumption method takes the least amount of time but at the expense of the structure stiffness. Both 2-variable optimizations produce almost identical results; however least-square minimization takes a little longer than active set method. The final 3-D topology of the curved cantilever using active-set method is shown in Figure 4-22.

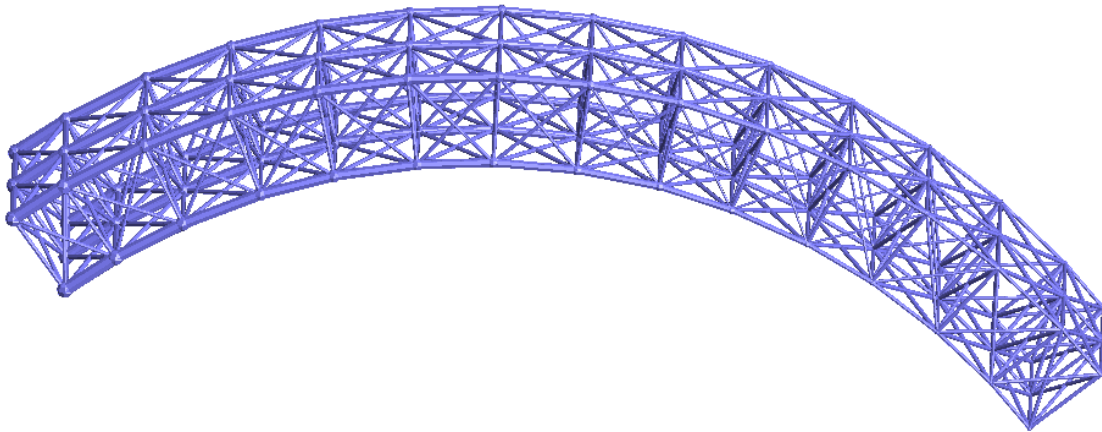


Figure 4-22: Final topology for the third selection scenario of the curved cantilever beam using active-set method

4.2.3.4 Selection Scenario 4

The final selection scenario has weighting values set at: $W_v = 0$, $W_{vn} = 1$, $W_p = 1$. The topology consists of 18 crossed configurations and 10 diagonal configurations. The complete topology of the curved cantilever beam is shown in Figure 4-23. A side view of the topology is also shown in Figure 4-24.

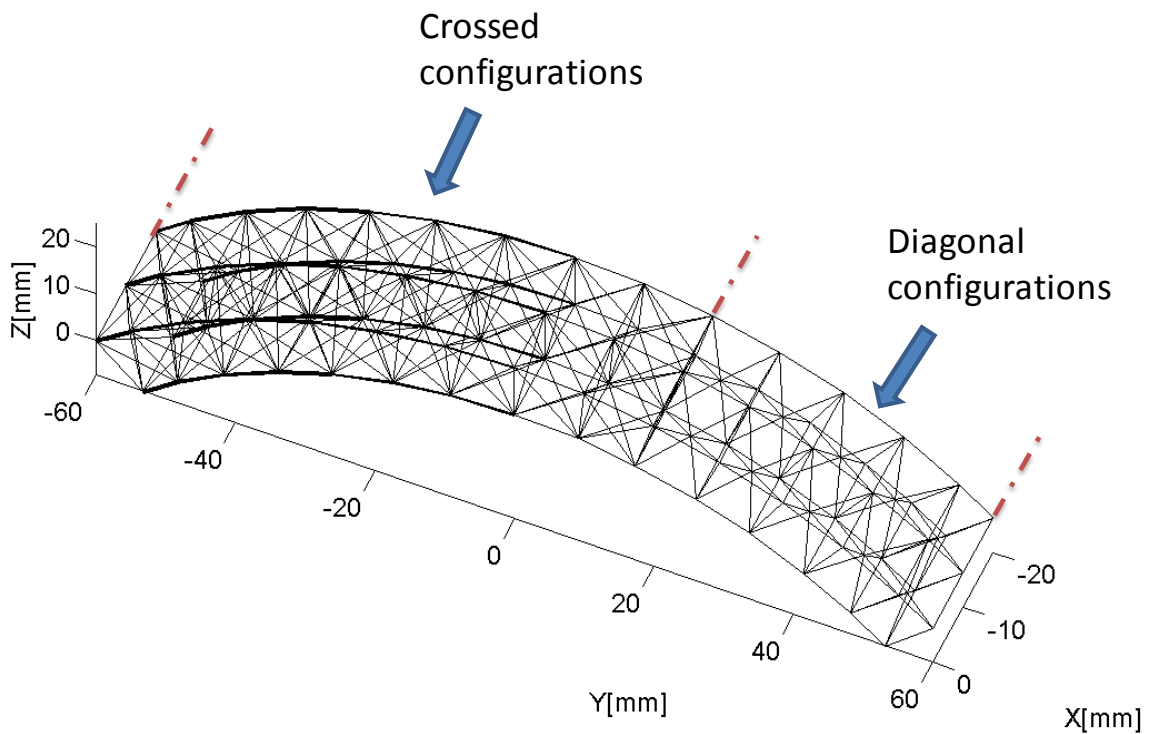


Figure 4-23: Topology for the final selection scenario of the curved cantilever beam

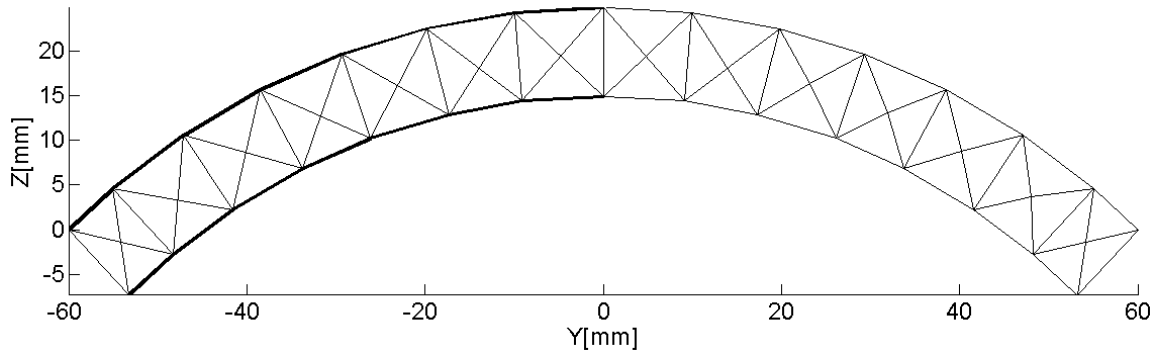


Figure 4-24: Side view of the final selection scenario of the curved cantilever beam

Table 4-11: Diameter results for the final selection scenario of the curved cantilever beam

| <u>Optimization Approach</u> | 28% Assumption | Active-Set | Least-square Minimization |
|-------------------------------------|-----------------------|-------------------|----------------------------------|
| Deflection(mm) | 1.595 | 1.066 | 1.066 |
| Volume (mm³) | 5502.4 | 5501.1 | 5501.1 |
| D_{min} (mm) | 0.96 | 0.41 | 0.41 |
| D_{max} (mm) | 2.19 | 3.67 | 3.67 |
| D_{cutoff} (mm) | N/A | N/A | N/A |
| Design Time (s) | 9.2 | 52.1 | 53.5 |

The strut diameter results are summarized in Table 4-11. Similar to those previous selection scenarios, the one-variable optimization returns results in the least amount of time but with the least desirable structure stiffness. Active-set method and least-square minimization produce almost identical result; however, active-set method converges faster than its counterpart. The final 3-D topology of the curved cantilever using active-set method is shown in Figure 4-25.

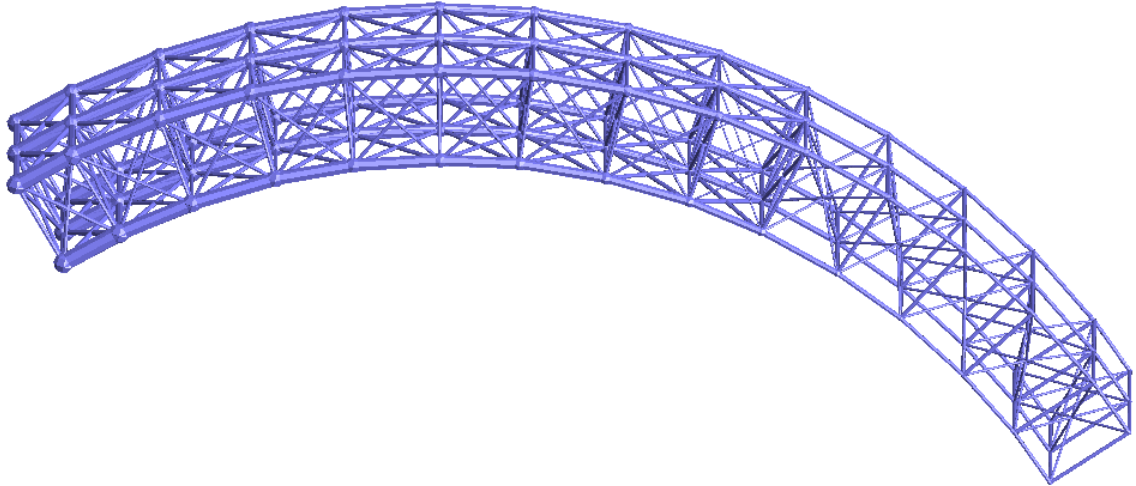


Figure 4-25: Final topology for the final selection scenario of the curved cantilever beam using active-set method

4.2.3.5 Result Comparison

The results from four unique selection scenarios are compared in this section. Table 4-12 presents the deflections results of the curved cantilever beam for each topology.

Table 4-12: Deflection results for curved cantilever beam

| <u>Selection Scenario</u> | SMS 28% Assumption | SMS Active-Set | SMS Least-square Minimization | LM Ground Truss |
|--|-----------------------------------|---------------------------|--|--------------------------------|
| Scenario 1 [28 diagonals] | 1.341 | 0.901 | 0.901 | 0.780 |
| Scenario 2 [4 paramount 1, 24 diagonal] | 1.379 | 1.049 | 1.049 | -- |
| Scenario 3 [28 crossed] | 2.231 | 1.908 | 1.908 | -- |
| Scenario 4 [18 crossed, 10 diagonal] | 1.595 | 1.066 | 1.066 | -- |

From Table 4-12, we can observe the following important trends:

- 28% assumption returns the worst structure stiffness. Active-set method and least square minimization produce almost identical results.

- Selection scenario 1 topology (28 diagonal configurations) has the best performance for this particular structure and loading condition. In contrast to Chang’s L-bracket example [15], this example suggests that crossed configuration is not the best configuration for all loading scenarios using SMS method. In fact, the structure consisting of cross configurations performed poorly.

The design time results for all four selection scenarios are provided in Table 4-13.

Table 4-13: Design time results for curved cantilever beam

| <u>Selection Scenario</u> | SMS 28% Assumption | SMS Active-Set | SMS Least-square Minimization | Ground Truss LM |
|---|-----------------------------------|---------------------------|--|--------------------------------|
| Scenario 1 [28 diagonals] 413 struts | 7.8 | 46.7 | 52.8 | 3260 |
| Scenario 2 [4 paramount 1, 24 diagonal] 427 struts | 8.9 | 49.9 | 55.5 | -- |
| Scenario 3 [28 crossed] 445 struts | 9.0 | 47.1 | 49.2 | -- |
| Scenario 4 [18 crossed, 10 diagonal] 435 struts | 9.2 | 52.1 | 53.5 | -- |

From Table 4-13, some key conclusions can be drawn:

- Two-variable optimization returns the best structure stiffness result but at the expense of the design time. There is a trade-off between design time and structure stiffness. The designer must make a decision on what is more important in his/her design process.
- The design time also increases when there are multiple configurations selected for the structure. For topologies consisting of the same number of configurations, the design time has a positive correlation with the number of struts in the structure.

That makes sense because the majority of optimization time is from the finite-element analysis of the truss structure

- Between the two variable approaches, the optimization time for active-set method is shorter than least-square optimization.
- When compared to topological optimization, it can be seen that the SMS method has comparable performance and is able to converge much more quickly, with over 70 and 400 times decrease in design time when using 2-variable and 1-variable optimization approach respectively.

4.2.4 Summary

For the 3-D curved cantilever beam problem, the augmented SMS method and the unit-cell library were utilized to generate an optimized topology. This example serves to demonstrate that the augmented SMS method can be used in structures with curved surfaces. Augmented SMS method give designers an alternative method to rigorous global topological optimization that is significantly faster while still returning reasonably good designs. The 28% assumption seems to always return diameter values faster than either of the two variables methods. However, faster design time comes at the expense of structure stiffness. For this particular structure under the given loading condition, the structure with 28 diagonal configurations returns the best possible stiffness result.

4.3 Micro Aerial Vehicle (MAV) Fuselage

4.3.1 Problem Description

The final design example is a micro aerial vehicle (MAV) fuselage. MAVs play a critical role in modern military operations as they allow easy surveillance in hazardous

environment. The next generation of these aerial robotic systems needs to have enhanced take-off and landing capabilities, better endurance, and be adaptable to mission needs in varying conditions [57]. In term of the design of the wings and fuselage of these MAVs, some types of structures and/or materials that are lighter, stronger and customizable are highly desired.

In this design example, the fuselage is designed to withstand the impact when landing or crashing. The design problem is shown Figure 4-26. There is a distributed load from the payload applied to the inner surface of the fuselage. The weight of the motor and the tail are modeled as point loads at their centers of mass. This is done in ANSYS using a rigid link element. The equivalent couple is applied to the truss structure. All these weights are scaled by a factor of ten to simulate impact when crashing or landing. The weight of the wing is small and assumed to have negligible contribution. A small area on the bottom of the fuselage is fixed to model the landing zone as the MAV is landing. Multiple views of the fuselage are shown in Figure 4-27 with key dimensions labeled. The objective is to achieve a target volume of $100,000 \text{ mm}^3$ or 65% porosity relative to the solid model while minimizing the deflection of the structure. The initial properties of the design problem are provided in Table 4-14.

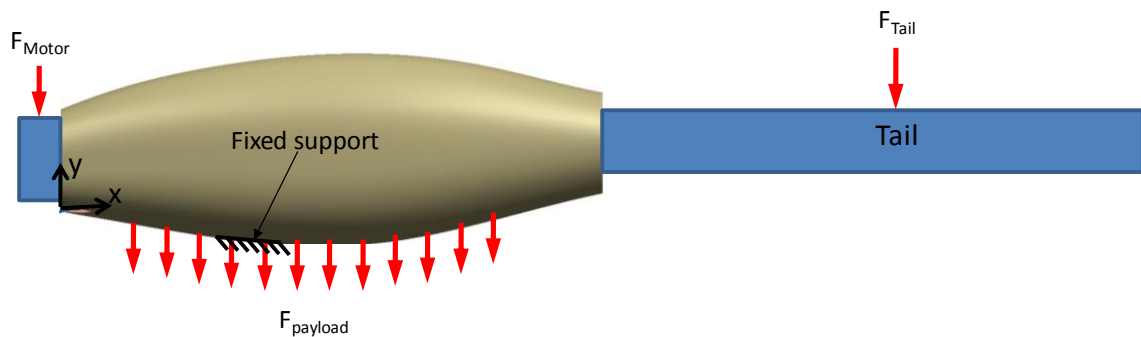


Figure 4-26: Loading and boundary condition on the fuselage

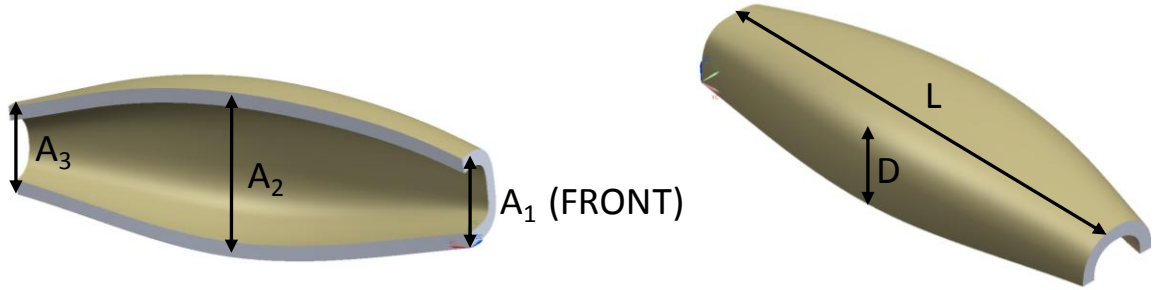


Figure 4-27: Multiple views of the fuselage

Table 4-14: Initial properties for the fuselage

| | | | |
|-------------------------------|----|---|---------|
| A_1 (mm) | 47 | L (mm) | 254 |
| A_2 (mm) | 90 | F_{motor} (N) | 5.9 |
| A_3 (mm) | 45 | F_{Tail} (N) | 2.7 |
| D (mm) | 45 | F_{payload} (N/mm ²) | 0.1 |
| Unit-cell size in-plane (mm) | 12 | Elastic Modulus (N/mm ²) | 1960 |
| Unit-cell size in-plane (mm) | 12 | Poisson Ratio | 0.3 |
| Unit-cell size out-plane (mm) | 8 | Target Volume (mm ³) | 100,000 |

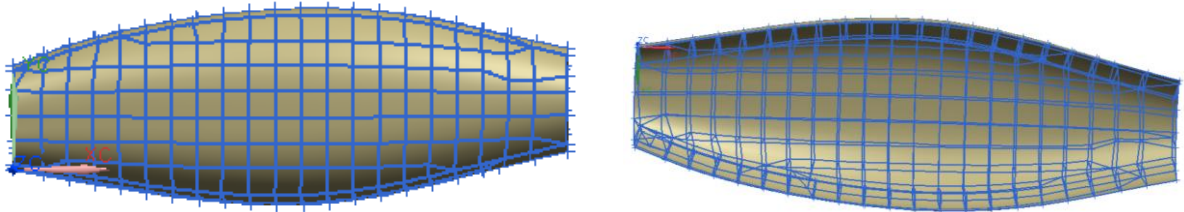


Figure 4-28: Multiple views of the ground structure for the fuselage

4.3.2 Ground Geometry and Solid Body Analysis

The ground structure for the fuselage is generated by TrussCreator with the desirable unit-cell sizes as provided in Table 4-14 . There are 214 unit cells in the ground structure. The previous implementations of the SMS method would not be able to generate the

ground geometry because it requires free-mesh approach. The solid-body finite-element analysis result is shown Figure 4-29. From the result, it can be seen that the highest stress occurs along the bottom of the fuselage as it makes impact when landing. Based on these observations, the method should allocate thicker struts along the bottom of the fuselage and thinner struts everywhere else.

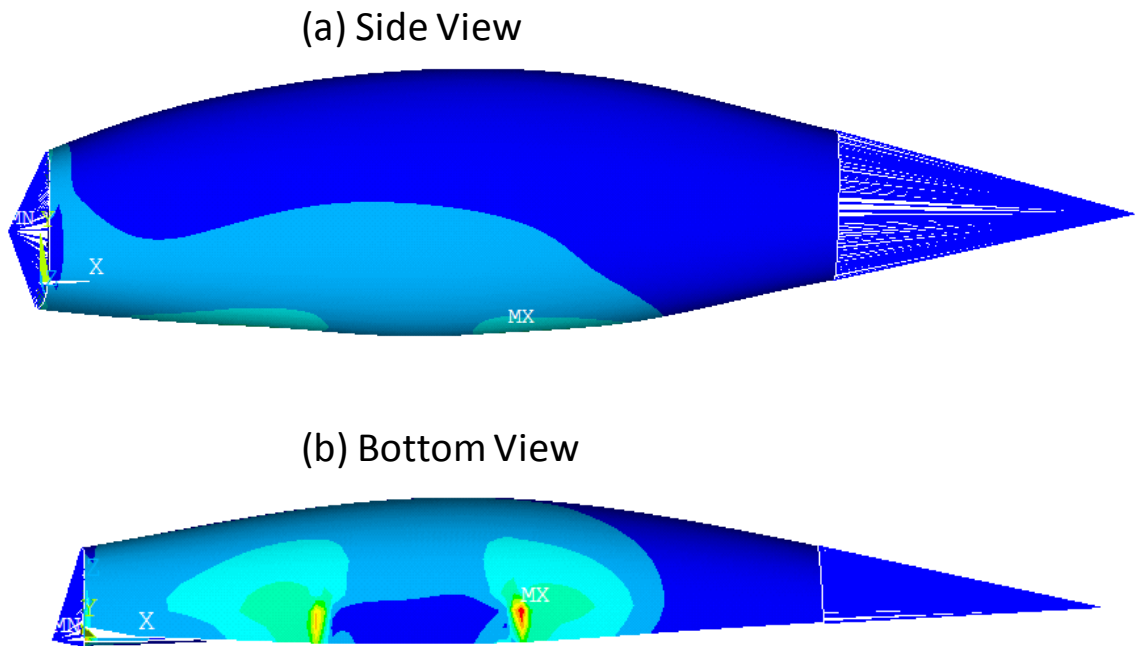


Figure 4-29: Solid-body analysis result for the fuselage

The stress results from the solid-body analysis are then mapped back the correct unit cells of the ground geometry and transformed to the local coordinate systems to allow correct topology generation for the truss structure. With the stress values are known, the unit-cell library can be used to determine unit-cell configuration and sizes of the struts to use in each unit cell.

4.3.3 Unit-Cell Library

In this section, four unique topologies of the fuselage will be created using the unit-cell library and selection scenario by varying weighting values in Equation 3-18. The resultant topology and struts diameter values are provided for each selection. For the selection scenario, which results in the best structural stiffness, a design space exploration/grid search is also conducted.

4.3.3.1 Selection Scenario1

For the first selection scenario, the weighting values from Equation 3-18 are set at: $W_v = 1$, $W_{nv} = 1$, $W_p = 0$. With the given weighting values, the topology was generated with 214 diagonal configurations. The complete topology of the structure is shown in Figure 4-30. A side view is also provided in Figure 4-31. The resultant topology appears to match the intuitive expectation for the topology of the structure based on the solid-body analysis. The average displacement of selected nodes on the top of the fuselage, where the large displacement occurs according to the solid-body analysis, is used as the metric for deflection.

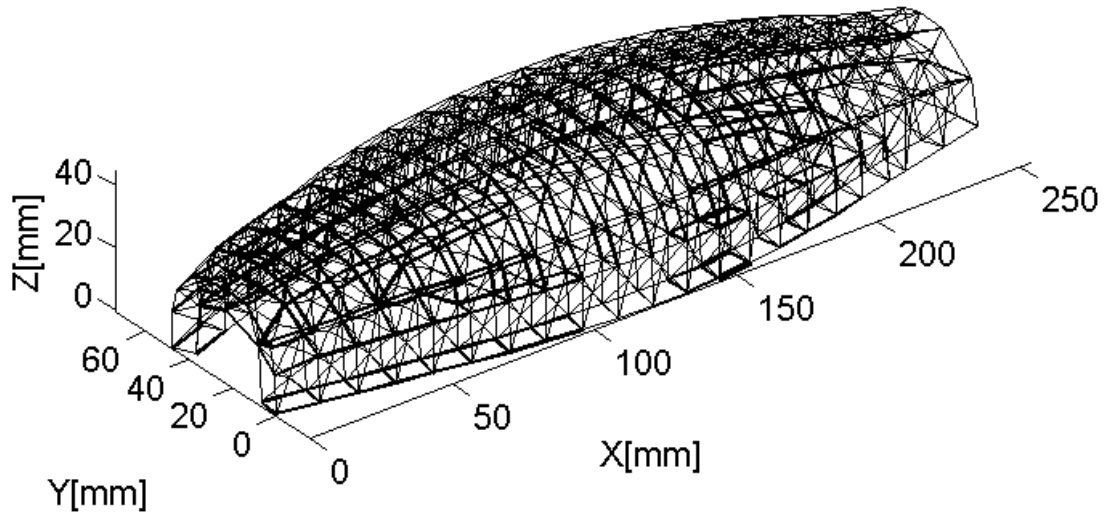


Figure 4-30: Topology for the first selection scenario of the fuselage

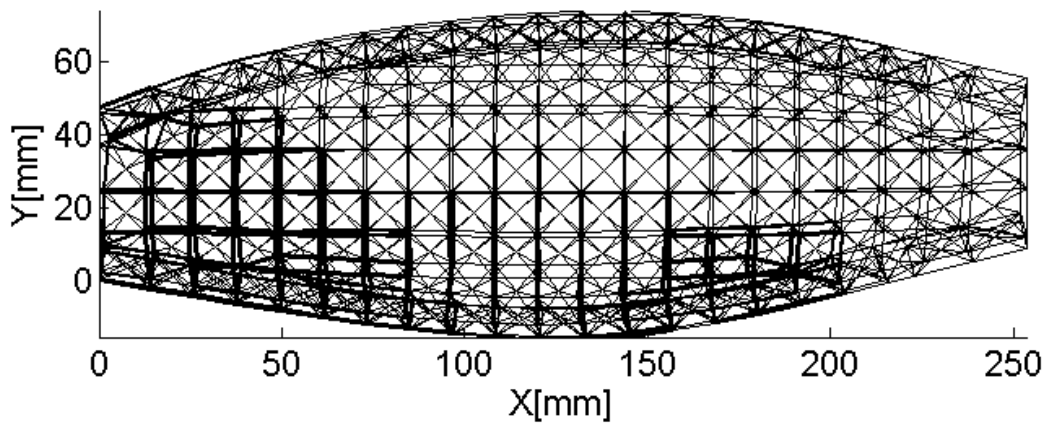


Figure 4-31: Side view of the first selection scenario of the fuselage

Table 4-15: Diameter results for the first selection scenario of the fuselage

| <u>Optimization Approach</u> | 28% Assumption | Active-Set | Least-square Minimization |
|-------------------------------------|-----------------------|-------------------|----------------------------------|
| Deflection(mm) | 0.419 | 0.428 | 0.413 |
| Volume (mm³) | 100010.0 | 100010.0 | 100000.0 |
| D_{min} (mm) | 0.98 | 1.83 | 1.77 |
| D_{max} (mm) | 3.49 | 3.29 | 3.50 |
| D_{cutoff} (mm) | N/A | N/A | N/A |
| Design Time (s) | 303.3 | 1650.5 | 395.5 |

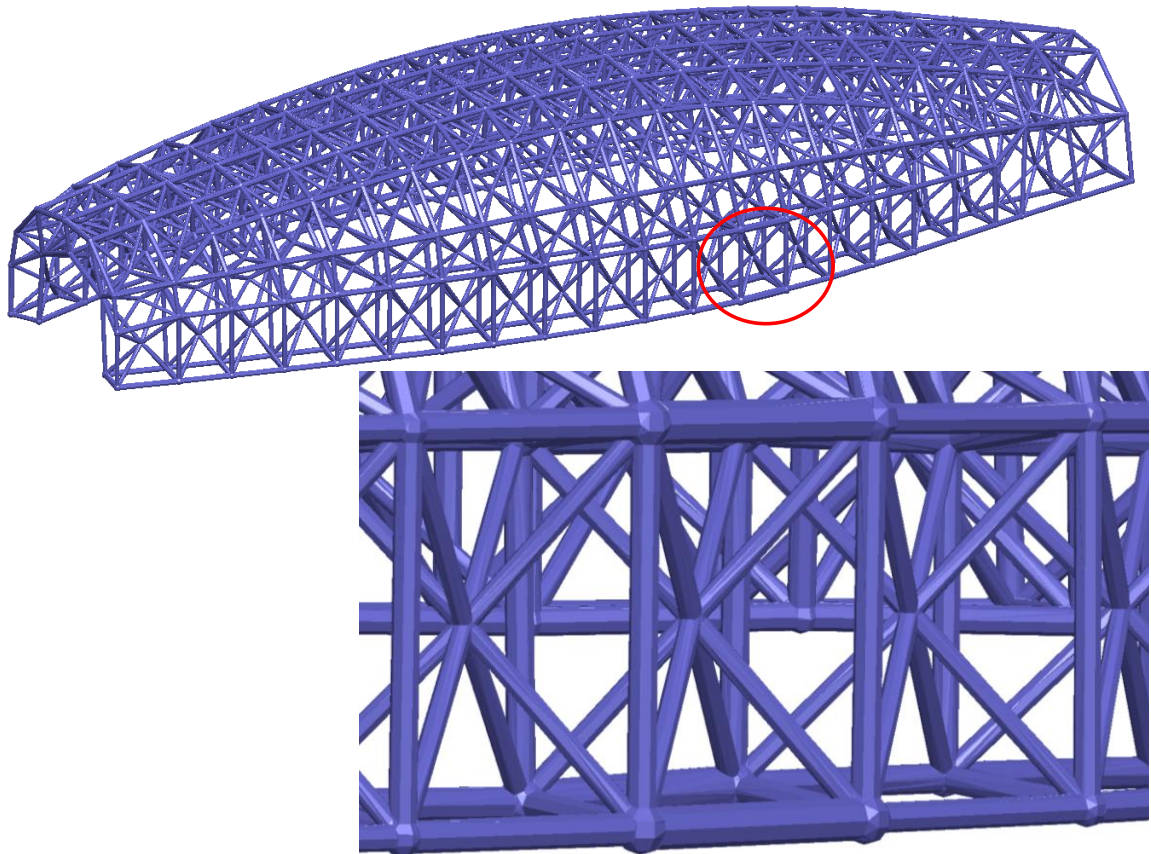


Figure 4-32: Final topology for the first selection scenario of the fuselage using least-square minimization

The strut diameter results are summarized in Table 4-15 . The results show that the 28% assumption method is able to converge the fastest. Between the 2-variable

optimization approaches, least-square minimization converges faster. In addition, it also returns the best deflection value. The final 3-D topology of the fuselage using least-square minimization is shown in Figure 4-32.

4.3.3.2 Selection Scenario 2

The weighting values in Equation 3-18 are set at: $W_v = 0$, $W_{nv} = 1$, $W_p = 0$ for this selection scenario. With these values, the topology of the structures contains 106 paramount 1 configurations and 108 diagonal configurations. The complete topology is shown Figure 4-33 . A side view of the topology is also provided Figure 4-34. The topology appears to match the intuitive expectation.

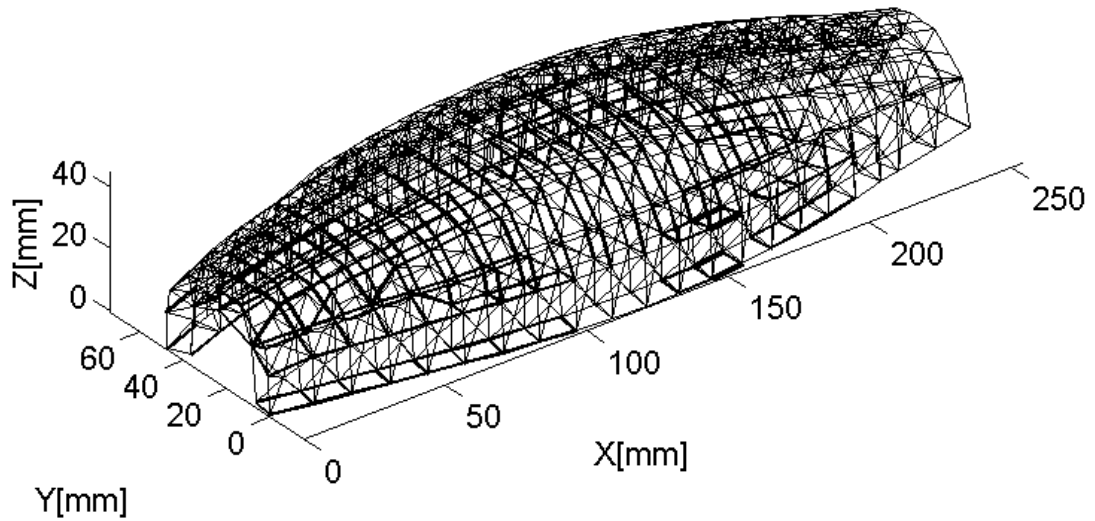


Figure 4-33: Topology for the second selection scenario of the fuselage

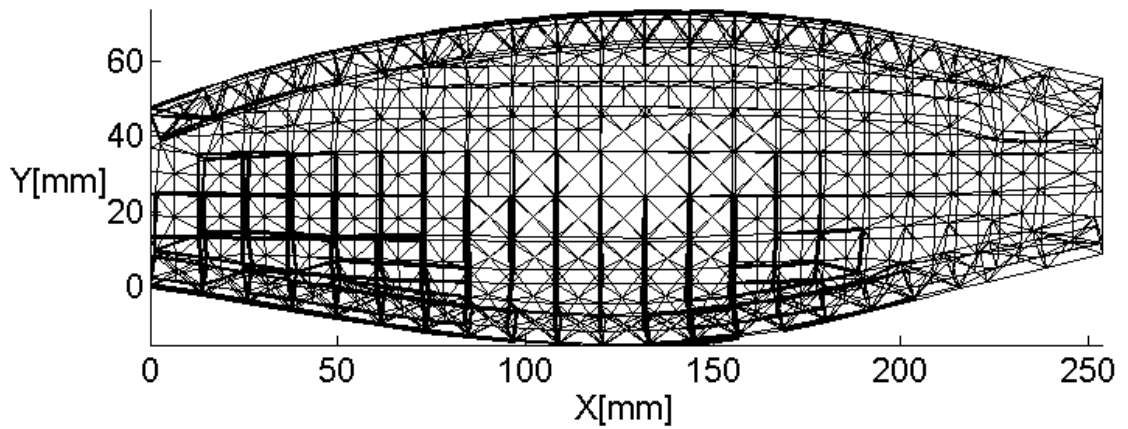


Figure 4-34: Side view of the second selection scenario of the fuselage

Table 4-16: Diameter results of the second selection scenario for the fuselage

| <u>Optimization Approach</u> | 28% Assumption | Active-Set | Least-square Minimization |
|-------------------------------------|-----------------------|-------------------|----------------------------------|
| Deflection(mm) | 0.403 | 0.384 | 0.417 |
| Volume (mm³) | 99997.0 | 99951.0 | 100000.0 |
| D_{min} (mm) | 0.98 | 1.50 | 1.69 |
| D_{max} (mm) | 3.49 | 3.86 | 3.35 |
| D_{cutoff} (mm) | N/A | N/A | N/A |
| Design Time (s) | 491.9 | 1943.8 | 624.3 |

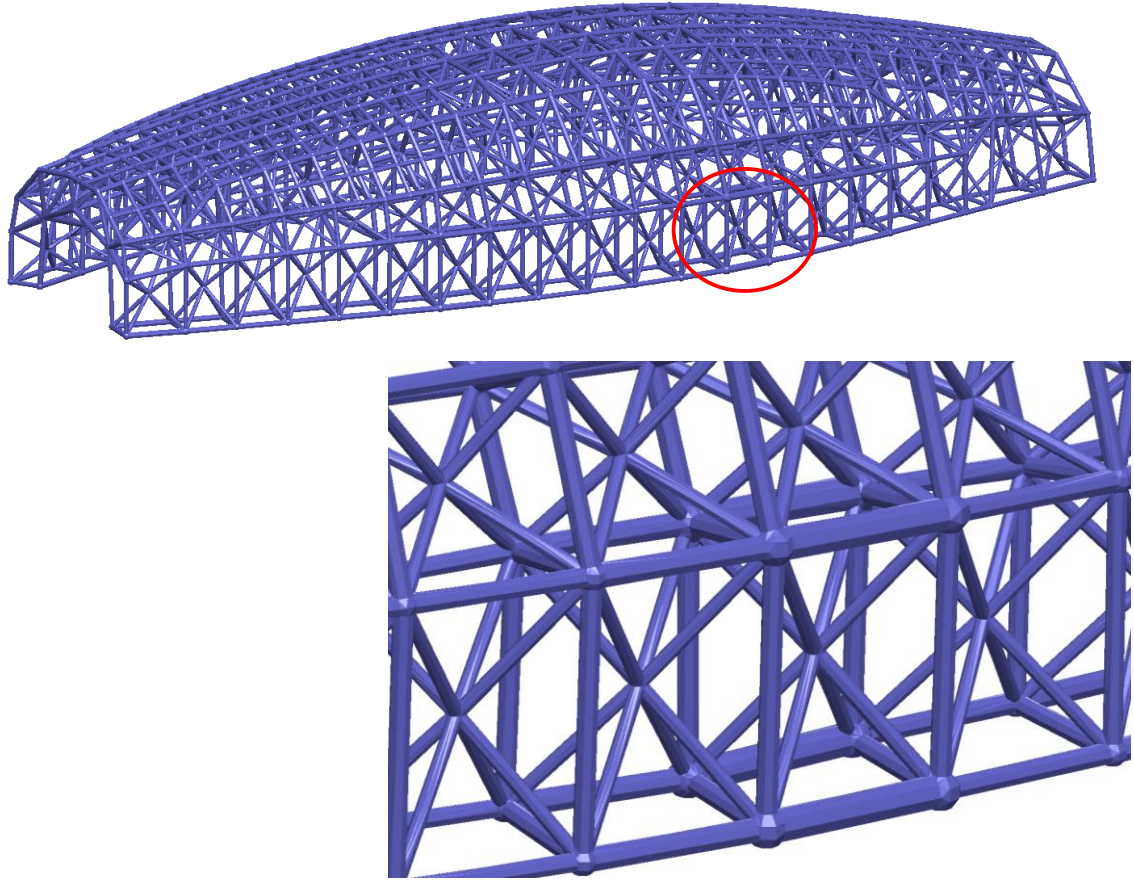


Figure 4-35: Final topology for the second selection scenario of the fuselage using active-set method

The strut diameter results are summarized in Table 4-16. Once again, the 28 % assumption took the least amount of time to return the result. Active-set method returned the best deflection value but at the cost of the design time with four times longer than the 28% assumption. The final 3-D topology of the fuselage using active-set method is shown Figure 4-35. The structure contains 106 paramount1 configurations and 108 diagonal configurations.

4.3.3.3 Selection Scenario 3

The third selection scenario has the weighting values in Equation 3-18 set at: $W_v = 0$, $W_{nv} = 1$, $W_p = 5$. With these weighting values, the topology is generated with 101 crossed

configurations and 113 diagonal configurations. The complete topology of the structure is shown in Figure 4-36. The side view of the topology is also provided in Figure 4-37. The topology matches the expectation based on the solid-body analysis.

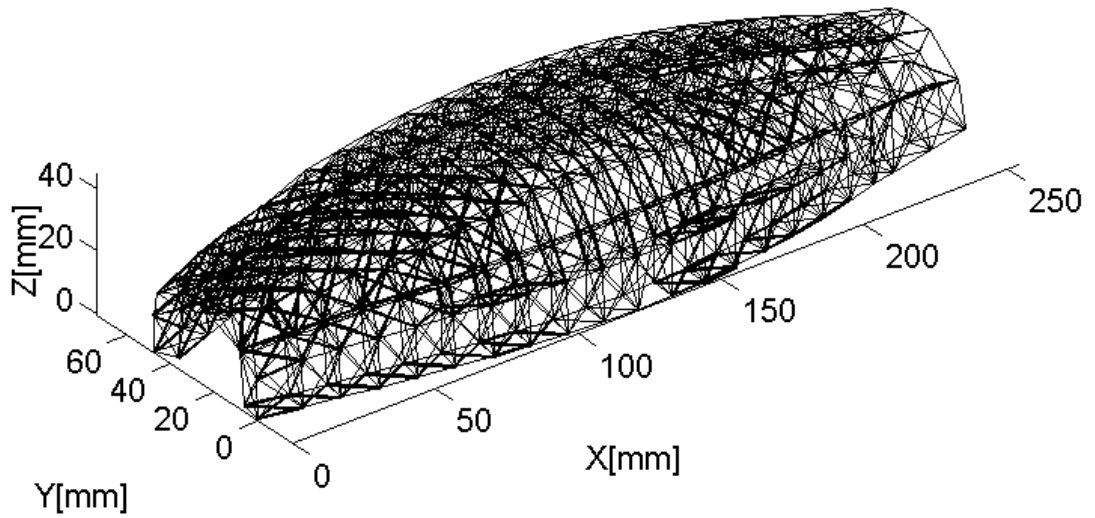


Figure 4-36: Topology for the second selection scenario of the fuselage

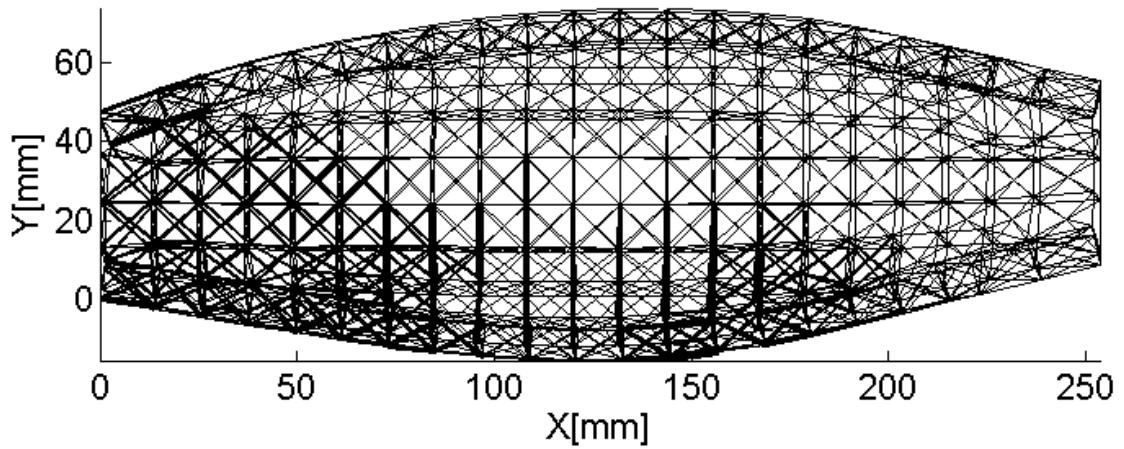


Figure 4-37: Side view of the third selection scenario for the fuselage

Table 4-17: Diameter results of the third selection scenario of the fuselage

| <u>Optimization Approach</u> | 28% Assumption | Active-Set | Least-square Minimization |
|-------------------------------------|-----------------------|-------------------|----------------------------------|
| Deflection(mm) | 0.327 | 0.299 | 0.319 |
| Volume (mm³) | 100000.0 | 99973.0 | 100010.0 |
| D_{min} (mm) | 0.85 | 0.65 | 1.12 |
| D_{max} (mm) | 3.04 | 4.16 | 3.29 |
| D_{cutoff} (mm) | N/A | N/A | N/A |
| Design Time (s) | 378.6 | 1630.9 | 508.9 |

The strut diameter results are summarized in Table 4-17. Active-set method returns the best deflection value but at the expense of design time with more than four times longer than the fastest method: 28% assumption. However, 28% assumption returns the worst deflection result compared to the two 2-variable approaches. The final 3-D topology of the fuselage using active-set method is shown Figure 4-38. The structure contains 101 crossed configurations and 113 diagonal configurations. As mentioned in example 1, it is important to note that the diameter results reported for SMS method are the actual diameters of structure after being scaled against the solid body analysis and unit cell library scaling factors. The pre-scaling D_{MIN} and D_{MAX} for the active set method are 0.5178mm and 7.1406mm respectively. In order to differentiate pre-scaling and scaling diameter value, D_{MIN} and D_{MAX} denotes pre-scaled values while D_{min} and D_{max} denotes scaled values.

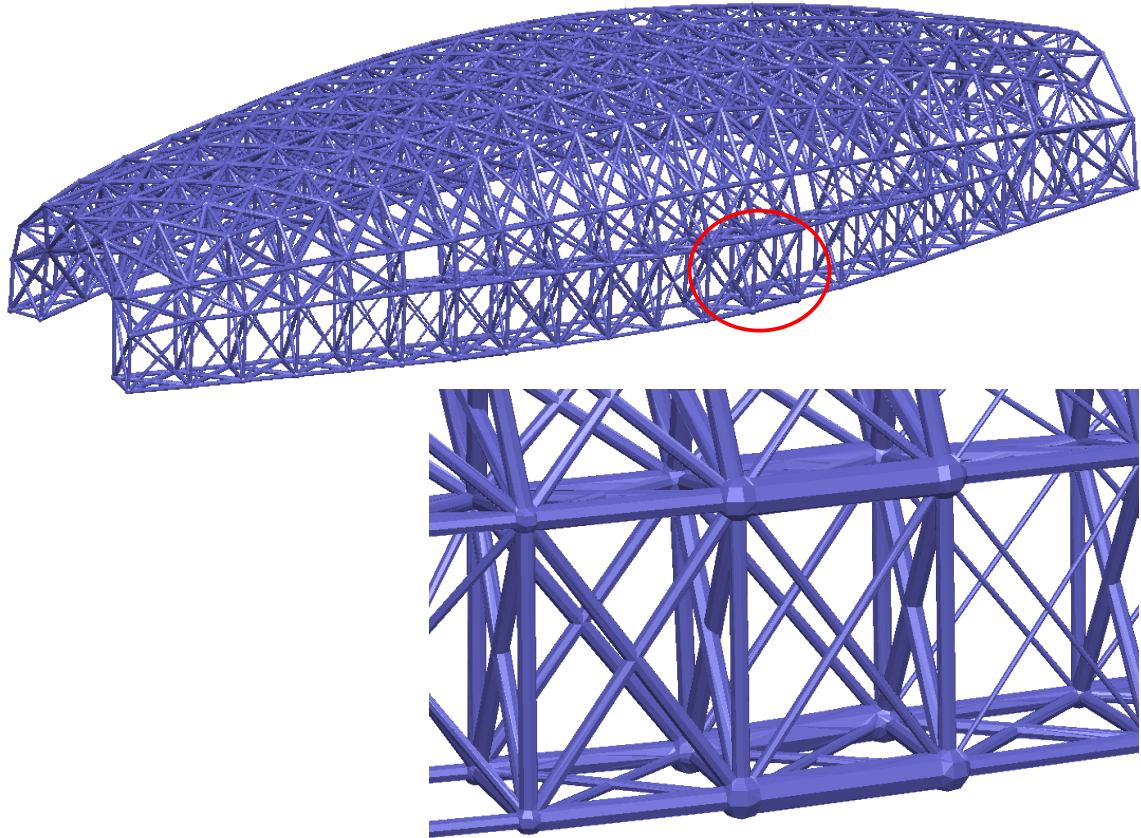


Figure 4-38: Final topology for the third selection scenario of the fuselage using least-square minimization

In addition to the three optimization approaches, design space exploration/grid search was conducted. The design space exploration is done using pre-scaling values of diameters. D_{MIN} and D_{MAX} were iterated from 0.1 mm to 10 mm and with an increment of 0.1 mm. The increment, 0.1 mm, is coarse to reduce analysis time. However, even with the coarse increment, the design space exploration already takes a long time to complete. Exhaustive search is not a feasible solution for structure with large number of struts. The result is plotted in Figure 4-39. A finer resolution of the design space was conducted around the apparent minimum by searching D_{MIN} from 0.4 to 0.6m and D_{MAX} from 7mm to 7.3 mm. with an increment of 0.01 mm. Figure 4-40 shows the design space zoomed

into the region of interest. The red diamond indicates in the minimum in the design space exploration. Diameter results that return the lowest objective function value are shown in Table 4-18. The first column is diameter values from the design space exploration before scaling. The second column is true diameters of the structure after they have been scaled using solid-body and unit-cell library scaling factors. These diameter values are found to be close to the values obtained from the SMS method. Both two-variable optimizations were able to return results with much lesser design time than the design space exploration. It can be seen from Figure 4-40, there is a valley in the design space exploration near the solution, which might cause the active set method to converge slowly because of the shallow gradient along one direction.

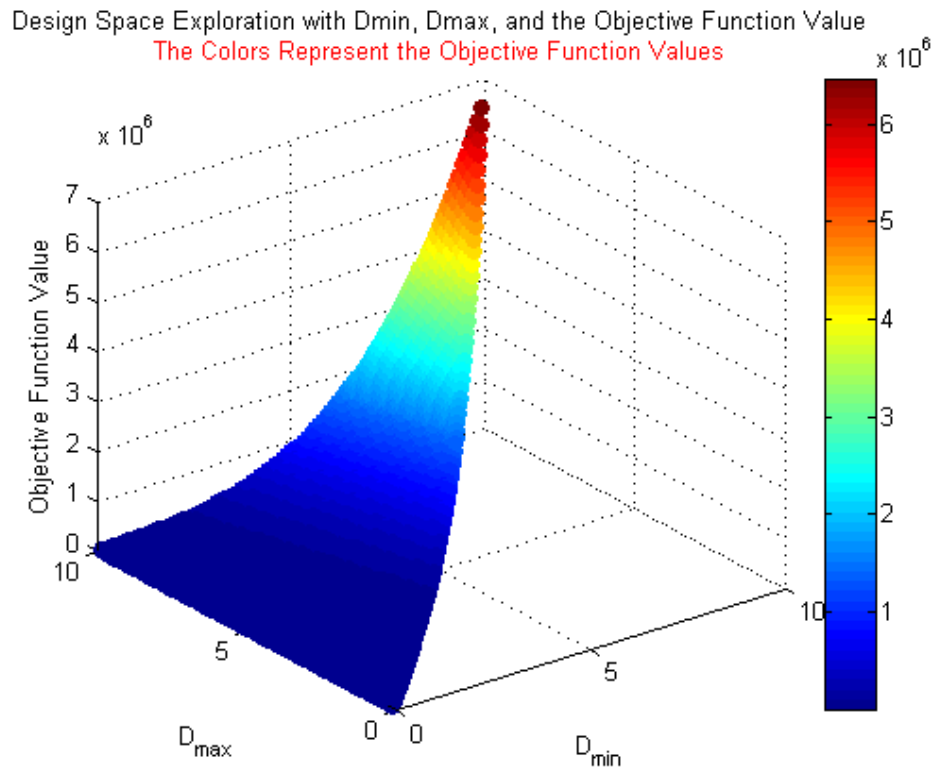


Figure 4-39: Design space for the third selection scenario of the fuselage

Table 4-18: Design space exploration results for the fuselage

| | Pre-scaled | Scaled |
|--------------------------------|------------|--------|
| Deflection(mm) | 0.296 | 0.296 |
| Volume (mm³) | 100000 | 100000 |
| D_{max} (mm) | 7.28 | 4.22 |
| D_{min} (mm) | 0.48 | 0.62 |
| D_{cutoff} (mm) | N/A | N/A |
| Design Time (s) | 76660 | 76660 |

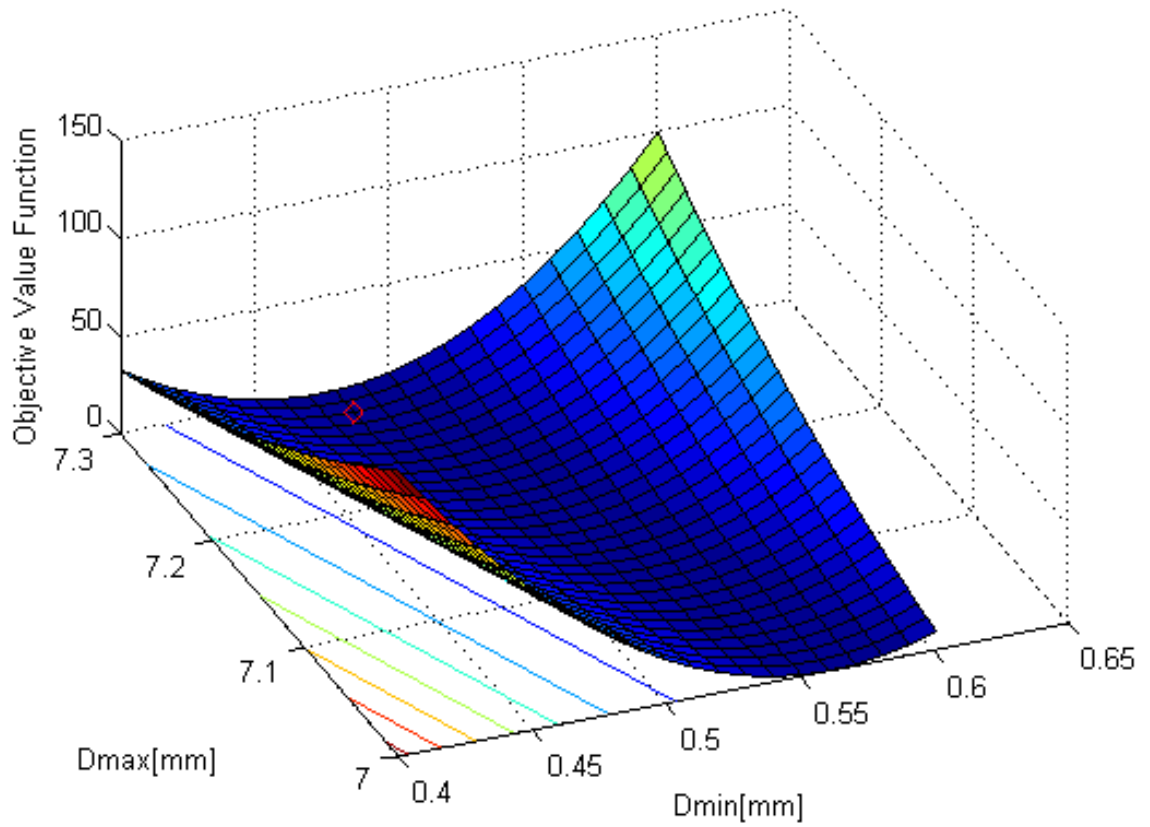


Figure 4-40: Zoomed-in design space of exploration for the third selection scenario of the fuselage

4.3.3.4 Selection Scenario 4

The final selection scenario has weighting values in Equation 3-18 set at: $W_v = 0$, $W_{nv} = 0$, $W_p = 1$. The topology consists entirely of 214 crossed configurations. The topology matches the expectation for the structure. The complete topology of the fuselage is shown in Figure 4-41. A side view of the topology is also shown in Figure 4-42.

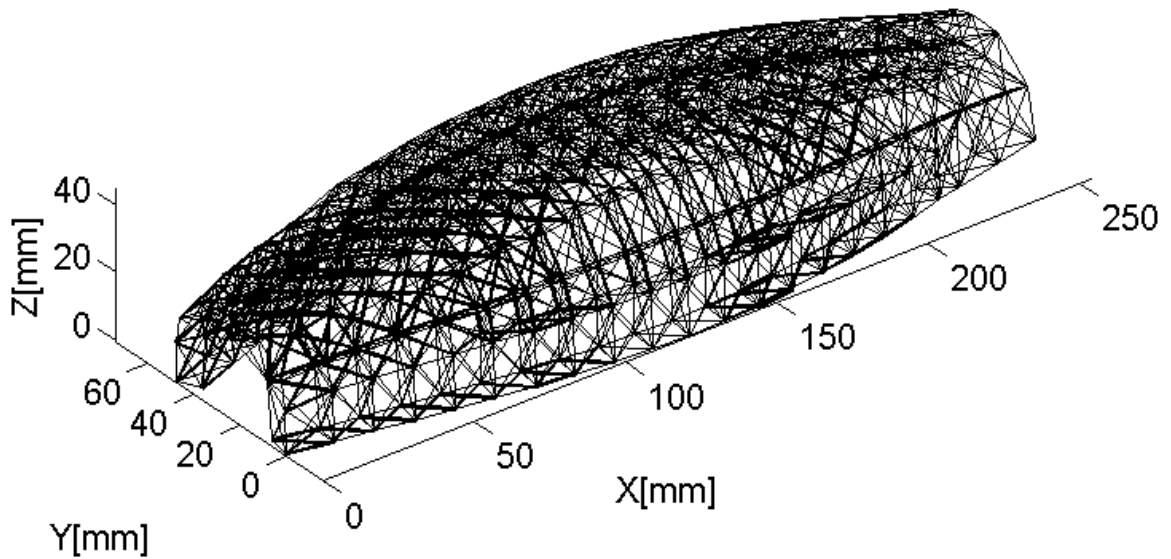


Figure 4-41: Topology for the final selection scenario of the fuselage

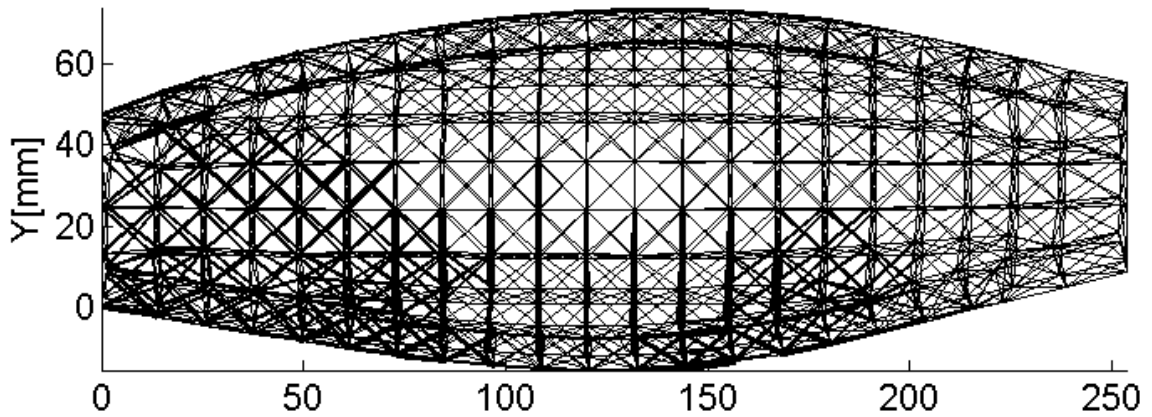


Figure 4-42: Side view of the final selection scenario for the fuselage

Table 4-19: Diameter results of the final selection scenario for the fuselage

| <u>Optimization Approach</u> | 28% Assumption | Active-Set | Least-square Minimization |
|-------------------------------------|-----------------------|-------------------|----------------------------------|
| Deflection(mm) | 0.393 | 0.391 | 0.376 |
| Volume (mm³) | 99997.0 | 100010.0 | 100000.0 |
| D_{min} (mm) | 0.77 | 0.91 | 0.66 |
| D_{max} (mm) | 2.75 | 3.18 | 3.99 |
| D_{cutoff} (mm) | N/A | N/A | N/A |
| Design Time (s) | 286.3 | 1550.1 | 447.3 |

The strut diameter results are summarized in Table 4-19. The results show that the 28% assumption method is able to converge the fastest. Between the 2-variable optimization approaches, least-square minimization converges faster. In addition, it also returns the best deflection value. The final 3-D topology of the fuselage using least-square minimization is shown in Figure 4-43. The structure contains 214 cross configurations.

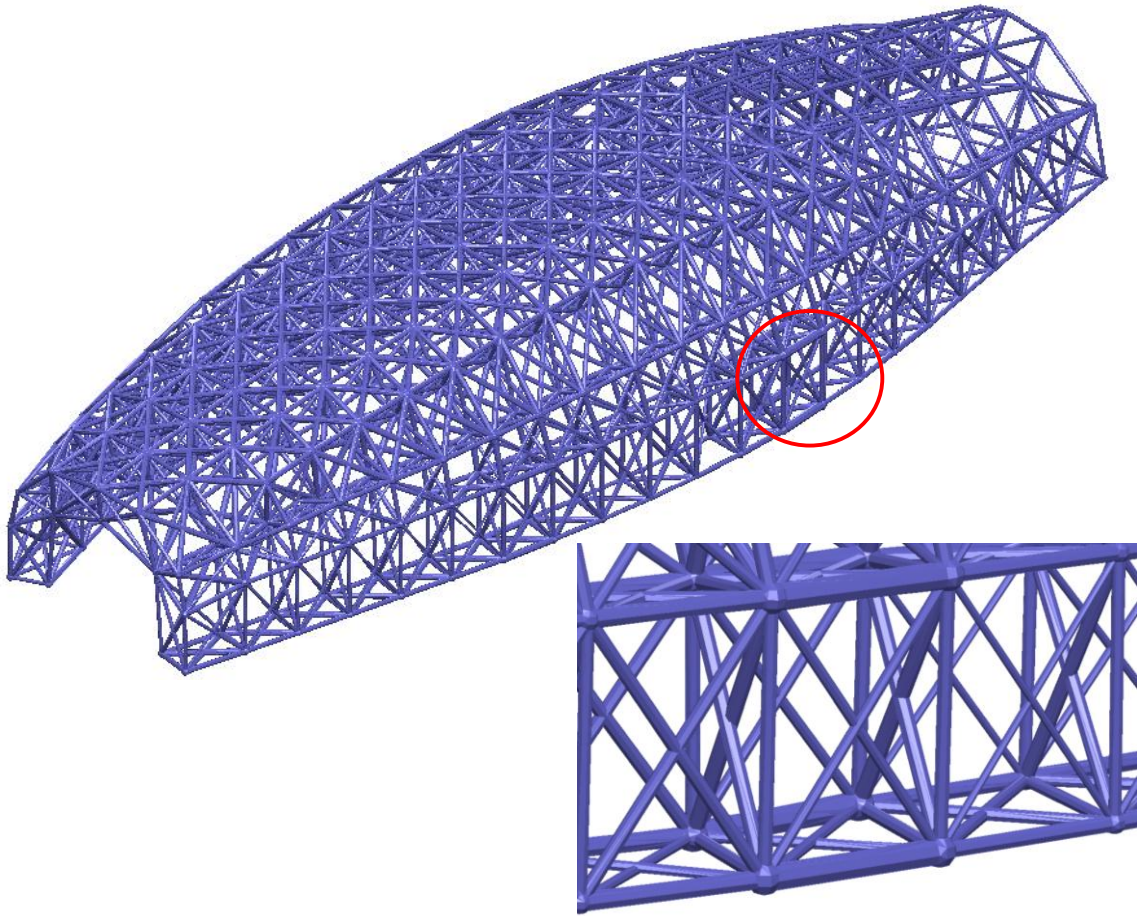


Figure 4-43: Final topology for the final selection scenario of the fuselage using least-square minimization

4.3.3.5 Result Comparison

The results from four unique selection scenarios are compared in this section. Table 4-20 presents the deflections results of the fuselage for each topology.

Table 4-20: Deflection results for the fuselage

| Selection Scenario | 28% Assumption | Active-Set | Least-square Minimization |
|---|-----------------------|-------------------|----------------------------------|
| Scenario 1 [214 diagonals] | 0.419 | 0.428 | 0.413 |
| Scenario 2 [106 paramount 1, 108 diagonal] | 0.403 | 0.384 | 0.417 |
| Scenario 3 [101 crossed, 113 diagonal] | 0.327 | 0.299 | 0.319 |
| Scenario 4 [214 crossed] | 0.393 | 0.391 | 0.376 |

From Table 4-20, we can observe the following important trends:

- Least-square minimization returns the best structural stiffness in selection scenario 1 and 2 when there is only one configuration selected while active- set method return the best deflection value in selection scenarios 2 and 3 when there are multiple configurations selected.
- Topology from selection scenario 3 (101 crossed, 113 diagonal) returns the best structural performance for this particular structure and loading condition.

Table 4-21: Design time results for the fuselage

| Selection Scenario | 28% Assumption | Active-Set | Least-square Minimization |
|---|-----------------------|-------------------|----------------------------------|
| Scenario 1 [214 diagonals] 2840 struts | 303.3 | 1650.5 | 395.5 |
| Scenario 2 [106 paramount 1, 108 diagonal] 3168 struts | 491.9 | 1943.8 | 624.3 |
| Scenario 3 [101 crossed, 113 diagonal] 2899 struts | 378.6 | 1630.9 | 508.9 |
| Scenario 4 [214 crossed] 2858 struts | 286.3 | 1550.1 | 447.3 |

Table 4-22: Number of function calls to objective functions for the fuselage

| Selection Scenario | 28% Assumption | Active-Set | Least-square Minimization |
|---|-----------------------|-------------------|----------------------------------|
| Scenario 1 [214 diagonals] | 23 | 128 | 24 |
| Scenario 2 [106 paramount 1, 108 diagonal] | 27 | 154 | 34 |
| Scenario 3 [101 crossed, 113 diagonal] | 28 | 120 | 33 |
| Scenario 4 [214 crossed] | 23 | 109 | 27 |

The design time results and number of function calls for all four selection scenarios are presented in Table 4-21 and Table 4-22.

From Table 4-21 and Table 4-22, some key conclusions can be drawn:

- In all selection scenarios, 28% assumption converges the fastest. This result is expected because there is one variable to be optimized as opposed to two variables.
- Between the two-variable optimization methods, the optimization time for least-square minimization is significantly shorter than the active-set method. Active-set method requires a significant more number of function calls than the other two approaches.
- The introduction of additional configuration to the topology seems to increase the overall optimization time.
- The number of the struts and number of function calls to the objective functions are proportional to the solution time.

- Topology with a combination of paramount and diagonal configurations appears to take the longest amount of time to converge because it has the most number of struts.

Figure 4-44 shows the typical convergence plot of the active set method, which takes the longest time to converge. The optimization seems to hit a plateau during iteration 2 and 3. This likely occurs because active-set method tries to follow the bound constraints and meets a small flat region in the function. There is a valley with a shallow gradient in one direction as shown in the design space exploration. Levenberg-Marquardt method, on the other hand, uses simple penalty function to impose bounds and does not follow bound constraints.

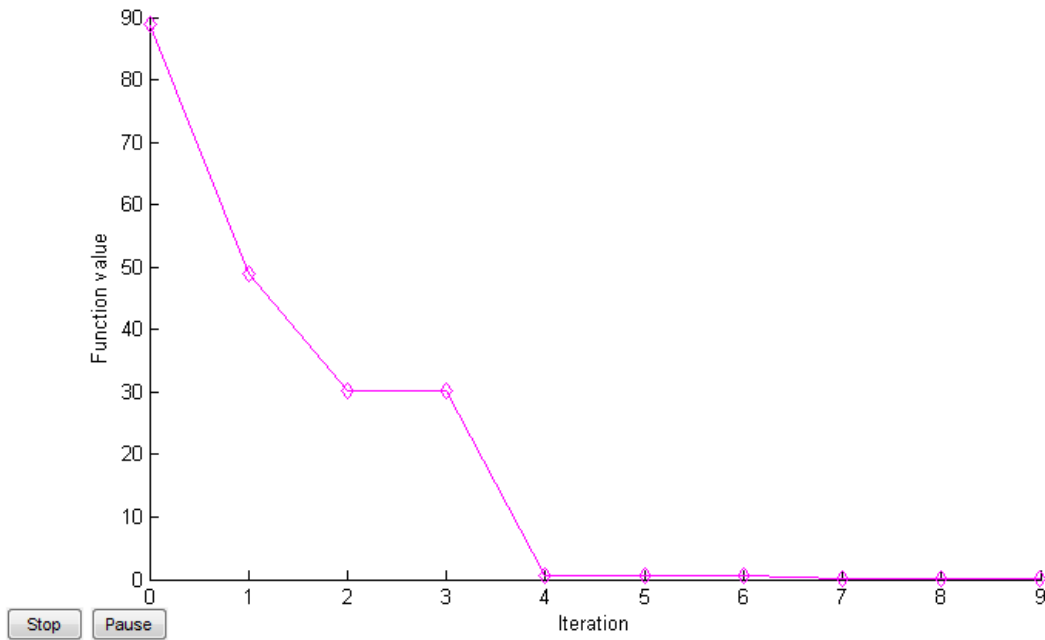


Figure 4-44: Convergence plot for active set method

4.3.4 Summary

The augmented SMS method and the unit-cell library were utilized to successfully generate the optimized topology for the fuselage. This example serves to demonstrate

that the augmented SMS method can be used to design and optimize complex-shaped structure. The one variable approach using 28 % assumption converges the fastest but at the expense of the overall structural performance. Between the two variable methods, active-set method converges more slowly than least-square minimization. For this particular structure under the given loading condition, the topology with a combination of cross and diagonal configuration returns the best possible stiffness result.

CHAPTER 5

CONCLUSIONS

5.1 Summary

Advances in additive manufacturing technologies have brought a new paradigm shift to both design and manufacturing. Designers now have access to a greater design space in which they can design and manufacture complex and customizable parts and products. One application of this technology is for fabrication of customized, light-weight material called meso-scale lattice structures (MSLS). MSLS are a type of cellular structure with strut diameters in the range of 0.1 to 10 mm and strut length on the order of centimeters. They have several advantages such as high strength to weight ratio, and strong thermal and acoustics insulation properties. Conventional CAD and CAE systems are computationally insufficient to handle MSLS-based designs because these structures can contain hundreds of thousands of individual struts. Furthermore, existing design methods for such structures are very limited due to the large number of design variables and options.

In previous research conducted by this laboratory, a new method, using a unit-cell approach, was developed to efficiently optimize MSLS. The MSLS optimization process is done by utilizing a heuristic that reduces the multivariable optimization problem to a problem of only two variables. The heuristic is based on the observation that the stress distribution in a MSLS will be similar to the stress distribution in a solid body of the same overall shape. Hence, a solid body is generated that envelopes the part model surfaces and the MSLS and a stress analysis is performed using finite-element analysis.

Based on the computed local stress states, unit cells from a predefined unit-cell library are selected and sized to support those stress states. The optimal diameters of these struts are then computed by performing a two-variable minimization. However, the method lacks a systematic methodology to efficiently generate the ground structure for the optimization process. The purpose of this research is to present the augmented SMS method, which integrates a free-mesh approach into its previous implementations, which allows the augmented method to efficiently optimize MSLS on complex shaped parts.

Chapter 2 is a literature review that covers all the relevant research. The review includes the research in the design and analysis of cellular structures, and the approaches for optimization of these structures.

Chapter 3 presents the augmented SMS method. This includes the integration of the free-mesh approach in the SMS method and modifications of existing method to be used for complex-shaped parts with curved and non-rectangular surfaces. The unit-cell library is also outlined in this chapter

Chapter 4 is a collection of example problems that demonstrate the capabilities of the augmented method. There are three examples including a 3-D cantilever beam, a 3-D curved cantilever beam, and a MAV fuselage.

Chapter 5 is this chapter, which summarizes the contributions, addresses the limitations, and provides the future work.

5.2 Conclusions

The goal of the research presented in this thesis is to develop a method to design and efficiently optimize MSLS on complex-shaped parts by integrating the free-mesh approach in generating conformal lattice structures for the ground structure generation

process. In order to achieve that goal, two subtasks are needed to be completed. The first task is to develop a new algorithm to correlate the finite element nodes from the solid-body analysis to the ground structure of the MSLS. The second task is to transform the stress from the global coordinate system to the local coordinate system of the unit cells to ensure correct topology generation. The followings are conclusions drawn from the research presented in this thesis.

The augmented SMS method was developed that can effectively design and optimize meso-scale lattice structure on complex shaped parts. Given a selected part model surface, MSLS can be generated to conform to the shape of a surface. A free-mesh approach to generate initial ground structure was integrated into the augmented method to design MSLS for complex-shaped parts including structures that have curved or non-rectangular surfaces. The software that embodies this ground structure generation process was integrated into Unigraphics NX, which allows the designer to set lattice size parameters through the graphical user interface. In step 3 of the augmented SMS method, a new algorithm was developed to determine which unit cell of the ground structure the finite-element nodes fall into. The new algorithm successfully maps the finite-element nodes to the correct unit cells in the ground structure so that the stress values of these nodes can be included in the calculation of stresses in the unit cells. Once the finite element nodes are mapped to the correct unit cells in the ground structure, a stress transformation from the global coordinate systems to local coordinate systems of the unit cells is conducted, which consists of a change of orthonormal basis made by rigid-body rotation. Utilizing the property of second-order tensor, the stress was transformed to its proper local state to generate the correct topology as shown in the examples.

The results from design example 1 agree well with the results from a similar design example done by Chang [15] in terms of design time and structural stiffness. It verifies that the integration of mesh-free approach and algorithm changes did not have any adverse effects on the topology and structure integrity of the cantilever beam.

Results from example 2 and 3 show that only three of seven configurations from the unit-cell library are selected in topology generation process due to their performance: the diagonal configuration, the cross configuration and the paramount 1 configuration. For these particular structures with the given loading conditions, topologies generated with diagonal configuration for example 2 and a combination of cross and diagonal configurations for example 3 return the best possible stiffness result. The weighting values W_v , W_{vn} , and W_p from Equation 3-18 should be set such that the topology is generated with diagonal configuration for example 2 and combination of crossed and diagonal configurations example 3. These weighting values are associated with $\sum V_\sigma$, V_{net} , and $\sum P$, respectively, in Equation 3-18. $\sum V_\sigma$ is biased toward diagonal configuration, while V_{net} favors diagonal and paramount 1 configurations. $\sum P$ is a performance parameter that always favor the cross configuration because it has the lowest strain energy. No generalized statement can be made on which unit-cell configuration should be selected because the method and the unit-cell library are only tested for a narrow set of design problems.

Between one-variable and two-variable optimizations, one-variable optimization using 28% assumption consistently returns diameter results much faster than either two-variable optimizations, but at the cost of the structure stiffness. The two two-variable optimizations produced very similar results in the first two design examples in terms of

stiffness and design time. However, least-square minimization outperformed active-set method in term of design time in the MAV example. Due to the trade-off between design time and structural stiffness, the designer must make a decision on what design criterion is more important in his/her design when choosing the optimization approach.

Overall, the augmented SMS method can be applied effectively in the design of conformal truss structure with highly optimized stiffness and volume for complex surface. For simpler structures such as design example 1 and 2, the augmented SMS method, using one-variable, can reduce design time up to 400 times compared to normal topology optimization and up to 70 times using two-variable approach. In cases where topological optimization is infeasible such as design example 3, the augmented SMS method can still effectively generate complex MSLS. This approach removes the need for a rigorous topology optimization, which is a main bottleneck in designing MSLS.

5.3 Contributions

The method developed in this thesis allows leveraging the advantages of additive manufacturing for designing complex truss structures. The major contribution of this thesis is the integration of free-mesh approach into the SMS method to efficiently design and optimize meso-scale truss structure on complex-shaped parts with curved or non rectangular surface, which was not possible with the previous implementation of the SMS method. This thesis is a stepping stone to develop an advanced CAD system which integrates design and analysis of MSLS.

5.4 Future Work

Although some critical key limitations of the previous implementations of the SMS method have been addressed in this research, there are still some improvements that can be added to make the SMS method more robust and effective.

5.4.1 Unit-Cell Library

Currently, there are 7 different configurations in the library. More unit-cell configurations can be added to the unit-cell library to improve the topology generated by the augmented SMS method.

Secondly, the selection method of the unit cell configurations for a given structure is currently based on the empirical understanding of the SMS method. It requires manual adjustments of different weighting values in order to generate different topology for a given structure. A more autonomous and systematic way can be developed to improve the selection process, which can consider factors such as designer's preference, stress distribution of the solid-body analysis, and interaction between neighboring unit cells with different configurations, etc.

The unit-cell library is currently formulated based on the assumption that the unit cell is significantly smaller than the overall structure allowing for the average stresses in the six independent normal and shear stress components in the unit cell to be the approximation of the stress distribution in that region. However, this assumption may not be valid for all problems. For such problems, it may be possible to include unit-cell configurations that handle the stress gradient by varying the strut diameter individually in each unit cell based on the distribution of each stress components.

5.4.2 Systems Integration

The entire MSLS design process can be streamlined by integrating the augmented SMS method to a commercial CAD system and FEA package. It would give the designers the ability to efficiently generate and represent meso-scale lattice structures, and create finite element and optimization models through the graphical user interface. Such integration would allow the SMS method to be used to design MSLS in industry setting.

5.5 Closure

MSLS have numerous benefits, including high strength to weight ratio, and strong thermal and acoustics insulation properties. With the advancement of additive manufacturing, it is now possible to fabricate these structures. This research has enabled the creation of design tools that help designers to design and optimize MSLS on complex-shaped parts, which could then be fabricated using additive manufacturing. We envision a future, where CAD software will be seamlessly integrated with analysis tools to help designers to improve and expand their designs.

REFERENCES

- [1] M. R. Legault and M. Musselman, "The rise of rapid manufacturing," *High Performance Composites*, vol. 17, pp. 32-37, July 2009.
- [2] D. W. Rosen, I. Gibson, and B. Stucker, *Additive Manufacturing Technologies: Rapid Prototyping to Direct Digital Manufacturing*: Springer, 2010.
- [3] P. F. Jabobs, *Rapid Prototyping & Manufacturing: Fundamentals of Stereolithography*. TX: Mcgraw-Hill, 1993.
- [4] T. Wohlers, "Wohlers Report 2008," 2008.
- [5] "Image: Invisalign braces," ed. <http://www.invisalign.com>.
- [6] "Image: Siemens hearing aid," ed. <http://www.medical.siemens.com>.
- [7] "Image: Aerospace ducts made using SLS," ed. <http://www.compositesworld.com/articles/rapid-manufacturing-part-ii-pioneer-applications>.
- [8] D. W. Rosen, "Computer-aided design for additive manufacturing of cellular structures," *Computer-Aided Design & Application*, vol. 4, pp. 585-594, 2007.
- [9] L. J. Gibson and M. F. Ashby, *Cellular Solids: Structure and Properties*. Cambridge: Cambridge University Press, 1997.
- [10] "Image: Cellular metal lattice structure," ed: http://ec.europa.eu/research/transport/projects/items/celpact_en.htm.
- [11] "Image: Foam-aluminum," ed: <http://www.facades.com/foamed-aluminum>.
- [12] M. F. Ashby, A. G. Evans, N. A. Fleck, L. J. Gibson, J. W. Hutchinson, and H. N. G. Wadley, *Metals Foams: A Design Guide*. Woburn, MA: Butterworth-Heinemann, 2000.
- [13] V. S. Deshpande, N. A. Fleck, and M. F. Ashby, "Effective properties of the octet-truss lattice material," *Journal of Mechanics and Physics of Solids*, vol. 49, pp. 1747-1769, 2001.
- [14] J. Chu, S. Engelbrecht, G. Graf, and D. W. Rosen, "A comparison of synthesis methods for cellular structures with application to additive manufacturing," *Rapid Prototyping Journal*, vol. 16, pp. 275-283, 2010.
- [15] P. Chang, "An Improve Size, Matching, and Scaling Synthesis Method for the Design of Meso-Scale Truss Structures," Master's Thesis, Georgia Institute of Technology, 2010.

- [16] G. Graf, "Development of specialized base primitive for meso-scale conforming truss structures," Master's thesis, Georgia Institute of Technology, 2009.
- [17] S. Engelbrecht, "Design of meso-scale cellular structure for rapid manufacturing " Master's thesis, Georgia Institute of Technology, 2009.
- [18] A.-J. Wang and D. L. McDowell, "Optimization of a metal honeycomb sandwich beam-bar subjected to torsion and bending," *International Journal of Solids and Structures*, vol. 40, pp. 2085-2099, 2002.
- [19] A.-J. Wang and D. L. McDowell, "Yield surfaces of various periodic metal honeycombs at intermediate relative density," *International Journal of Plasticity*, vol. 21, pp. 285-320, 2005.
- [20] J. C. Wallach and L. J. Gibson, "Mechanical behavior of a three-dimensional truss material," *International Journal of Solids and Structures*, vol. 38, pp. 7181-7196, 2001.
- [21] S. R. Johnston, M. Reed, H. V. Wang, and D. W. Rosen, "Analysis of mesostructure unit cells comprised of octet-truss structures," presented at the Solid Freeform Fabrication Symposium, Austin, TX, 2006.
- [22] H. Wang, "A unit-cell approach for lightweight structure and compliant mechanism," PhD Thesis, Georgia Institute of Technology, 2005.
- [23] H. Wang, Y. Chen, and D. W. Rosen, "A hybrid geometric modeling method for large scale conformal cellular structures," presented at the ASME Computers and Information in Engineering Conference, 2006.
- [24] M. P. Bendsøe and O. Sigmund, *Topology Optimization: Theory, Methods and Applications*. Berlin: Springer, 2003.
- [25] M. P. Bendsøe, *Optimization of Structural Topology, Shape and Material*. . Berlin Heidelberg: Springer-Verlag, 1995.
- [26] G. Allaire, *Shape Optimization by the Homogenization Method*. New York: Berlin, 2002.
- [27] P. Pedersen, "On optimal shapes in materials and structures," *Structure Multidisciplinary Optimization*, vol. 19, pp. 169-182, 2000.
- [28] G. I. N. Rozvany, *Topology Optimization in Structural Mechanics*: Springer, 2003.
- [29] A. G. M. Michell, "Limits of economy material in frame structures," *Philosophy Magazine*, vol. 6, pp. 589-597, 1904.
- [30] P. Dewhurst and S. Srithongchai, "An Investigaton of minimum-weight dual-material symmetrically loaded wheels and torsion arms," *Journal of Applied Mechanics*, vol. 72, pp. 196-202, 2005.

- [31] G. I. N. Rozvany, O. M. Querin, J. Lógó, and V. Pomezanski, "Exact analytical theory of topology optimization with some pre-existing members or elements," *Structural Multidisciplinary Optimization*, vol. 4, pp. 585-594, 2007.
- [32] S. V. Selyugin, "On optimal geometrically non-linear trusses," *Structure Multidisciplinary Optimization*, vol. 29, pp. 113-124, 2005.
- [33] K. Tai, G. Y. Cui, and T. Ray, "Design synthesis of path generating compliant mechanisms by evolutionary optimization of topology and shape," *Journal of Mechanical Design*, vol. 124, pp. 492-500, Sep 2002.
- [34] R. J. Yang and C. H. Chuang, "Optimal topology design using linear programming," *Computers & Structures*, vol. 52, pp. 265-275, 1994.
- [35] M. P. Bendsøe and N. Kikuchi, "Generating optimal topologies in structural design using a homogenization method " *Computer Methods in Applied Mechanics and Engineering*, vol. 71, pp. 197-224, 1988.
- [36] R. Haber, M. P. Bendsøe, and C. Jog, "A new approach to variable topology shape design using a constraint on the perimeter," *Structural Optimization*, vol. 11, pp. 1-12, 1996.
- [37] M. Zhou, Y. Shyy, and H. Thomas, "Checkerboard and minimum member size control in topology optimization," *Structural Multidisciplinary Optimization*, vol. 21, pp. 152-158, 2001.
- [38] Y. Wang, "A study on microstructures of homogenization for topology optimization," PhD Thesis, School of Architecture, Civil and Mechanical Engineering, Victoria University of Technology, 2003.
- [39] W. Dorn, R. Gomory, and H. Greenberg, "Automatic design of optimal structures," *Journal Mechanical*, vol. 3, pp. 25-52, 1964.
- [40] W. Achtziger, "On simultaneous optimization of truss geometry and topology," *Structural Multidisciplinary Optimization*, vol. 33, pp. 285-304, 2007.
- [41] S. A. Burns, *Recent Advances in Optimal Structural Design*: American Society of Civil Engineers, 2002.
- [42] J. Patel and S. Choi, " Classification Approach for Reliability-based Topology Optimization using Probabilistic Neural Networks," *Structural and Multidisciplinary Optimization*, 2011.
- [43] S. C. Chapra and R. P. Canale, *Numerical Method for Engineers*, 6 ed.: McGraw-Hill, 2010.
- [44] G. I. N. Rozvany and M. Zhou, "The COC algorithm, Part I: Cross-section optimization or sizing," *Computer Methods in Applied Mechanics and Engineering*, vol. 89, pp. 281-308, 1991.

- [45] B. Hassani and E. Hinton, "A review of homogenization and topology optimization III - topology optimization using optimality criteria," *Computers and Structures*, vol. 69, pp. 739-756, 1998.
- [46] K. Zhou and J. Li, "The exact weight of discretized Michell trusses for a central point load," *Structural Multidisciplinary Optimization*, vol. 28, pp. 69-72, 2004.
- [47] W. H. Press, S. A. Teukolsky, W. T. Vetterling, and B. P. Flannery, "Chapter 15," in *Numerical Recipes in C*, 2nd ed Cambridge, UK: Cambridge University Press.
- [48] N. Gould, D. Orban, and T. Philippe, "Numerical methods for large-scale nonlinear optimization," *Acta Numerica*, vol. 24, pp. 299-361, 2005.
- [49] "Matlab r2011a documentation, optimization toolbox: fmincon active set algorithm," ed. [online] <http://www.mathworks.com/help/toolbox/optim>.
- [50] J. Kennedy and R. C. Eberhart, "Particle Swarm Optimization," in *IEEE International Conference on Neural Networks*, Piscataway, NJ, 1995, pp. 1942-1948.
- [51] R. E. Peres and K. Behdinan, "Particle swarm optimization in structural design," in *Swarm Intelligence: Focus on Ant and Particle Swarm Optimization*, F. T. S. Chan and M. K. Tiwari, Eds., ed Vienna, Austria: Itech Education and Publishing, 2007, pp. 373-394.
- [52] S. Engelbrecht, L. Folgar, D. W. Rosen, G. Schulberger, and J. Williams, "Cellular Structures for Optimal Performance," in *Solid Freeform Fabrication Symposium*, Austin, TX, 2009.
- [53] C. C. Seepersad, J. K. Allen, D. L. McDowell, and F. Mistree, "Robust design of cellular materials with topological and dimension imperfections," *Journal of Mechanical Design*, vol. 128, pp. 1285-1297, 2006.
- [54] J. Nguyen, S.-I. Park, and D. W. Rosen, "Cellular structure design for lightweight components," in *5th International Conference on Advanced Research and Rapid Prototyping*, Leiria, Portugal, 2011.
- [55] L. E. Malvern, *Introduction to the Mechanics of a Continuous Medium*. Upper Saddle River, NJ: Prentice-Hall, Inc, 1969.
- [56] "Matlab r2011a documentation, optimization toolbox: fminbnd," ed. online: <http://www.mathworks.com/help/toolbox/optim/ug/fminbnd.html>.
- [57] C. Voorhees. (2011, 4/05/2012). *DARPA Asks, "Can You Design, Build, and Fly the Next Generation UAV?"*. Available: <http://science.dodlive.mil/2011/05/25/darpa-asks-can-you-design-build-and-fly-the-next-generation-uav-video/>